UNIVERSITAT POLITÈCNICA DE CATALUNYA
DEPARTAMENT D'ENGINYERIA DEL TERRENY I CARTOGRÀFICA
ESCOLA TÈCNICA SUPERIOR D'ENGINYERS
DE CAMINS, CANALS I PORTS

NONISOTHERMAL MULTIPHASE FLOW OF BRINE AND GAS THROUGH SALINE MEDIA

TESIS DOCTORAL

PRESENTADA POR:
SEBASTIÀ OLIVELLA PASTALLÉ

DIRIGIDA POR:
JESÚS CARRERA RAMÍREZ
ANTONIO GENS SOLÉ

BARCELONA – JUNIO DE 1995

ABSTRACT

A new formulation for the coupled analysis of thermo- hydro- mechanical problems in saline media is presented. The work ranges from the establishment of the mass, momentum and energy balance equations to its numerical solution by means advanced numerical techniques, including the derivation of some constitutive laws. The resulting computer program (CODE_BRIGHT) can be used to analyze real problems of sealing systems built with porous salt aggregates, which was the original motivation of the work.

The balance equations have been formulated taking into account that three main species or components are present in saline media. These are: salt, water and air. One of the peculiarities of saline media with respect to other geological media is that solid phase dissolves at elevated concentrations in the liquid phase which is referred as to brine. Another interesting aspect is the presence of brine inclusions in the solid phase. Dissolution and precipitation of salt leads to a creep strain mechanism. The shape of grains changes by dissolution of salt in zones of stress concentration while recrystallization takes place in zones of lesser stress level. In addition the grains also deform by the ductile behaviour of the crystalline solid. We have derived a new constitutive law for stress- strain behaviour of porous salt aggregates, which is based on coupling an idealized geometry of grains with the basic strain mechanisms.

Once the computer code was developed and verified, it has been used to study different phenomena. We present the analysis of porosity variations induced by temperature gradients in unsaturated porous salt aggregates. Temperature differences induce a flux of water vapour counteracted by an opposite brine flux. This flux drags dissolved salt, hence a salt flux towards the hot side takes place. This phenomenon, which may cause strong variations of porosity, has not been studied before. Secondly, the analysis of the behaviour of a brick dam subject to compression in the mine gallery is presented. We show that the hydromechanical coupling is crucial to understand what happens. Initially, there is a brine flux towards the dam because of its large suction. When the pores of the backfill reach saturation, the flux is reversed because convergence of the rock salt cause pore pressure to build up at the dam. A few applications to other problems related to nonsaline media show that the formulation is very versatile.

RESUMEN

Presentamos una formulación nueva para el análisis de problemas termo- hidro-mecánicos en medios salinos. Esta formulación incluye, desde la obtención de ecuaciones de balance de masa, momento y energía hasta su resolución numérica, incluyendo la derivación de algunas ecuaciones constitutivas. El programa de cálculo resultante (CODE_BRIGHT) puede usarse para analizar problemas reales de sistemas de sellado construidos con agregados porosos de sal, que era la motivación original de este trabajo.

Las ecuaciones de balance se han formulado teniendo en cuenta que en un medio salino existen tres especies o componentes mayoritarios. Éstos son: la sal, el agua y el aire. Uno de los aspectos diferenciadores respecto a otros medios geológicos es que la fase sólida se disuelve a concentraciones elevadas en la fase líquida a la que se llama salmuera. Otro aspecto interesante es la presencia de inclusiones de salmuera en la fase sólida. La disolución y precipitación de la sal da lugar a un mecanismo de deformación por fluencia. La forma de los granos de sal cambia por disolución en las zonas donde se concentran las tensiones y recristalización en las zonas de menor estado tensional. Además los granos también se deforman por al carácter muy dúctil del propio sólido cristalino. Hemos derivado una nueva ley constitutiva tensión- deformación para los agregados porosos de sal, que se basa en acoplar una geometría idealizada de los granos con los mecanismos fundamentales de deformación.

Una vez que se ha desarrollado y verificado el programa de cálculo, éste ha sido aplicado para el estudio de diferentes fenómenos. Presentamos el análisis de las variaciones de porosidad inducidas por gradientes de temperatura en agregados porosos de sal no saturados. Las diferencias de temperatura inducen un flujo de vapor que es contrarrestado por un flujo de salmuera. Éste arrastra la sal disuelta y da lugar a un flujo de sal hacia zonas de temperatura más alta. Este fenómeno, que puede producir variaciones de porosidad muy grandes, no se había estudiado con anterioridad. En segundo lugar se analiza el comportamiento de una barrera de ladrillos de sal al verse sometida a compresión en una galería de una mina. Como demostramos, el acoplamiento hidromecánico es crucial para entender el comporamiento. Inicialmente hay un flujo de salmuera hacia el relleno al tener mayor succión. Cuando en los poros del relleno se llega a saturación, el flujo se invierte porque la convergencia de la roca causa un aumento brusco de la presión intersticial en el relleno. Algunas aplicaciones a otros problemas en medios no salinos muestran que la formulación es muy versátil.

ACKNOWLEDGEMENTS

Firstly, I will thank the people that have guided this research work. I would like to express my acknowledgement to Jesús Carrera for having drawn me to this extraordinary field that is research. Sincerely, I believe that Jesús Carrera has exceptional qualities in lots of aspects. Good results are due to his adequate supervision. This thesis has been cosupervised because geomechanical aspects were also studied. I would like to acknowledge Antonio Gens for having led to obtain good results in this work. Jesús Carrera and Antonio Gens were among the best professors during my graduation studies. I also would like to acknowledge Eduardo Alonso and Antonio Lloret for their dedication to my work. All them are excellent people. All these professors know very well the meaning of 'laisser-faire' which, I believe, produces good results and, sometimes, is not so easy to apply. I also would like to thank all the people in the Departmento de Ingeniería del Terreno for their help at any moment. Particularly, to Beatriz and Miguel.

Secondly, I will thank the funding institutions. I acknowledge ENRESA which is doing an investment in research, sometimes without immediate results, to solve the problem of radioactive waste disposal, one of the major problems of our society. Particularly I would like to acknowledge Fernando Huertas who was responsible of the project. We have attended several meetings and I thisnk he has a contribution in this work. I also thank the European Commision through B. Haijtink with the contract FI.2W-CT90-0068. I have been beneficiary of a grant from the Generalitat de Catalunya and other additional economical supports from the Universitat Politècnica de Catalunya.

Finally, I would like to thank my wife Núria Farell for her constant and unconditional help and support. Without any doubt she has also believed in this project. I also thank her parents for support at any moment. I would like to thank my parents that funded my graduation, with sacrifice. Without this graduation it would not have been possible to do this thesis.

AGRADECIMIENTOS

En primer lugar agradeceré a las personas que han guiado de un modo u otro este trabajo de investigación. Quiero expresar mi más sincero agradecimiento a Jesús Carrera por haberme atraido hacia este campo extraordinario que es la investigación. Sinceramente, creo que Jesús Carrera tiene unas cualidades excepcionales en muchos sentidos. Los resultados obtenidos son fruto de una supervisión muy adecuada. La existencia de dos codirectores de tesis doctoral ha sido motivada por el carácter que tomó la investigación hacia temas geomecánicos. Estoy muy agradecido a Antonio Gens por haber sabido también obtener buenos resultados en este trabajo. A Jesús Carrera y Antonio Gens ya los había considerado entre los mejores profesores de la carrera. También agradezco a Eduardo Alonso y Antonio Lloret por la dedicación que han prestado a mi trabajo. Ambos también son merecedores de un calificativo excelente. Todos estos profesores conocen muy bien el sentido de 'laisser-faire' que creo que a tan buenos resultados puede dar lugar y que, estoy convencido, a veces no resulta tan fácil de aplicar. También quiero agradecer a todas las personas del Departmento de Ingeniería del Terreno que en algún momento, y quizás sin darse cuenta, hayan podido poner su grano de arena. En particular, a Beatriz y a Miguel.

En segundo lugar agradeceré a los que han financiado económicamente esta investigación. Estoy muy agradecido con ENRESA que está realizando una inversión en investigación, a veces con resultados no inmediatos, para resolver el problema del almacenamiento de residuos radioactivos, sin duda un problema de nuestra sociedad. En particular quiero agradecer a Fernando Huertas que ha sido responsable del proyecto que motivó este trabajo. Hemos compartido la asistencia a algunas reuniones con expertos de otros paises. Él también tiene una parte en este trabajo. También agradezco la financiación del la Comisión Europea a través de B. Haijtink con el contrato número FI.2W-CT90-0068. Por otro lado he sido beneficiario de una beca de la Generalitat de Catalunya y de ayudas por parte de la Universitat Politècnica de Catalunya.

En tercer lugar quiero agradecer a mi mujer Núria Farell por su ayuda y apoyo constantes e incondicionales. Sin duda alguna ella también a creido en este proyecto y me ha alentado a hacerlo realidad. También a sus padres por su apoyo en todo momento. Estoy muy agradecido con mis padres que, con su sacrificio, sacaron adelante mis estudios hasta la graduación, incluso realizando lo imposible para financiarlos. Sin estos estudios no se habría podido hacer realidad esta tesis doctoral.

TABLE OF CONTENTS

Abstract i

Resumen ii

Acknowledgements iii

Agradecimientos iv

Table of contents v

List of figures viii

List of tables xiii

1. INTRODUCTION 1
   1.1 Motivation and objectives 1
   1.2 Organization and scope 2

2. REVIEW OF THE HYDROMECHANICAL BEHAVIOR OF SALINE MEDIA 5
   2.1 Introduction 5
   2.2 Basic properties and processes 7
   2.3 Mechanical behavior 13
   2.4 Hydraulic behaviour 22
   2.5 Concluding remarks 26
   2.6 References 26

3. NONISOTHERMAL MULTIPHASE FLOW OF BRINE AND GAS IN SALINE MEDIA 29
   3.1 Introduction 29
   3.2 Notation 32
   3.3 Macroscopic approach 33
   3.4 Problem formulation 34
   3.5 Mass balance equations 37
   3.6 Stress equilibrium equation 41
   3.7 Energy balance equation 41
   3.8 Constitutive theory 43
   3.9 Equilibrium restrictions 47
   3.10 Summary 48

3.11 Algebraic transformation of balance equations 49
3.12 References 51

4. MECHANICAL CONSTITUTIVE MODEL FOR CREEP DEFORMATION OF POROUS SALT AGGREGATES 55
4.1 Introduction 55
4.2 Mechanical behaviour of porous salt aggregates..... 56
4.3 Model predictions 72
4.4 Conclusions 76
4.5 References 78

5. COMPUTATIONAL APPROACH FOR COUPLED THERMO- HYDRO-MECHANICAL PROBLEMS IN SALINE MEDIA 79
5.1 Introduction 79
5.2 Numerical approach 79
5.3 Discrete form of the mechanical constitutive model 81
5.4 Mechanical problem including creep deformation 82
5.5 Mass and energy balance equations 85
5.6 Porosity variations 90
5.7 Conclusions 91
5.8 Balance equations 91
5.9 References 93

6. VERIFICATION OF THE PROGRAM CODE-BRIGHT 95
6.1 Heat flow, a mathematically linear problem 96
6.2 Gas flow, a nonlinear problem 96
6.3 Rock salt creep. COSA-project benchmark 98
6.4 Thermal convection. HYDROCOIN-project benchmark 100
6.5 Concluding remarks 106
6.6 References 106

7. POROSITY VARIATIONS IN SALINE MEDIA CAUSED BY TEMPERATURE GRADIENTS COUPLED TO MULTIPHASE FLOW AND DISSOLUTION/ PRECIPITATION 109
7.1 Introduction 109
7.2 Notation 111
7.3 Theoretical basis. Background 113
7.4 Dimensionless form of balance equations 114
7.5 Numerical approach used to develop CODE_BRIGHT 120
7.6 Porosity variation due to dissolution/precipitation 122
7.7 Conclusions 129
7.8 Equilibrium restrictions and constitutive equations 130
7.9 Balance equations 135
7.10 References 136

8. APPLICATION TO ANALYZE THE BEHAVIOUR OF A SEALING DAM 139
8.1 Introduction 139
8.2 Conditions of the analysis 139
8.3 Results of the analysis 143
8.4 Conclusions 147

9. APPLICATION TO PROBLEMS RELATED TO NONSALINE GEOENVIRONMENTS 157
9.1 Analysis of heat flow from buried pipelines 158
9.2 Two phase flow of water and oil in porous media 177
9.3 Preliminary analyses for a heating test in a clay barrier 180
9.4 References 181

10. CONCLUSIONS AND FUTURE WORK 183
10.1 Conclusions 183
10.2 Future research work 184

A. APPENDIX: PROPERTIES OF LIQUID AND GAS 187
A.1 Properties of liquid phase 187
A.2 Properties of gas phase 192
A.3 References 195

LIST OF FIGURES

2.1: Schematic representation of a repository in salt rock during operation, showing location of dams (above); and schematic section of test dam (below). Actual dams will have abutments at both ends. (After Engelmann et al., 1989). 6

2.2: Idealized inclusion with parallell and planar faces subject to temperature gradient (after Yagnik, 1983). 11

2.3: Deformation mechanism map for grain size d = 1mm, fluid pressures between 0.1 and 20 Mpa, σ is deviatoric stress, μ is elastic shear modulus, T is temperature and Tm is meelting temperature. (Adapted from Spiers et al., 1986) 14

2.4: Constant strain rate ($\dot{\varepsilon} = 2.1 \times 10^{-5} s^{-1}$) tests for diferent confining pressures for Cheshire rock salt (After Farmer and Gilbert, 1981). ... 17

2.5: Constant strain rate ($\dot{\varepsilon} = 2.1 \times 10^{-5} s^{-1}$) tests for diferent confining pressures for Asse rock salt (After Spiers et al., 1986). 17

2.6: Deviatoric stress versus strain rate (steady state case) including results from different authors. (After Munson and Dawson, 1981). 18

2.7: Deviatoric stress versus strain rate (steady state case) proposed by Dusseault, 1987. 18

2.8: Argon gas permeability measurements versus distance from opening wall (Asse's mine gallery $\sim$ 800 m depth). Open symbols are for 2.5 MPa confining pressure during test and closed are for 5.0 MPa). 23

2.9: Experimental results of permeability in deformed crushed salt. Asterisks are for dry compacted material, square symbols represent data obtained from samples with high initial porosity (38.8%), circular symbols correspond to low initial porosity (24.8%) and "diamonds" correspond to ultrafine NaCl powder. Closed symbols represents permeability vs. total porosity and open vs. connected porosity). (After Spiers et al., 1988). 25

3.1: Schematic representation of the porous medium composed by salt grains, brine and gas. 35

4.1: Stress/temperature deformation mechanism map for NaCl of 1 mm grain size. Adapted from Spiers (1986). 58

4.2a: Idealized geometry using polyhedrons (see 4.2b for variable definitions and derived expressions) 59

4.2b: Definition of variables and derived expressions corresponding to the idealized geometry (see 4.2a). Relative pore size and contact size are variables that only depend on void ratio. They tend to zero and one, respectively, as void ratio vanishes 60

4.3: a) Fluid assisted diffusional transfer mechanism. Dissolution of salt takes place in contacts and precipitation in pores as a consequence of differences in chemical potential. b) Assumed distribution of stresses in the grain for the dislocation creep mechanism. 63

4.4: Dependence of strain rate on degreee of saturation. Strain rate as a function of brine degree of saturation (S_l). Linear and square root relationships are included. Experimental data from Spiers et al (1988). 66

4.5: Void ratio functions. g_I^v, g_I^d, (corresponding to mechanism FADT) and g_{II}^v, g_{II}^d, (corresponding to mechanism DC). 67

4.6: Flow rule used for the nonlinear counterpart of the model (DC mechanism). 70

4.7: Strain rates under isotropic stress computed with the model as a function of several variables. Temperature is 20 °C and grain size is 500 μm. The contribution of DC and FADT mechanisms is shown separately in order to demonstrate that one of them may predominate over the other. 72

4.8: Comparison of the model (FADT mechanism) predictions with experimental results for isotropic deformation of saturated medium at 4.3 MPa, 21 °C and grain size 50-75 μm and 125-150 μm. Data adapted from Schutjens, (1991). 74

4.9: Comparison of the model (DC) predictions (for oedometric deformation) with experimental results of oedometric deformation at 16.5 MPa and 100 °C (after Stührenberg, 1990) and 8.0 MPa and 22 °C (after Spiers, 1988). 75

4.10: Comparison of oedometric test results with model (both mechanisms) predictions (for oedometric deformation). Creep strain rates as a function of void ratio for the different stress level periods. 76

4.11: Comparison of oedometric test results with model (both mechanisms) predictions (for oedometric deformation). Time evolution of void ratio, (*) creep deformation combined with linear elasticity and (**) creep deformation combined with non-linear elasticity 77

5.1: Representation of a cell in a finite element mesh. 87

6.1: Linear radial flow, analytical and numerical predictions 97

6.2: Non-linear radial flow, gas pulse test, field test results (Kloska et al. 1989) and numerical simulations with CODE_BRIGHT and NOCONF 97

6.3: Description of the first Benchmark of the COSA intercomparison project 99

6.4: Typical finite element mesh 100

6.5: Time evolution of displacement at inner boundary (nodes 1 and 2) and at the outer boundary (nodes 31 and 32). The difference between nodes 31 and 32 is caused by the non-symmetry of the grid. Continuous lines define the max. and min. values according to the COSA project 101

6.6: Time evolution of equivalent stress at selected points. The computed values tend to the analytical ones. Theoretical values are drawn for times greather than 10^{10} seconds 101

6.7: Equivalent stress variation with distance and for different times. Continuous lines define the max. and min. values according to the COSA project. (The differences for 10^6 seconds are probably caused by the kind of elements used, see text for discussion) 102

6.8: Finite element grid (249 nodes) used in the thermal convection problem. Axisymmetry is around the vertical (y) axis (left vertical boundary). The coordinate origin ($x = 0, y = 0$) is at the centre of the sphere. Sphere radius is R_o =250 m. Total simulated region is 1500-radius $\times$ 3000-height 103

6.9: Time evolution of temperature at selected points. Computed (symbols) and analytical (dashed lines) results 104

6.10: Time evolution of liquid pressure at selected points. Computed (symbols) and analytical (dashed lines) results 105

7.1: Hydrothermal coupled phenomena in saline media. Except for salt dissolution and precipitation, the processes are the same as those considered by Bear et al (1991) 110

7.2: Schematic representation of the idealized microstructure of the porous saline media 114

7.3: Porous salt sample subject to a temperature gradient. Mass transfer is not permitted accross the boundary, only heat in or out is possible according to the condition of prescribed temperature. The temperatures that have been imposed in the hot and cold walls are: $T_1 = 82^oC$ and $T_2 = 22^oC$ 123

7.4: Evolution of porosity, degree of saturation and liquid flux. Case 0 (see Table 7.IV). Curves are for several dimensionless times ($t_D = t/t_0$, $t_0 = x_0^2/D$, see text). Dimensionless distance is obtained as $x_D = x/x_0$ 126

7.5: Influence of intrinsic permeability. Evolution of porosity, degree of saturation and brine flux. Curves for the last time of the simulated period (dimensionless time $t_D = 594.05$). Case 0: $k_0 = 1.0 \times 10^{-12}m^2$; Case 1: $k_0 = 1.0 \times 10^{-13}m^2$; in both cases for ϕ_0=0.30 127

7.6: Influence of retention curve. Evolution of porosity, degree of saturation and brine flux. Curves for the last time of the simulated period (dimensionless time $t_D = 594.05$). Case 0: $P_0 = 0.001$ MPa; Case 2: $P_0 = 0.01$ MPa 128

8.1: Schematic representation of the problem to be modelled 140

8.2: Finite element mesh used for the analysis and initial stress distribution 144

8.3: Porosity distribution in the seal from analysis after 3241 and 4051 days 149

8.4: Degree of saturation from analysis after 3241 and 4051 days 151

8.5: Time evolution of porosity and volumetric brine content at four points within the seal 153

8.6: Time evolution of brine pressure and degree of saturation at four points within the seal 154

8.7: Time evolution of total and net mean stress at four points within the seal 155

9.1: Basic geometry of the problem 159

9.2: Dependence of water viscosity on temperature 161

9.3: Typical mesh for the study of heat output from buried pipelines 163

9.4: Distribution of temperatures from analysis for thermal conduction only, T_p=150°C 167

9.5: Distribution of temperatures from analysis for coupled conduction and convection, T_p=150°C 169

9.6: Water velocity field from analysis for coupled conduction and convection, T_p=150°C 171

9.7: Distribution of water density from analysis for coupled conduction and convection, T_p=150°C 173

9.8: Contours of the ratio between heat loss rate computed in coupled analysis (convection and conduction) and heat loss rate computed in uncoupled analysis (conduction only) 175

9.9: Water degree of saturation profile at 100000 days after injection started. Consistent approximation of relative permeability 179

9.10: Water degree of saturation profile at 100000 days after injection started. Alternative approximation of relative permeability 180

A.1: Variation of salt solubility with temperature 188

A.2: Variation of brine density with concentration for three values (25, 50, 75 °C) of temperature 188

A.3: Variation of liquid (pure water and brine) density with temperature. Solubility relationship has been used 190

A.4: Variation of brine viscosity on concentration for three different temperatures 191

A.5: Variation of liquid (pure water and brine) viscosity with temperature. Solubility relationship has been used 191

A.6: Surface tension of pure water and saturated brine 193

A.7: Variation of relative vapour pressure on concentration under planar surface 194

A.8: Variation of gas, air and vapour density on temperature 196

A.9: Dependence of gas viscosity on temperature 196

LIST OF TABLES

2.I: Most frequent evaporitic minerals 8

3.I: Equation and variable summary 36

7.I: Equation and variable summary 115

7.II: Examples of characteristic times for linear problems 118

7.III: Characteristic times (t_0) for transport processes 118

7.IV: Material parameters used in the computations 124

8.I: Material parameters and initial conditions used in the analysis 142

9.I: Intrinsic permeability of sand, k (m^2) 162

CHAPTER 1

INTRODUCTION

1.1 Motivation and objectives

This thesis was originally motivated by the need to model the long-term behaviour of a sealing system for the access galleries of high level radioactive waste repositories in rock salt. However, the basic nature of the investigations makes the results applicable well beyond their original motivation. The study of saline media, specially porous salt aggregates, is necessary to understand the behaviour of several man-made structures.

A sealing system has been proposed by the german research centres DBE (Deutsche Gesellschaft zum Bau und Betrieb von Endlagern für Abfallstoffe GmbH, German Institute for Construction and Operation of Waste Final Repositories) and GSF (Gessellschaft für Strahlen- und Umweltforschung, Institute for Radiation and Environmental Investigation) and assumed by ENRESA (Empresa Nacional de Residuos, Waste National Company) and ANDRA (Agence Nationale des Déchets RadioActifs, Radioactive Waste National Agency). It consists of several components. The one that is expected to ensure long-term sealing is made of crushed salt bricks, which should become nearly impervious once the surrounding rock salt converges and compresses them. Modelling this process involves understanding the mechanical behaviour of both bricks and rock, as well as the evolution of their hydraulic properties. Research on the mechanical behaviour of rock salt had been very intensive but it was unclear that a full understanding had been achieved. The hydraulic behaviour of these media was even less well characterized. Hence, it is not surprising that much remained to be done in coupling hydraulic and mechanical problems.

Because of the high solubility of evaporites in water, physico-chemical processes should be taken into account. The hygroscopic character of mineralogic constituents produces air moisture condensation on rock surface, affecting brine content. At the same time, fluid (brine) salinity influences suction at the meniscus with respect to low salinity water situations. Recrystallization, which is important for explaining some aspects of mechanical behaviour and will play an important role in evaluating the long-term evolution of bricks, is strongly affected by the

presence of brines. This is important both for modelling the system and for designing hydraulic tests. In order to couple the mechanical and hydraulic behaviours, it is necessary to study the influence of water content, suction, temperature, stress paths and strain rate paths. Viscous constitutive laws have commonly been proposed to model the mechanical behaviour of salt and its creep characteristics. Some of those have been developed for rock salt and they are based on dislocation theory of crystalline solids.

Dam construction represents an essential component of the multibarrier safety concept for a repository for radioactive waste in salt formations. Their basic role is to isolate backfilled and abandoned areas of the repository from operating mine openings during the operational phase and to provide a barrier against short-cicuiting during the post-operational phase. The proposed design of the dam consists of several parts. The long-term sealing system is expected to provide tightness in the post-operational phase and will be built with compacted bricks made of fine grained crushed salt. The hydraulic sealing system should become effective shortly after construction of the dam and consists of several sealing and protecting elements. Abutments at both ends are made of salt concrete (i.e., concrete made with crushed salt as granular material and brine as mixing water) and aim at providing mechanical stability.

The long-term sealing system is based on the concept that, due to mine convergence, the system will be compressed. This will lead to compaction which will result in increased mechanical resistance and reduced permeability. Presumably, the salt brick wall should evolve towards a material with properties hardly distinguishable from those of natural rocksalt. A detailed analysis of such evolution cannot be done without a thorough understanding of the processes involved (heat flow, water and vapour flow, salt diffusion, mechanical deformation, dissolution/ precipitation, etc).

In this context, a CEC-funded project was set up by DBE, GSF, ANDRA and ENRESA in 1991. The objectives of the project were:

(1) to provide proof of the tightness of the long-term seal by means of experimental investigations and,

(2) prognosticate its behaviour over long time periods via model calculations.

This thesis is aimed at providing the framework for achieving such objectives.

1.2 Organization and scope

The organization of this thesis is related to several papers that have been

prepared for submission to international journals. For this reason, the chapters are self contained. In this regard, the introduction to each chapter incorporate a brief description of the general problem that is investigated.

A review of the hydromechanical behaviour of saline media is presented in Chapter 2. This review was written before any investigation in salts had started. Probably, if we had to do another review today, it would be different to what was done at that moment. However, today, we would miss the innocence of a researcher that does not know about a topic and the review would have become less objective. Since we think that this review was very motivating, we have kept on it in its original form, although it may not be completely up to date. Yet, we still think that the important points are outlined.

We propose a general formulation for non-isothermal multiphase flow of brine and gas through saline media in Chapter 3. Its development mainly consists of obtaining balance equations and constitutive relationships. The balance equations include mass balance (three species), equilibrium of stresses and energy balance (total internal energy). Salt, water and air mass balance equations are established. The balance of salt allows the derivation of the equation for porosity evolution due to solid skeleton deformation, dissolution/precipitation of salt and migration of brine inclusions. Water and air mass balance equations are also obtained. Two equations are required for water: total water in the medium and water present in solid phase brine inclusions. The mechanical problem is formulated by means of the equation of stress equilibrium. Finally, the balance of internal energy is established assuming thermal equilibrium between phases. Some general aspects of the constitutive theory are also presented.

A new constitutive model for mechanical behaviour of porous salt aggregates is presented in Chapter 4. The model concentrates on creep deformation because saline media behave in a ductile way. An idealized geometry is used as a common framework to obtain macroscopic laws of strain based on two mechanisms: fluid assisted diffusional transfer creep and dislocation creep. The model can predict strain rates for volumetric and deviatoric creep deformation. The predictions are compared with results from laboratory tests under isotropic and oedometric conditions. Macroscopic laws are written under a nonlinear viscoelastic approach. This form is necessary in order to combine the constitutive model with the stress equilibrium equations.

The numerical approach for simulating thermo-hydro-mechanical problems in porous media, particularly, saline media is presented in Chapter 5. The equations of the mechanical constitutive model are transformed to its discretized form and then introduced in the weighted residual form of the stress equilibrium equation. Details of the numerical implementation of the mass and energy balance equations

are included. The methodology for implementing different types of terms is presented.

The verification of the program CODE_BRIGHT is presented in Chapter 6. Exercises for relatively simple problems are presented. Verification of such a complex approach is difficult because it is restricted to the cases for which analytical solutions are available. We are aware of the need of further verification. In this context, i should be mentioned that we are involved in an european exercise which is intended for validation of codes that simulate gas migration and two phase flow.

We present a theoretic-numerical investigation of porosity variations in unsaturated saline media induced by temperature gradients in Chapter 7. It is known that temperature variations cause humidity variations which lead to liquid flow towards and vapour flow away from the hot source. When this phenomenon occurs in saline media, the liquid is salt saturated brine, so that evaporation causes salt precipitation and the ensuing porosity reduction near the hot side. This process may be important in the case of heat generating waste because it suggests that self sealing may take place. An experimental investigation is currently in progress.

The study of a sealing dam, which in fact was the original motivation of this work, is presented in Chapter 8. A very interesting coupled phenomenon is simulated in this application example. Brine flow, initially from the host rock towards the seal is suddently reversed as saturation of pores takes place. Degree of saturation increases mainly induced by volumetric creep deformation, that is, by porosity reduction.

Finally, Chapter 9 is devoted to the application of the model to problems related to non saline environments. First, the study of the thermo/hydraulic behaviour of a soil in which a heat generating pipeline is buried is presented. Natural convection occurs for relatively high permeability and the coupled analysis allows us to evaluate the contribution of conduction and convection to heat losses. Second, an example of two phase flow in a one-dimensional medium is used to show different numerical strategies which may lead to different results in this kind of problems. Sometimes, the most consistent form is not the one that produces best results.

General conclusions and future work are outlined in Chapter 10. Each chapter contains a section with its specific conclusions, the corresponding reference list, and, in some cases, appendices.

CHAPTER 2

REVIEW OF THE HYDROMECHANICAL BEHAVIOR OF SALINE MEDIA

2.1 Introduction

The concept of a multibarrier system is based on the idea that several isolating levels should provide safety independently. In other words, the probability of damage is reduced because when one element fails the other keep guarantying the isolation. Perhaps the main component of the multibarrier system is the host rock. However, in terms of design possibilities, the engineered barrier is important because it can be constructed with very well defined properties.

The engineered multibarrier system is constituted by the following components: the borehole plug, the backfilled disposal rooms and drifts, the dams and the shaft sealing (see Figure 2.1). The dam is made of compacted porous bricks. In the other components crushed salt is used with different degrees of compaction. For instance, the borehole plugs are backfilled with a more compacted material than the disposal rooms. The dam construction represents an important component of this multibarrier safety concept. Also in figure 2.1 the schematic representation of a field test at 1:1 scale is shown. This test represents only a half of the complete sealing structure which is foreseen with abutments at both ends. Further details on the dam concept are described by Engelmann et al. (1989).

The long-term sealing system is compressed by mine convergence. The required confinement is provided by the abutments. In this way deformation will take place under nearly isotropic conditions. Reduction of porosity causes increase in the mechanical resistance and reduction of permeability. It is expected that these long-term seals transform into a very compacted medium with similar properties as the host rock. It is then clear that there will be an interaction between the sealing structures and the host rock, both, mechanical and hydraulical.

This chapter was aimed at reviewing existing literature on the mechanical and hydraulic behaviour of salts, as a basis for guiding subsequent modelling efforts. In turn, these should help in designing and interpreting laboratory and field experiments. This chapter is organized as follows. Section 2.2 describes basic

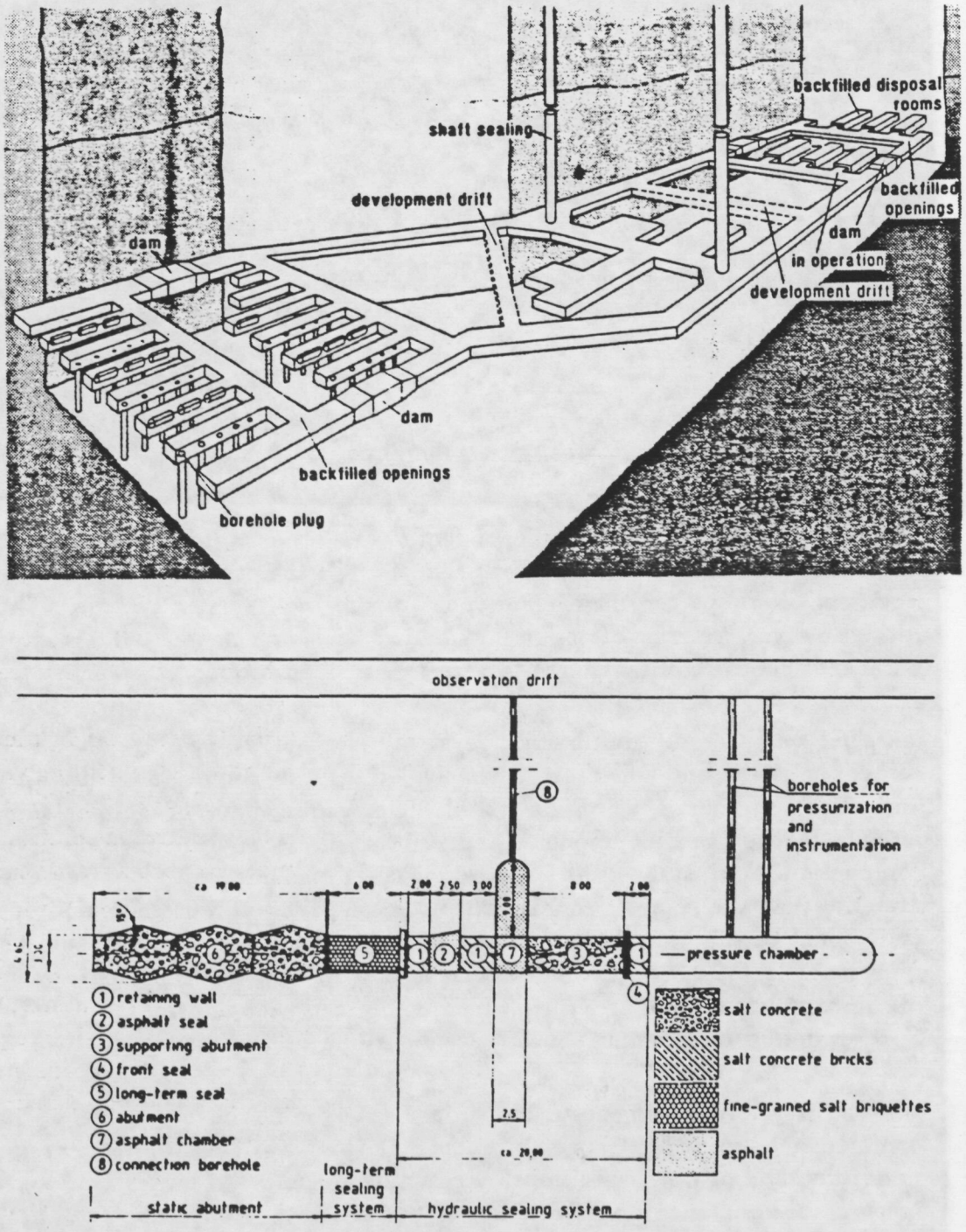

Figure 2.1: Schematic representation of a repository in salt rock during operation, showing location of dams (above); and schematic section of test dam (below). Actual dams will have abutments at both ends. (After Engelmann et al., 1989).

properties of salts. Mechanical and hydraulic behaviors are the subject of Sections 2.3 and 2.4, respectively.

Significant research efforts have been devoted to the study of rocksalts. Yet, at the begining of this thesis, we felt that a comprehensive picture of their hydro-mechanical behavior was still missing. The situation was worse for porous salt aggregates, which have become the focus of research only very recently. Therefore, what follows should be understood as a synthesis of current ideas on salts syntetized at the begining of this thesis. The reader should not expect definite statements about the behavior of salt. In this chapter, the notation is not uniform with the other parts of the thesis because here it has been kept with the same symbols as in the different literature references.

2.2 Basic properties and processes

2.2.1 Microstructure of rock salts

Rocksalts are composed of several evaporitic minerals. The most frequent ones are listed in Table 2.I. Most natural rocksalts, both from domes and bedded deposits, are basically composed of halite (NaCl), which crystallizes in the cubic system forming a regular cubic net that alternates Na and Cl atoms in the vertices. The net is ionic, which leads to high melting temperature (T_m= 800.8 °C) and low solubitity in non-polar solvants. Crystallization from oversaturated solutions may result in large crystals (several cm). However, deformational processes (formation of anticlines, diapires, domes, etc) may lead to granular microstructures. Grain sizes of samples from widely different origins range mostly between 1 and 10 mm (Horseman, 1981; Carter and Hansen, 1983; Spiers et al , 1986). Deffects in the net (point deffects and dislocations) tend to concentrate at grain boundaries, where the crystalline structure is highly disordered. Triple joint at approximately 120° are frequent. A subgranular structure, with sizes between 50 and 400 μm can often be seen in the grain interiors (Carter and Hansen, 1983). These internal boundaries show a lesser concentration of crystalline deffects.

Most abundant impurities (frequently above 1%) include anhydrite ($Ca\ SO_4$) and polyhalite ($K_2\ SO_4 \cdot 2CaSO_4 \cdot Mg\ SO_4 \cdot 2H_2O$), which crystallize in the rombic and triclinic systems, respectively. These crystals or grains can be observed within the micrograin halite structure. Clay and silt impurities are also frequent in bedded rock formations. In such cases they tend to be stratified with the halite (Roedder, 1984).

In defining the porosity structure of rock salts, two types of voids can be distinguished: interconnected and isolated. The first group refers to grain

boundary microfissures, whose thickness may range between 0.01 and 5 μm and increases as the confining pressure is reduced. The non connected void fraction consists of inclusions. The small ones (up to 1 mm) are regular and shaped as negative crystals. The larger ones show irregular or elongated shapes. Superficial voids located at grain boundaries may be either connected or isolated. Inclusions tend to concentrate on grain (not subgrain) edges. Inclusions in grain interiors are usually of the regular type, having sometimes migrated from the boundaries by deformational processes (Spiers et al., 1986).

Table 2.I: Most frequent evaporitic minerals

Mineral	Formula	Density	Solubility*	Crystall.
Halite	NaCl	2.1 a 2.2	0.36	Cubic
Sylvite	KCl	2.0	0.34	Cubic
Carnallite	K Cl· Mg Cl_2· $6H_2O$	1.6	0.56 ($MgCl_2$)	Rombic
Anhydrite	$CaSO_4$	2.9 a 3.0	$2{\cdot}10^{-3}$	Rombic
Kieserite	$MgSO_4{\cdot}H_2O$	2.6	0.35	
Polyhalite	$K_2SO_4{\cdot}$ $2CaSO_4{\cdot}$ $\cdot MgSO_4 \cdot 2H_2O$	2.7 a 2.8	0.11 (K_2SO_4)	Triclinic

* gr solute per gr H_2O at 18°C

According to Roedder (1984) inclusions may contain gas (at about 0.1 MPa), brine or both. He suggest that the gas may have formed as a result of the pressure release during sampling because gas pressure is close to atmosferic.

About 80 to 90% of Asse Mine inclusions contain brine and gas, the rest of brine being fluid film. The resulting gravimetric water content ranges between 0.05 and 0.1% although part of it may be attributed to polyhalite hydration (Spiers et al, 1986). These authors point out that water content under natural conditions may be slightly larger because some voids may have lost part of its water as a result of sampling decompression.

2.2.2 Crushed salt

Crushed salts have recently become the focus of several studies because of their importance for backfilling and closing cavities open in rock salt formations. Both

Kappei et al (1984) and Liedtke (1984) have studied the mechanical and hydraulic behavior of two diferent crushed salts: the first follows a Fuller granulometry, with $d_{max} = 64$ mm, $d_{60} = 25$ mm and $d_{10} = 0.8$ mm, while the second follows a PHM (grain distribution obtained from the excavation engine) granulometry with $d_{60} = 3$ mm and $d_{10} = 0.3$ mm. On the other hand, Spiers et al (1988) work with less graded but finer materials (mean sizes ranging from 87 to 410 μm), although they also study mixtures of several size fractions. Yet, for backfilling materials, they suggest using a coarser fraction (15 to 20% in the 10 to 50 mm range). Salt bricks to be used in the sealing systems (DBE-GSF-ANDRA-ENRESA) are within the granulometric range studied by Spiers et al (1988) although the size distribution is less uniform ($d_{50} \simeq 0.16$ mm and $d_{85} \simeq 0.25$ mm, according to Walter, 1991).

According to Spiers et al. (1988), microstructure of these artificial fine grained materials shows different aspect according to the degree of compaction:

(1) Uncompacted material, composed of regular cubic crystals.

(2) Slightly compacted material, with dented and truncated grain boundaries depending on the presence of brine and compaction.

(3) Very compacted material, in which the grains are no longer cubic and tend to polygonal shapes.

(4) Granular (recrystallized) structure with texture and grain sizes very similar to those of rock salt.

Experiments on crushed salts always require a certain compaction. Published results are based on materials much less compacted (initial porosity in the 0.3 to 0.4 range) than those of the salt bricks intended for the dam (initial porosity around 0.1). However, backfilling galleries is forseen with these large porosity materials.

2.2.3 Hygroscopy

This phenomenon is known since ancient times and consists in the condensation of atmosferic water vapour on the surface of evaporite minerals. Water molecules are fixed to the mineral surface by electromagnetic Van der Waals forces, tending to form a thin water film so that partial pressure of water vapor in the air equals the evaporation pressure in the liquid phase, which is a function of the concentration and nature of solute. Since salts are very easily dissolved, the water film becomes virtually saturated very quickly. This leads to two consequences. First, precipitation and crystallization do occur when evaporation takes place. Second, the vapor pressure at which condensation and evaporation equilibrate is basically a function of the solute. The corresponding relative humidity is called

"critical humidity". For NaCl, this humidity is equal to 76.4% at 0°C and 74.2% at 100°C. Other salt minerals show much greater hygroscopic effects, with lower critical humidities (i.e., around 30% for carnallite).

Obviously, the medium still contains water, mostly retained by capillarity, at lower air humidities. The equilibrium vapor pressure under suction can be derived from the psycrometric law (Edlefson and Anderson, 1943):

$$P_v(\psi,T) = P_{vo}(T,\omega)h_r = P_{vo}(T,\omega)\exp(-\frac{\psi \cdot V_m}{RT}) \tag{2.1}$$

where P_v is vapor pressure (FL^{-2}) in equilibrium with brine at absolute temperature T (K) and under suction ψ (FL^{-2}), P_{vo} is the vapor pressure in equilibrium with planar surface; V_m is the molar volume of brine (M^3) and R is the gas universal constant (8.31 J/mol/°K). This relationship was originally stablished for pure water. However, since it refers to matric suction there is no reason for not using it with brine. For this reason, it is assumed that P_{vo} is a function of temperature and concentration, and V_m is the molar volume of brine.

2.2.4 Movement of inclusions

It has been shown experimentally that inclusions move in response to temperature gradients (Roedder, 1984). Due to irregularities in the crystal structure (dislocations, impurities, grain boundaries, etc), the movements of inclusions is somewhat erratic. In fact, when inclusions reach grain boundaries, they become part of the connected porosity. The model proposed by Yagnik (1983) to describe the movement of essentially planar inclusions can be expressed by (see Figure 2.2)

$$\boldsymbol{v} = \frac{\boldsymbol{j}_s}{\rho_s} \tag{2.2}$$

where $\boldsymbol{v}$ is the inclusion velocity and $\boldsymbol{j}_s$ is mass flux salt, given by:

$$\boldsymbol{j}_s = -D_1\nabla c - D_1 C^{sat}\sigma\nabla T \tag{2.3}$$

which can be written as:

$$\boldsymbol{j}_s = -D_1 C^{sat}[(\frac{1}{C^{sat}}\frac{dC^{sat}}{dT} + \sigma)\nabla T + \frac{\xi_h + \xi_c}{L}\boldsymbol{n}] \tag{2.4}$$

where ρ_s is solid density (ML^{-3}), C^{sat} and D_1 are solubility and coefficient of molecular diffusion of NaCl in water, respectively, σ is Soret coefficient, L is the

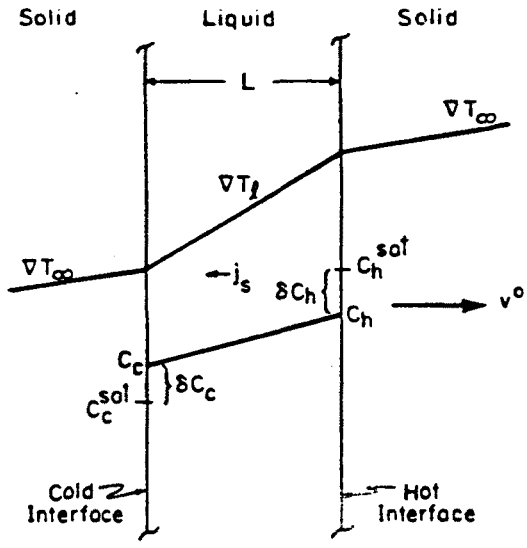

Figure 2.2: Idealized inclusion with parallell and planar faces subject to temperature gradient (after Yagnik, 1983).

size of the inclusion, n is its orientation and ξ_h and ξ_c are relative subsaturation and oversaturation in the hot and cold faces of the inclusion respectively.

In this model it is implicity assumed that molecular diffusion is the factor controlling the inclusion velocity. That is, other processes, such as precipitation or dissolution, are assumed to be much faster so that their effect on velocity can be neglected. Under reasonable temperature gradients, inclusion velocities may range between 0.1 and 10 cm/year, experimental values wich are consistent with the above models.

In large voids (above 1 cm), natural convection cells may develop, favoring the displacement of inclusions in response to temperature gradients.

Though never mentioned in the literature, it is postulated here that inclusions may move in response to stress gradients, a phenomenon that may be important near underground openings. As discussed later, chemical potential changes in response to stress variations, favoring dissolution at the most compressed zones and precipitation at the least compresed. This mechanism could be tested by bending a crystal with a fluid inclusion, which should move towards the compressed side.

2.2.5 Movement of NaCl

This section is devoted to mass transfer at the molecular level, favored by the presence of water. Strain effects and their mechanisms will be discussed in coming sections.

The first mechanism is transfer by solid state diffusion of the ionic species that form the crystalline structure of salt. This mechanism can be described of ions (or voids) across the grains (Nabarro-Herring effect) or its boundaries (Coble effect), from the contact zones towards the pore walls. Solid state diffusion takes place only at high temperatures, well above 250°C (Munson and Dawson, 1981).

Mass transfer at lower temperatures is mainly caused by diffusion through the fluid within microfissures at grain contacts. Spiers et al. (1988) distinguish two types of mechanisms: fluid assisted diffusion transfer (FADT) and pressure induced solution transfer (PIST): FADT is caused by the gradient in free energy due to stress variations between grain contacts and pores. That is, chemical potential near a high stress zone should be larger than at the pores. This favors dissolution near the contacts and transfer by molecular diffusion towards the pores, where the salt precipitates. Sprunt and Nur (1977) describe an experiment that demonstrates this mechanism. The experiment consists of applying a simple compression load to a parallepipedic crystal in which a circular hole has been perforated perpendicularly to the compression. The sample is kept inmersed in brine. As a result of loading (say in the 0^o- 180^o with respect to the circle), points at 90^o and 270^o are under a compression state, so that salt tends to be dissolved. On the other hand, points at 0^o and 180^o are under a tensile stress, which favors precipitation and recrystallization. As a result, the circle becomes an ellypse. This mechanism (FADT) is relevant for low stress states (efective stress between 5 and 10 MP_a) and temperatures below 200°C.

PIST, on the other hand, takes place under larger stresses by release of material from zones with plastic strains at the edge of grain contacts and subsequent diffusion throught the liquid phase. The driving force in this case is plastic strain (concentration of deffects in the crystalline net). If adjacent grains show differences in plastic strain energy, then mass transfer through the fluid from the most deformed leads to a displacement of the boundary. In turn, this results in recrystallization in a material microstructure. Tada and Siever (1985) describe and experiment illustrating PIST. It basically consists of cleaving a small salt ridge between two grooves with a sharp knife quartz. Again, the sample is kept inmersed in brine. It is possible to observe dissolution caused by this mechanism.

2.3 Mechanical behavior

This section is devoted to the analysis of phenomena associated salt strain behaviour. Phenomena related to the presence of brine have already been described in Section 2.2.

2.3.1 Strain mechanisms in rocksalt deformation

Crystalline rocks such as salts consist of grains with varying sizes and zones with varying degrees of perfection in the crystalline structure (orientation changes, dislocations, voids or impurities). These imperfections, specially dislocations, may play an important role when studing the deformational behaviour of salts. Dislocations can be viewed as discontinuity in the crystal structure ideally caused by a shear stress that tends to displace ions in one face of the dislocation with respect to the other. After slipping, they become bonded again so that the only visual remnant is the dislocation "line" at the end of the slippage surface, where unbonded ions exist. Dislocation lines may be contained on a single or several planes, in which case they form a curved line. The change from one plane to another is referred to as dislocation climb. As discussed earlier, crystal imperfections concentrate at grain boundaries, which act as sink and sources of dislocations and point deffects (voids and impurities) during deformation processes.

The type of mechanism controlling strain behavior depends on temperature and stress tensor. Spiers et al. (1986) propose the map shown in Figure 2.3 to identify the main creeping mechanism as a function of deviatorial stress and temperature. Based on this map, we describe the various mechanisms on what follows.

Fluid assisted diffusion transfer creep (FADT) is the deformation mechanism most directly linked to masss transfer mechanisms discussed in section 2.2, although it also includes grain boundary sliding. On the basis of idealized geometries, and assuming that dissolution and precipitation rates are much faster than diffusion in the liquid phase, Spiers et al (1986, 1988, 1990) have established the following model for the strain rate of a policrystal salt aggregate:

$$\dot{\beta} = AV_m \frac{Z^*}{T} \frac{\sigma_e}{d^3 e_v^a} \tag{2.5}$$

for the compaction of granular materials, and

$$\dot{\epsilon} = 5\, V_m \frac{Z^*}{T} \frac{\sigma}{d^3} \tag{2.6}$$

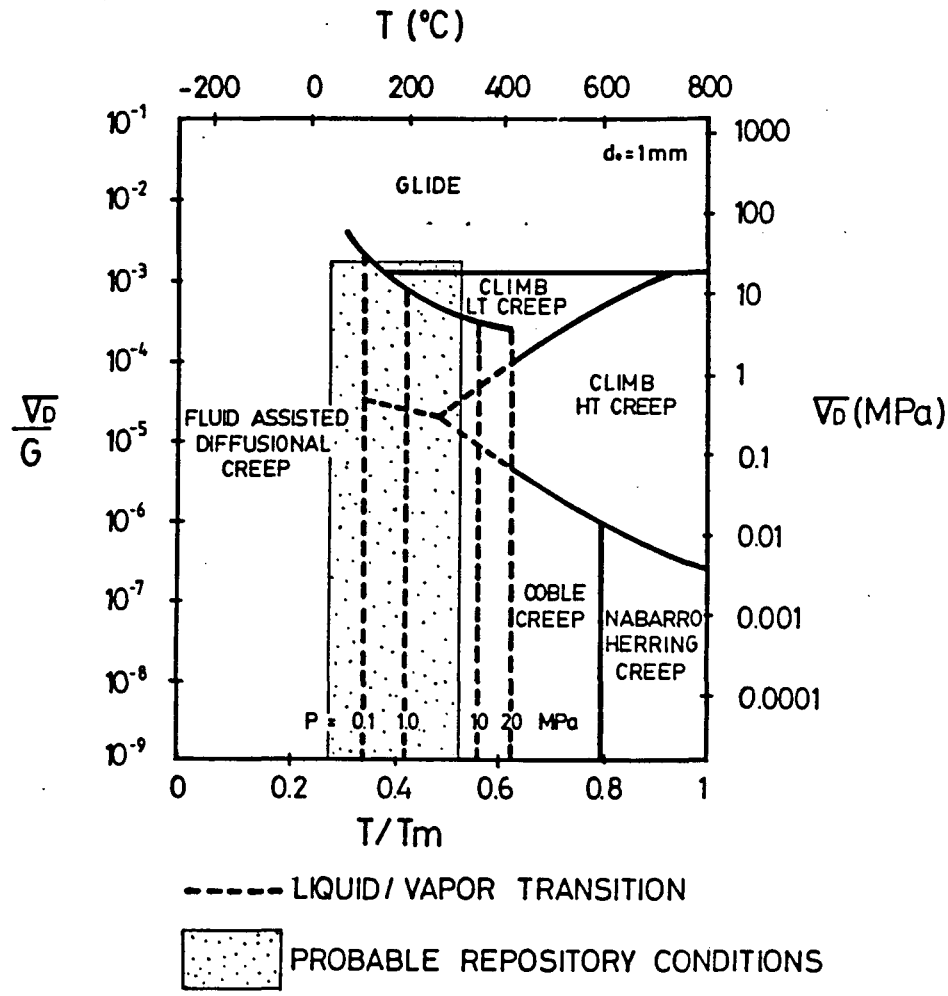

Figure 2.3: Deformation mechanism map for grain size d = 1mm, fluid pressures between 0.1 and 20 Mpa, σ is deviatoric stress, μ is elastic shear modulus, T is temperature and Tm is meelting temperature. (Adapted from Spiers et al., 1986)

for the axisymmetric case in dense aggregates (e.g. rock). In these equations, $\dot{\beta}$ is volumetric strain rate $[T^{-1}]$; e_v is the volumetric strain; A is a constant that depends on grain shape, packing, etc.; V_m is the molar volume of the solid phase ($2.693 \times 10^{-5}\ m^3/mol$); Z^* equals DCS, where D, C and S are, respectively the diffusion coefficient, average concentration and average thickness in the fluid

at grain boundaries; σ_e is effective stress (stress minus brine pressure; assumed hydrostatic or isotropic); T is absolute temperature; a is an exponent that depends on grain shape and packing ($2 \leq a \leq 4$); $\dot{\epsilon}$ is the strain rate for the axisymmetric case; and σ is the deviatoric stress for such case.

Values of D and C are temperature dependent. Based on theory of solutions, Spiers et al. (1990) presume that they exhibit an Arrhenius dependence so that Z^* can be written as:

$$Z^* = D_o C_o S \exp(-\frac{Q}{RT}) \tag{2.7}$$

where Q is activation energy for grain boundary diffusion and D_0 and C_0 are the values of D and C as $1/T \rightarrow 0$.

The dependence of $\dot{\beta}$ and $\dot{\epsilon}$ with σ, d and e_v (Eqs. 2.5 and 2.6) has first been derived theoretically, under the assumption of spherical grains, and then adjusted to experimental results. Theoretically based strain rates are much faster than those derived empirically.

Literature models for explaining solid state diffusion creep (Coble and Nabarro-Herring creep) are similar to Equation 2.6. We will not discuss them here because these effects only become relevant for large temperatures. The remaining mechanisms of Figure 2.3 can be studied in the framework of dislocation theory. Dislocation glide (displacement) is the dominant factor for large stress, while dislocation climb becomes relevant at lesser stresses. A large number of mathematical models are available for expressing strain rates for these mechanisms (e.g., Langer, 1981; Carter, 1983; Munson and Dawson, 1981; and others). However, they appear to converge towards expressions of the form:

$$\dot{\epsilon} = A_1 \exp(-\frac{Q_1}{RT})(\frac{\sigma}{\mu})^{n_1} + A_2 \exp(-\frac{Q_2}{RT})(\frac{\sigma}{\mu})^{n_2} +$$

$$+ |H| [B_1 \exp(-\frac{Q_1}{RT}) + B_2 \exp(-\frac{Q_2}{RT})] \mathrm{sh}(\frac{q(\sigma - \sigma_0)}{\mu}) \tag{2.8}$$

where Q_i are activation energies; H is Heaviside's scalar function of $(\sigma - \sigma_0)$ and A_i, B_i, q and n_i are empirical constants. This formulation, that expresses steady-state creep, consists of three adding mechanisms: (1) dislocation climb; (2) an undefined low stress and temperature creep mechanism (possibly FADT) and (3), at high stresses, dislocation slip.

Recrystallization deserves further comments. Experimental evidence is shown by several researchers (Urai, 1985). Strain induced recrystallization refers to changes in the crystal structure caused by external supply of strain or thermal

energy. While these mechanisms may be very important at high temperatures, recrystallization at low temperature is usually stress induced, in which case no external energy supply is required. As discussed earlier, stress induced recrystallization is fluid assisted.

2.3.2 Elastic behavior of rocksalt

Elastic strains take place in response to small and fast ($\dot{\varepsilon} < 10^{-4} s^{-1}$) loads. Beyond this, creep will occur if the load is maintained. Elastic behaviour is difficult to isolate because, even for small stresses, one can observe permanent strains, which increase with the applied load and time. Yet, despite the marked ductile nature of rocksalts, their early time mechanical behaviour is not significantly different from that of other geological materials for which elastic properties have been measured. For instance, Horseman et al. (1981) have obtained the following elastic parameters for rocksalt from Atwick (Hornsea, UK):

Tangent modulus (3^{rd} load cycle)	: $E = 2.7 \times 10^4$ MPa
Poisson modulus	: $\nu = 0.23 - 0.32$
Volumetric modulus	: $K = 2.5 \times 10^4$ MPa

2.3.3 Creep and viscoelasticity of rock salt

Instantaneous loads in underground cavities are mainly restricted to the excavation stage. Convergence measurements in existing galleries suggest strain rates of about $10^{-9} s^{-1}$. This value seems to indicate that viscous strains are dominant. A significant effort has been devoted to characterizing the viscous behaviour of rocksalts. Laboratory experiments on small samples for this purpose can be classified in creep (constant stress), relaxation (constant strain), constant strain rate and constant stress rate (the first and third being the most frequent). Variables controlling the mechanical behaviour of salts and, therefore, experimental results include the following: temperature, water content and/or ambient humidity, strain mechanisms and nature of sample (mineralogy, grain size, porosity, ...).

Figures 2.4 and 2.5 illustrate the response to axisymmetric compression under constant strain rate ($\dot{\varepsilon}$ of the order of $10^{-5} s^{-1}$) before reaching steady state creep. Comparing these figures it is difficult to establish the frontiere between dilating and non dilating behaviors. Notice, however, that strain rates for these experiments are very high. Under more realistic rates much smaller minimun confinements are required for preventing dilation.

A number of mechanisms favor the development of a steady-state creep, so

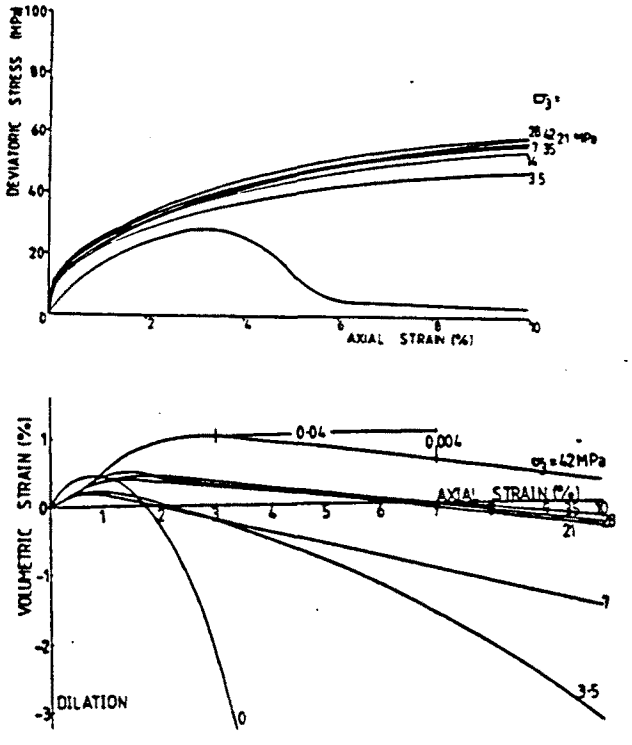

Figure 2.4: Constant strain rate ($\dot{\varepsilon} = 2.1 \times 10^{-5} s^{-1}$) tests for diferent confining pressures for Cheshire rock salt (After Farmer and Gilbert, 1981).

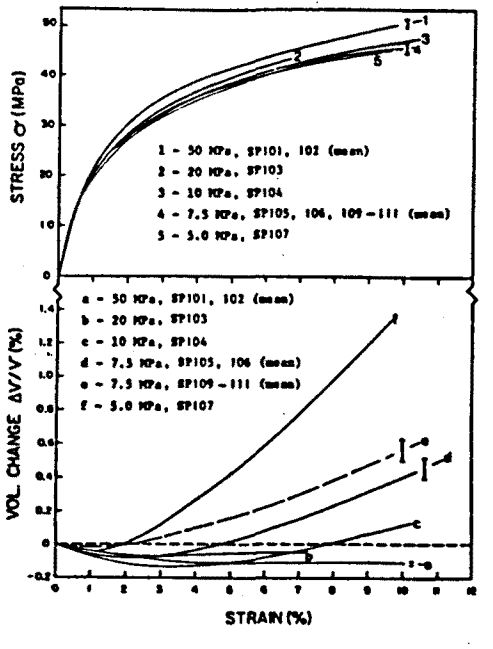

Figure 2.5: Constant strain rate ($\dot{\varepsilon} = 2.1 \times 10^{-5} s^{-1}$) tests for diferent confining pressures for Asse rock salt (After Spiers et al., 1986).

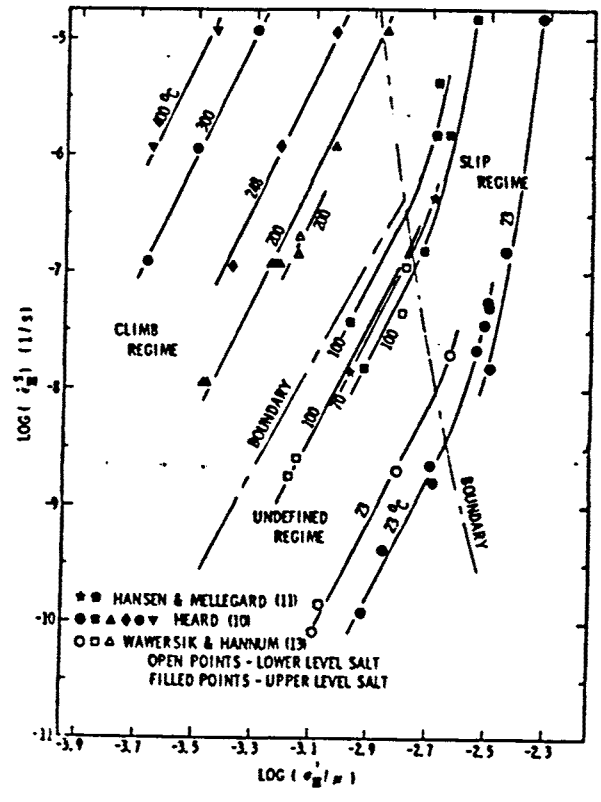

Figure 2.6: Deviatoric stress versus strain rate (steady state case) including results from different authors. (After Munson and Dawson, 1981).

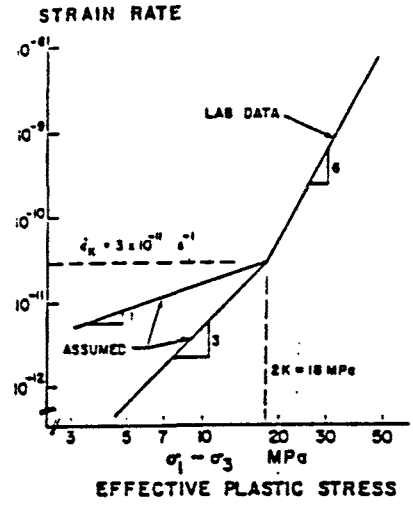

Figure 2.7: Deviatoric stress versus strain rate (steady state case) proposed by Dusseault, 1987.

that a biunivocal relationship between deviatoric stress (σ) and strain rate ($\dot{\varepsilon}$) could be stablished. The relationship between σ and $\dot{\varepsilon}$ is non-linear and depends on the total stress state. Figures 2.6 and 2.7 illustrate the relationship for two cases. Notice that different zones of the $\sigma - \dot{\varepsilon}$ map can be associated to different dominant strain mechanisms. Also, under low stresses, the $\sigma - \dot{\varepsilon}$ relationship can be considered linear, which would support models based on fluid assisted diffusion transfer, such as Equations 2.5 and 2.6.

As a viscoelastic non-linear material, the constitutive model for saltrocks can be written as:

$$\dot{\varepsilon}_{ij} = \dot{\varepsilon}^{e}_{ij} + \frac{3}{2}\frac{\dot{\varepsilon}}{\sqrt{3J_2}}s_{ij} \tag{2.9}$$

where $\dot{\varepsilon}^{e}_{ij}$ is the elastic strain tensor, s_{ij} is the deviatoric stress tensor, J_2 is the second invariant of s_{ij} ($J_2 = \frac{1}{2}s_{ij}s_{ij}$, summation implied); $\dot{\varepsilon}$ is a function of T, J_2 and crystalline structure that expresses the viscous behavior under deviatoric stress (usually used (2.8)). One of the important limitations of (2.9) is the implicit assumption about lack of volumetric strains. Therefore, both dilation and compaction mechanisms are ignored.

Other mechanical behavior aspect that has received significant attention is the transient evolution, prior to a steady creep, caused by variations in loads, temperature, etc. Important efforts have also been devoted to the rock salt memory of the stress history. Yet, work on transient behavior has been critized by Berest (1989) on the basis that laboratory stress paths bear little relationship with natural ones. Furthermore, laboratory tests are performed for very short durations compared with natural creep times. Hence, for example, tests in which significant behavior variations are observed in response to order of magnitude changes in strain rates may be irrelevant for understanding the behavior of salts under natural conditions. Similar criticisms are made with regard to memory effects.

2.3.4 Creep of granular aggregates

Volumetric strain, which is often neglected when studying rocksalts, becomes an important parameter for granular aggregates. The complexity of the mechanical behavior of salt backfillings is illustrated by the early work of Liedtke (1984) and Kappei (1984), who present some interesting results. Kappei worked with two different granulometries on Asse mine salt (recall Section 2.2). He performed oedometric tests on normally consolidated aggregates with different initial densities and obtained consolidation coefficients, C_c, in the range from 0.1 to 0.4 ($e - e_o = -C_c log_{10}(\sigma'/\sigma'_o)$). Liedtke (1984) performed similar experiments, but he also analized unloading and deviatoric and creep behaviors. From his results, C_c can

be estimated around 0.12 for dry conditions and 0.30 for saturated conditions. The swelling coefficient, C_s, may reach values around 0.01. Regarding delayed effects, Liedtke analized the behavior under constant stress, reaching empirical expressions that cannot be extrapolated. Recently, Spiers et al (1988, 1990) have proposed an empirically supported model for the isotropic deformational behavior of salts. As discussed before, their model is based on strain mechanisms controlled by masss transfer through the fluid. The basic assumption is that excess in free energy at grain contacts above pores can be expressed as:

$$\Delta\mu = (\sigma_n - P_f)\Omega \tag{2.10}$$

where μ is molecular free energy; σ_n is normal stress at the contact, P_f is fluid pressure and Ω is the solid molecular volume. This excess energy is dissipated in salt dissolution and precipitation and molecular diffusion in the liquid phase. The slowest of these three processes, usually assumed to be molecular diffusion, controls strain rate. Regarding the nature of grain contacts, also an important factor, two hypothesis can be made: first, a continuous fluid film exists between the grains and, second, solid "islands" connect the grains. Assuming the molecular diffusion is the controlling process, one obtains Equation 2.5. On the other hand, if strain rate is controlled by dissolution or precipitation, a similar equation is obtained, but with a unit exponent for grain size.

Spiers and coworkers also performed consolidation (oedometric and isotropic) experiments under constant effective stress (up to 8 MPa) for different grain sizes (between 100 μm and 400 μm) and temperature (from 22 to 90^{o}C) and for dry and with varying water content samples. Regarding the last parameter, it is interesting to notice that variations in water content are only relevant up to approximately 10% in weight water contents. Fitting experimental results leads to:

$$\dot{\beta}_{sat} = A \exp(-\frac{\Delta H}{RT}) \frac{\sigma_e^{1.325}(\phi_o - e_v)^{5.042}}{e_v^{1.228}\ d^{2.678}} \tag{2.11}$$

where A is a constant (fitted value $1.05 \cdot 10^6$); σ_e (MPa) is the isotropic effective stress; ϕ_o is initial porosity; e_v is volumetric strain; d is an averaged grain size (μm) and ΔH is activation energy for intergranular diffusion (24600 J/mol). The volumetric strain rate below saturation can be written as:

$$\dot{\beta} = Q\,\dot{\beta}_{sat} \qquad Q = B(\frac{1-\phi_o}{\phi_o - e_v})F \tag{2.12}$$

where F is brine content (expressed as percentage in weight) and B is a constant. The term $(\phi_o - e_v)$ in (2.11) has been added (it does not appear in the theoretical model) to ensure that $\dot{\beta}$ tends to zero with the porosity.

Regarding experiments performed on dry samples, the proposed model is based on Heard's creep law for axisymmetric strain.

$$\dot{\beta}_{dry} = K_1 \exp(-\frac{\Delta H}{RT})\exp[\frac{\sigma_e}{K_2}(\frac{\phi}{\phi_o - \phi})^{0.8}] \tag{2.13}$$

where K_1 and K_2 are fitting constants equal to 31257 and 2.0391, respectively, and ΔH equals 108784 J/mol.

Notice that (2.13) does not depend on grain size. This is a consequence of the fact that the model is based on solid deformation mechanisms, which are independent of grain size.

2.3.5 Failure

Rocksalts may become brittle at high strain rates. This type of failure may occur near the walls of underground cavities, specially shortly after excavation and also in heavily loaded pillars. Inasmuch as failure behavior depends on many factors, mainly strain rate and temperature, it is difficult to establish general failure criteria. Furthermore, when using empirical criteria, it is critical to bear in mind the conditions under which they were derived.

Hunsche and Albrecht (1990) present results of true triaxial test and propose using a extended Drucker-Prager criterion. This is a function of a failure octaedric shear stress, which is temperature dependent, octaedric normal stress and Lode's parameter. These test were performed under constant stress rates of 7.6 MPa/min for 30.2 MPa /min for the isotropic phase and between 15.1 and 30.2 MPa/min for the deviatoric phase. On the other hand, Hambley et al. (1989) have a proposed a combined failure criterion which, in its linear part, is the extended Mohr-Culomb criterion. Strain rates for these tests range between 10^{-3} and 10^{-5} s^{-1}, much faster than those to be expected under natural conditions.

A general form to the computation of fracture strains that can be written as:

$$\dot{\varepsilon}^f_{ij} = \frac{1}{\eta} < F > \frac{\partial F}{\partial \sigma_{ij}} \tag{2.14}$$

where $F = F(I_1, J_2)$ is the extended Drucker-Prager criterion ($< F >$ equals 0 if $F \leq 0$ and equals F, otherwise) $\dot{\varepsilon}^f_{ij}$ is the strain rate tensor at failure, I_1 is the first invariant of the stress tensor and J_2 is the second invariant of the deviatoric stress tensor and η is the viscous parameter that may depend on state variables.

2.4 Hydraulic behaviour

2.4.1 Permeability of rock salt

Because of their low permeability, rock salts were historically considered impervious and, to this day, scant efforts have been devoted at characterizing them. Probably, the earliest studies are those of Gloyna and Reynolds (1961), who performed a large number of permeability laboratory experiments on both dome (Grand Saline) and bedded salt (Hutchison) samples from approximately 200 m deep. Despite the low permeability of the rock, experiments were performed under steady-state flow conditions with different permeation fluids (brine, helium, natural oil and kerosene). Estimated intrinsic permeabilities ranged between 10^{-15} and 10^{-17} m^2 for dome samples and between 10^{-17} and 10^{-18} m^2 for bedded salt samples.

The viscous nature of rocksalt makes it difficult to uncouple the mechanical and hydraulic behaviours. Hence, results of permeation experiments have to be given in the framework of the mechanical conditions under which they were performed. Gloyna and Reynolds used confining pressures similar to the "in situ" lithostatic stress in order to account for opening of fissures during sampling. Furthermore, permeation was started only after volumetric changes became negligible. Yet, permeability reductions of up to an order of magnitude were observed during the experiments, which lasted less than 36 days. The relationship between net confining pressure and permeability displays two distinct slopes. A significant increase in slope can be observed between 5 and 10 MPa, which is consistent with the variations in mechanical behavior described earlier.

Another consequence of the low permeability of rock salts is the extremely low diameter of flow paths. As a result, liquid-solid interactions may become significant, which leads to a fluid dependent permeability, in contradiction with elementary theory of flow through porous media. Knudsen diffusion (Klinkenberg effect) has been reported by several authors. Under low pressures, free path of molecules can become comparable to path diameter, leading to an apparent slippage at the fluid- solid interphase. As a result, measured gas intrinsic permeability can be larger than the corresponding measurement with liquid. Other types of interactions may also be important, depending on the polar nature of the liquid molecules. For example, Gloyna and Reynolds report permeability values for brine which, in the average, are 32% of those for kerosene.

Sutherland and Cave (1980) present more recent experimental results for bedded salt samples (SE New Mexico, approx. 640 m deep). Their permeabilities were obtained using the transient pressure pulse with argon gas and ranged

between 10^{-18} and 10^{-19} m^2. They studied the temporal evolution of permeability for confining pressures of about 14 MPa.

Peach et al (1987) have used both methods (steady-state brine flow and transient pulse with brine and argon gas). They studied the permeability of both natural deformed dome salt samples (Asse II, 800 m). An interesting result from their experiments on underformed samples taken from several distances from the gallery is the permeability reduction with such distance (Figure 2.8). Also, samples tested under dilatant conditions ($\sigma_3 = 5$ Mpa, $\dot{\epsilon} = 3 \cdot 10^{-5}\ s^{-1}$) increased its permeability from initial values around 10^{-21} m^2 to approximately 10^{-17} m^2 for axial strains of 4%. Permeability increases flattened out from there on, reaching 10^{-16} m^2 for a strain of 10%.

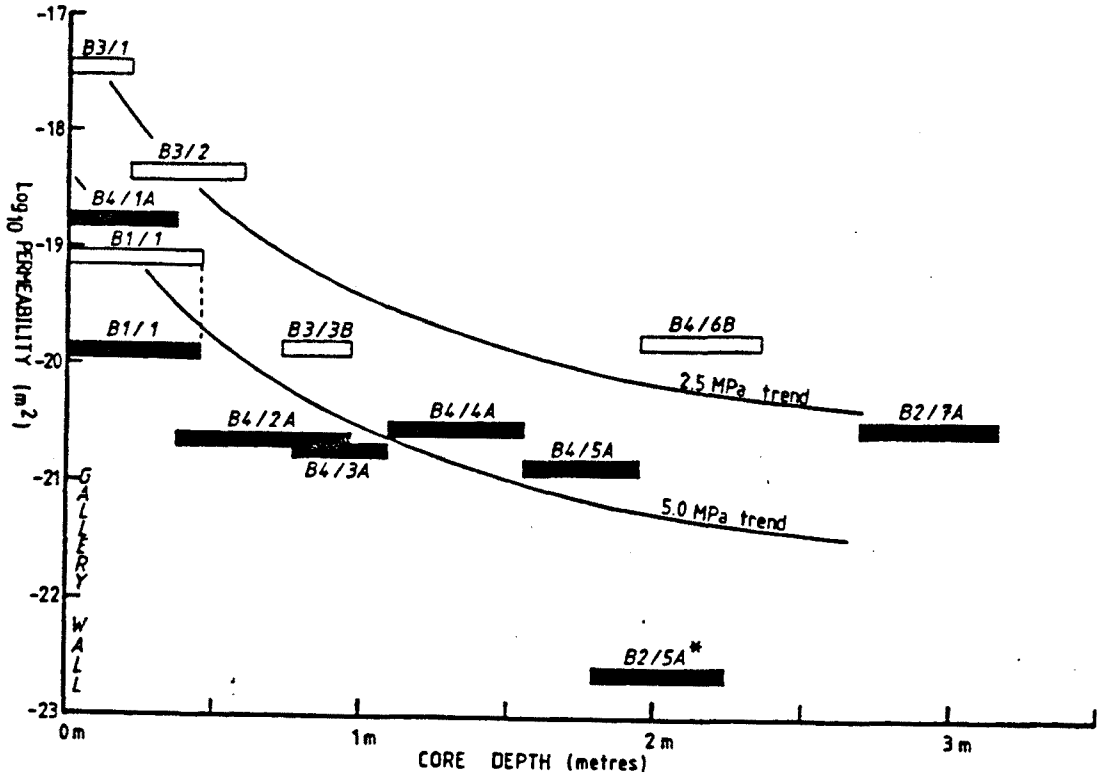

Figure 2.8: Argon gas permeability measurements versus distance from opening wall (Asse's mine gallery ~ 800 m depth). Open symbols are for 2.5 MPa confining pressure during test and closed are for 5.0 MPa).

Peach et al (1987) also studied temporal variations of permeability on deformed samples using two types of experiment. The first one which is similar to that of

Sutherland and Cave (1980), consists of performing quasi-stationary measurements of permeability for several sequential time intervals. Their permeability reductions were not as marked as those of Sutherland and Cave, which is not surprising since the sample (dry) permeability was about 10^{-16} m^2, two orders of magnitude above that of the latter. The second set of experiments consist of brine steady flow tests, alternating flow and no flow periods and changing the flow direction sequentially. Permeability reduction rates for this latter case were much higher than for the dry case and the highests, those with flow, though permeabilities were smaller (between 10^{-17} and 10^{-18} m^2). These rates were comparable to those of Sutherland and Cave, whose samples were dry and not previously deformed.

Peach et al. used a fluorescent dye in conjunction with the tests. These left a tracer throughout the sample.

2.4.2 Permeability of granular aggregates

Spiers et al. (1988) used the argon gas transient pulse technique for determining the permeability of granular aggregates composed of: 75-80% of NaCl with grain size of 275± 25μm, 15-20% with grain sizes between 10 and 50 mm and 2-3% of Fe_2O_3 and anhidrite. Two different initial values of 0.25 and 0.40 were used for porosity. A first set of experiments were performed on dry samples and brine was added for the second set (approximately $\sim$ 5% in weight). Tests were performed for different compaction levels. Results are summarized in Figure 2.9, which also displays $k - \phi$ relationship for an ultrafine grain aggregate (grain size 100 μm) previously dry compacted at 2 MPa.

Result suggest that porosity is the permeability controlling factor. Permeability dependence on other parameters (grain size, initial porosity, geometry of connected porosity, which should vary in response to variations in deformatial mechanisms and brine content, etc) is weak, at most. Therefore, Spiers et al. (1988) propose the log K- log ϕ linear relationship derived from Figure 2.9.

On the basis of observed microstructure variations, they concluded that fluid assisted diffusion transfer (FADT) was the dominant deformational mechanism for wet samples. Plastic strains dominate the deformation behavior of dry samples. Recrystallization in the pores and grain contact migration for low porosities could be observed. On the other hand, when using high compaction, microstructure of the ultrafine aggregate approached that of natural rock salt, with grain sizes around 2 to 3 mm.

Permeabilities computed by Gloyna and Reynolds (1961) for dome rock salt were one to two orders of magnitude larger than those derived from Figure 2.9.

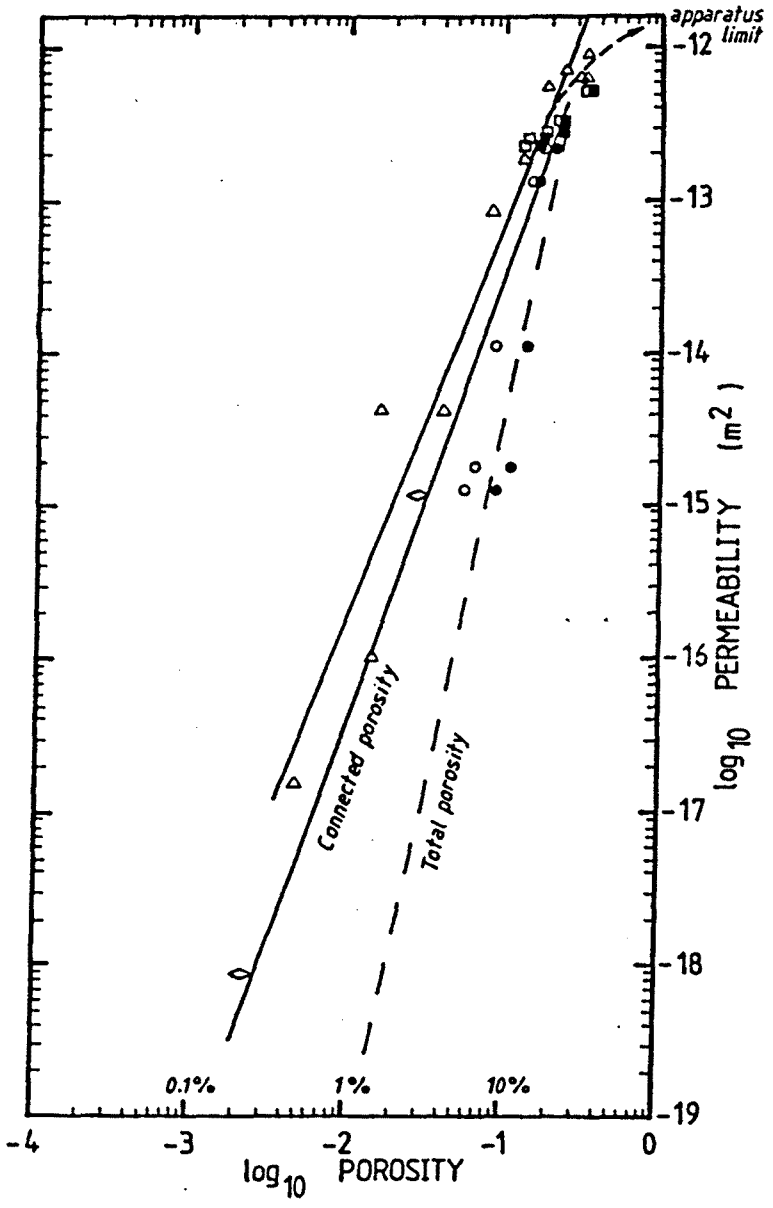

Figure 2.9: Experimental results of permeability in deformed crushed salt. Triangles are for dry compacted material, square symbols represent data obtained from samples with high initial porosity (38.8%), circular symbols correspond to low initial porosity (24.8%) and "diamonds" correspond to ultrafine NaCl powder. Closed symbols represents permeability vs. total porosity and open vs. connected porosity). (After Spiers et al., 1988).

2.5 Concluding remarks

This review was performed with the objective of learning and understanding the physical mechanisms regarding mechanical and hydraulic behaviour of saline media that were considered relevant in the literature. It has to be seen as an introduction to this research topic but probably today it is incomplete because other investigations have been performed in the recent years. However, the pretended objective was completely accomplished because an interesting research started from this work which, certainly, will continue in the future. The contents of this thesis are partially based on the learnings obtained in this review but general theories of geohydromechanics were also reviewed and recalled later. From the author's point of view, this review served as a motivation to begin a very interesting investigation work.

2.6 References

Berest, P. (1989): "Viscoplasticity in rock mechanics", in Geomaterials, constitutive equations. F. Darve (ed.), Elsevier: 239-262.

Carter, N.L. and F.D. Hansen, (1983): "Creep of rock salt", Tectonophysics, 92: 275-333.

Dusseault, M.B., L. Rothenburg and D.Z. Mraz, (1987): "The design of openings in saltrock using multiple mechanism viscoplastic law", Proc. of 28th US Symp. on Rock Mechanics, Tucson: 633-642.

Edlefson, N.E. and A.B.C. Anderson, (1943): "Thermodynamics of soil moisture". Hilgardia, 15(2): 31-298.

Engelmann, H.J., P.W. Broochs, W. Hänsel and L. Peters, (1989): "Dams as sealing systems in rock salt formations test dam construction and determination of permeability", Sealing of radioactive waste repositories. Proc. of an NEA/CEC workshop , OECD: 151-162.

Farmer, I.W. and M.J. Gilbert, (1981): "Time dependent strength reduction of rock salt", Proc. 1st Conf. Mech. Behaviour of Salt, Penn. State Univ.: 3-18.

Gloyna, E.F. and T.D. Reynolds, (1961): "Permeability measurements of rock salt". Journal of Geophysical Research, Vol. 66, n. 11: 3913-3921.

Hambley, D.F., C.J. Fordham and P.E. Senseny, (1989): "General failure criteria for saltrock", in Rock Mechanics as a Guide for Efficient Utilization of Natural Resources, Khair (ed.), Balkema: 91-98.

Horseman, S. T. and E. Passaris, (1981): "Creep tests for storage cavity closure prediction". Proc. 1st Conf. Mech. Behaviour of Salt, Penn. State Univ.: 119-157.

Horseman, S.T., (1984): "Moisture content - A major uncertainty in storage cavity closure prediction", Proc. 2nd Conf. Mech. Behaviour of Salt, Penn. State Univ.: 53-68.

Hunsche, U. and H. Albrecht, (1990): "Results of true triaxial strength tests on

rock salt", Engineering Fracture Mechanics, Vol. 35, no. 4/5: 867-877.
Kappei, G. and K. Gessler, (1984): "In situ tests on the behaviour of backfill materials", Proc. 2^{nd} Conf. Mech. Behaviour of Salt, Penn. State Univ.: 311-328.
Kascheev, V.A., P.P. Poluektov, A.S. Polyakov, (1989): "The role of convection in the process of liquid transfer under temperature gradient in crystalline massives of halite", Proc. Symp. on Safety Assessment of Radioactive Waste Repositories, NEA-OECD: 1001-1003.
Langer, M. (1981): "The rheological behaviour of rock salt", Proc. 1^{st} Conf. Mech. Behaviour of Salt, Penn. State Univ.: 201-240.
Liedtke, L. and W. Bleich, (1984): "Convergence calcultation for back-filled tunnels in rock salt", Proc. 2^{nd} Conf. Mech. Behaviour of Salt, Penn, State Univ.: 551-580.
Munson, D.E. and P.R. Dawson, (1981): "Salt constitutive modeling using mechanism maps", Proc. 1^{st} Conf. Mech. Behaviour of Salt, Penn. State Univ.: 717-737.
Peach, C.J., C.J. Spiers, A.J. Tankink, H.J. Zwart, (1987): "Fluid and ionic transport properties of deformed salt rock", Nuclear Science and Technology, CEC Vol. EUR 10926 EN.
Roedder, E., (1984): "The fluids in salt 1", American Mineralogist, Vol. 69: 413-439.
Spiers, C.J., J.L. Urai, G.S. Lister, J.N. Boland, H.J. Zwart, (1986): "The influence of fluid-rock interaction on the rheology of salt rock", Nuclear Science and Technology, CEC, EUR 10399 EN.
Spiers, C.J., C.J. Peach, R.H. Brzesowsky, P.M.T.M. Schutjens, J.L. Liezenberg, H.J. Zwart, (1988): "Long-term rheological and transport properties of dry and wet salt rocks", Nuclear Science and Technology, CEC. Vol. EUR 11844 EN.
Spiers, C.J., P.M.T.M. Schutjens, R.H. Brzesowsky, C.J. Peach, J.L. Liezenberg and H.J. Zwart, (1990): "Experimental determination of constitutive parameters governing creep of rocksalt by pressure solution", Deformation Mechanisms, Rheology and Tectonics, Knipe, R.J. and Rutter, E.H., Geological Society Special Publication, no. 54: 215-227.
Sprunt, E.S. and A. Nur, (1977): "Experimental study of the effects of stress on solution rate", Journal of Geophysical Research, Vol. 82, no. 20: 3013-3022.
Sutherland, H.J. and S.P. Cave, (1980): "Argon gas permeability of New Mexico rock salt under hydrostatic compression", Int. J. Rock Mech. Min. Sci. and Geomech. Abstr., Vol. 17: 281-288.
Tada, R. and R. Siever, (1985): "Experimental knife-edge pressure solution of halite". Geochimica et Cosmochica Acta, Vol. 50: 29-36.
Urai, J.L. (1985): "Waste enhanced dynamic recrystallization and solution transfer in experimentally deformed carnallite". Tectonophysics, Vol. 120: 285-317.
Wallner, M. (1986): "Stability demonstration concept and preliminary desing calculations for the Gorleben reporsitory", Workshop on mathematical

modelling for radioactive waste repositories. Enresa. Madrid: 29-47.
Walter, (1991): Personal comunication.
Yagnik. S.K., (1983): "Interfacial stability of migrating brine inclusions in alkali halide single crystals supporting a temperature gradient", Journal of Crystal Grouth, 62: 612-626.

CHAPTER 3

NON-ISOTHERMAL MULTIPHASE FLOW OF BRINE AND GAS THROUGH SALINE MEDIA

3.1 Introduction

Salt rock (rock formed by salt minerals of which halite (NaCl) is the most important and common) geologic formations are being considered as one of the possible media for radioactive waste disposal. Salt rock appears to be suitable for this purpose because of its low permeability, adequate mechanical and thermal behaviour, possibility of healing natural or induced defects, relative ease of excavation, occurrence of large formations and low economical value.

The isolation of waste from the environment is achieved by sealing systems. Porous salt granular aggregates are used to fill cavities and galleries where waste has been disposed and also to build sealing systems such as brick dams (Engelmann et al. 1989). Salt bricks are manufactured by compaction of salt powder and used to construct parts of the sealing system. Slightly consolidated raw material is used to fill different kinds of openings. Initial porosities and particle sizes may vary according to the objectives of the system, its hydromechanical behaviour or other factors.

The ductile behaviour of salt rock, which is crucial for achieving self sealing of natural and induced defects, produces very large convergences in mine galleries, sometimes closing them completely. Therefore, fills and seals will be compressed and their porosity will be reduced. This deformation can lead to low porosity materials, hardly distinguishable from natural salt rock. Environmental physical conditions strongly affect the rates of deformation.

The complex behaviour of such systems requires new theoretical and applied developments and suitable laboratory and field experiments. Due to the unusual processes that take place in saline media, a comprehensive theory should couple hydraulic, mechanical and thermal (eventually chemical) problems. An example of the coupled phenomena that occur is that volumetric strain rates due to creep

deformation change over orders of magnitude under field variations of temperature and relative humidity. This leads to porosity changes which in turn influence brine, gas and heat transport.

On the other hand, saline environments show phenomena on unusually short time scales. An excavated gallery for mining purposes can converge completely in a time comparable to a human lifetime. But the fundamental processes are similar as those that take place over geological time scales in other media. Therefore, saline media must be investigated not only for the sake of the necessary knowledge of salt itself but also because salt can provide interesting explanations of the processes and phenomena that take place in other media.

In this chapter, the macroscopic governing equations (continuous level) for non-isothermal multiphase flow of brine and gas through porous deformable saline media are presented. The formulation presented here is used to develop a numerical finite element model to handle COupled DEformation, BRIne, Gas and Heat Transport (CODE-BRIGHT).

Non-isothermal moisture transport in non-saturated porous media has been the topic of the research of different authors. Philip and de Vries (1957) presented what has been the basis for further investigations. Based on it, Milly (1982) established the equations for moisture and heat transport, extending their applicability to hysteretic and inhomogenous porous media. Most authors in this field assume that gas pressure is constant in space and time. Under such conditions, no balance equation is necessary to characterize the gaseous phase. This assumption is adequate when dealing with partially saturated soils (Bear et al., 1991). The theory has been extended to overcome this practical simplification (Pollock, 1986; Pruess, 1987). When gas pressure cannot be neglected, two mass balance equations are established, one for each species (water and air), which can be present either in the liquid phase or in the gaseous phase. In all cases, thermal equilibrium of phases (Milly, 1982) is assumed and only one equation for energy balance is required.

An isothermal multiphase flow model has also been established for problems of organic compounds transport which is another field of research related to what we are presenting here. Abriola and Pinder (1985) and Pinder and Abriola (1986) have presented the equations for multiphase flow of water, air and a nonaqueous compound. The formulation involves two liquid phases and one gaseous phase, each one containing several species.

Closely related research is performed in the field of geothermal reservoirs. Faust and Mercer (1979) established the governing equations both for liquid dominated and for vapour dominated hydrothermal systems. Two assumptions

make this theory specific: (1) only the aqueous species (liquid, vapour or both) are present in the pores and (2) capillary pressure effects are neglected. Therefore, one fluid pressure value is the unknown associated to one mass balance equation for the only species considered. Thermal equilibrium is also assumed. Lewis et al. (1989) coupled the deformation of the rock matrix with multiphase flow in geothermal reservoirs.

Hassanizadeh and Gray (1979a,b) presented formal developments for multiphase systems employing averaging theory. Hassanizadeh (1986a,b) derived the basic equations of mass transport in porous media, obtaining macroscopic balance laws and generalized Darcy's and Fick's laws. This author considered the possibility of high solute concentrations and solid/liquid phase interchange, and a particular case of the formulation for saturated brine was also included. Bachmat and Bear (1986) and Bear and Bachmat (1986) also presented theoretical developments for macroscopic modelling of transport phenomena in porous media. This latter group of works provides theoretical and mathematical basis to develop formulations for specific problems.

While the above works are very relevant to our objectives, none of them accounts for all peculiarities of saline media that must be taken into account to ensure adequate predictive capabilities. These include:

(1) Salt solubility is high and depends on both temperature and pressure. This will lead to both micro and macroscopic variations of porosity and related variables (permeability, compressibility, etc). In fact, the very fast creep behaviour of wet salts can be attributed to pore scale dissolution/precipitation of salt caused by local stress variations (Spiers et al., 1990; Olivella et al., 1992, 1993). Variations in solubility also imply density variations.

(2) Hygroscopy of salt. The classical form of the psychrometric law is not valid for brines. In fact, quite low relative humidities in the gas phase may be in equilibrium with a nearly saturated porous medium. For example, a halite brine at atmospheric pressure is in equilibrium with 75% relative humidity air, so that wetter air (still far from saturation with fresh water) will tend to condensate.

(3) Solid matrix deformation of salt is large and time dependent. Instantaneous and creep strains are relevant. Therefore, deformation of the solid body must be taken into account both because of its effects on brine, gas and heat storage and because of variations in transport properties, e.g. in permeability.

(4) Phase changes in saturated brines imply not only latent heat release or uptake, but also dissolution (condensation) or precipitation (evaporation) of salt and, as a consequence, variations in porosity.

(5) Brine inclusions in the solid phase. Migration of small brine bubbles inside grains, possibly leading to source/sink at grain boundaries, should be taken

into account. In dry salts, for example, a relatively important amount of brine is supplied to the connected porosity in this way. In turn, this amount may suffice to increase creeping rates dramatically. A possible mechanism for inclusion migration is due to salt molecular diffusion inside the brine bubble caused by concentration differences induced by temperature gradients.

3.2 Notation

$\boldsymbol{b}$	body forces vector in equilibrium equation
C^e	is the elastic compliance matrix.
d	ratio between volume and surface of the grains
d_o	grain size
D_s^w	effective diffusion coefficient for inclusion migration
D_α^i	dispersion tensor ($i = h,\ w$ for $\alpha = l$ and $i = w,\ a$ for $\alpha = g$)
E_α	internal energy of α-phase per unit mass of α-phase
E_α^i	internal energy of i-species in α-phase per unit mass of i-species
f^i	external mass supply per unit volume of medium ($i = h,\ w,\ a$)
f^E	internal/external energy supply per unit volume of medium
f_s^w	internal sink of water in fluid inclusion equation
$\boldsymbol{g}$	gravity vector
i	species index, h salt (halite), w water and a air (superscript)
$\boldsymbol{i}_\alpha^i$	nonadvective mass flux of i-species in α-phase
$\boldsymbol{i}_c$	nonadvective heat flux
$\boldsymbol{j}_{E\alpha}$	advective energy flux in α-phase with respect to a fixed reference system
$\boldsymbol{j}'_{E\alpha}$	advective energy flux in α-phase with respect to the solid phase
$\boldsymbol{j}_\alpha^i$	total mass flux of i-species in α-phase with respect to a fixed reference system
$\boldsymbol{j}'^i_\alpha$	total mass flux of i-species in α-phase with respect to the solid phase
$\boldsymbol{K}_\alpha$	permeability tensor ($\alpha = l,\ g$)
$\boldsymbol{k}$	intrinsic permeability tensor
$k_{r\alpha}$	α-phase relative permeability ($\alpha = l,\ g$)

M_w	molecular mass of water
P_α	fluid pressure of α-phase ($\alpha = l,\ g$)
q_α	volumetric flux of α-phase with respect to the solid matrix ($\alpha = l,\ g$)
R	constant of gases
S_α	volumetric fraction of pore volume occupied by α-phase ($\alpha = l,\ g$)
T	temperature
$\dot{\boldsymbol{u}}$	solid velocity vector
$\boldsymbol{v}_s^w$	velocity of brine inclusions in the solid phase
α	phase index, s solid, l liquid and g gas (subscript)
$\dot{\boldsymbol{\varepsilon}}$	strain rate tensor
θ_α^i	$(= \omega_\alpha^i \rho_\alpha)$ mass of i-species per unit volume of α-phase
μ_α	dynamic viscosity of α-phase ($\alpha = l,\ g$)
∇	gradient vector
ρ_α	mass of α-phase per unit volume of α-phase
$\boldsymbol{\sigma},\ \boldsymbol{\sigma}'$	stress tensor (total and net)
$\dot{\boldsymbol{\sigma}}$	stress rate tensor
ϕ	porosity
ω_α^i	mass fraction of i-species in α-phase

3.3 Macroscopic approach

The macrosopic balance of any thermodynamic property ψ (per unit mass) in a continuum can be expressed by:

$$\frac{\partial}{\partial t}(\rho\psi) + \nabla \cdot (\boldsymbol{j}_\psi) - f^\psi = 0 \tag{3.1}$$

where ρ is the mass of species per unit volume containing ψ, $\boldsymbol{j}_\psi$ is the total flux of ψ with respect to the reference system and f^ψ is the rate of production/decay of ψ per unit volume (internal or external). It is important to stress here that $\boldsymbol{j}_\psi$ is expressed in relation to a fixed system because corrections will be needed to account for the fact that the solid indeed moves. This total flux can be decomposed into an advective (phase motion) and a nonadvective (species motion inside the phase) counterparts, that is: $\boldsymbol{j}_\psi = \rho\psi\boldsymbol{v}_\psi + \boldsymbol{i}_\psi$, where $\boldsymbol{v}_\psi$ is the mass weighted mean velocity and $\boldsymbol{i}_\psi$ is the nonadvective flux. Using this decomposition, equation (3.1) would be the general equation given by Hassanizadeh (1986a) and used by Abriola and Pinder (1985), who called $\boldsymbol{i}_\psi$ nonadvective flux. It is also possible to use volume weighted velocities to define the advective flux (e.g. Bear and Bachmat, 1986).

It is necessary to make a further comment on the advective flux. The velocity of a fluid phase is decomposed into two terms: motion with respect to the solid phase and motion of the solid phase with respect to a fixed reference. These two terms will not be treated identically. To obtain the flux of ψ due to solid motion it is necessary to multiply solid velocities by the amount of ψ per unit volume of medium. For a fluid phase, its motion with respect to the solid is expressed as volumetric flux (q_α, that is, volume of fluid crossing the unit area of porous medium per unit time). Hence, this flux is multiplied by the amount of ψ per unit volume of fluid in order to obtain a mass flux. We will use this form because it maintains the concept of discharge as in the original Darcy's law. This treatment is also consistent with the fact that Darcy's flux represents a mass weighted flux because Darcy's law can be viewed as an expression of momentum conservation (Bear and Bachmat, 1986).

3.4 Problem formulation

The porous medium under study consists of three phases [solid (s), liquid (l) and gas (g)] and three main species [salt (h), water (w) and air (a)]. Figure 3.1 is an schematic representation of the medium. Without significant loss of generality, we will assume a uniform salt composition and will not consider chemical processes (except dissolution/precipitation controlled by solubility) which can occur due to the presence of different minerals. Salt is the species that forms the solid phase and it is also dissolved at high concentrations in the liquid phase. Water is the main species in the liquid phase (brine); it is also present in the gaseous phase as vapour and it can also be present in the solid phase as brine inclusions. These fluid inclusions are filled with saturated brine, i.e. at chemical equilibrium. Dry air is considered a single species, it is the main component of the gaseous phase and it is also dissolved in the liquid phase. Finally, it would be easy to include a contaminant at low concentration, assuming that it is non-reactive with the other species and that the properties of the fluid phases remain unaffected by its presence. Considering more than one saline species would require to address chemical interactions which are beyond the scope of the work presented here.

Full description of the hydro-thermo-mechanical state of the medium is given in terms of a large number of variables. Solution requires specifying an equal number of equations. Both are listed in Table 3.I, in which we have associated every equation with one variable. Obviously, this association is somewhat arbitrary, as every equation relates several variables. The variable associated to each equation in Table 3.I should be understood as the one we will be solving for in subsequent derivations. Implicit in Table 3.I is the choice of state (independent) variables from which all other will be derived through constitutive or equilibrium constraints. Thus, state variables are as follows: solid velocity, $\dot{\boldsymbol{u}}$ (in three spatial directions);

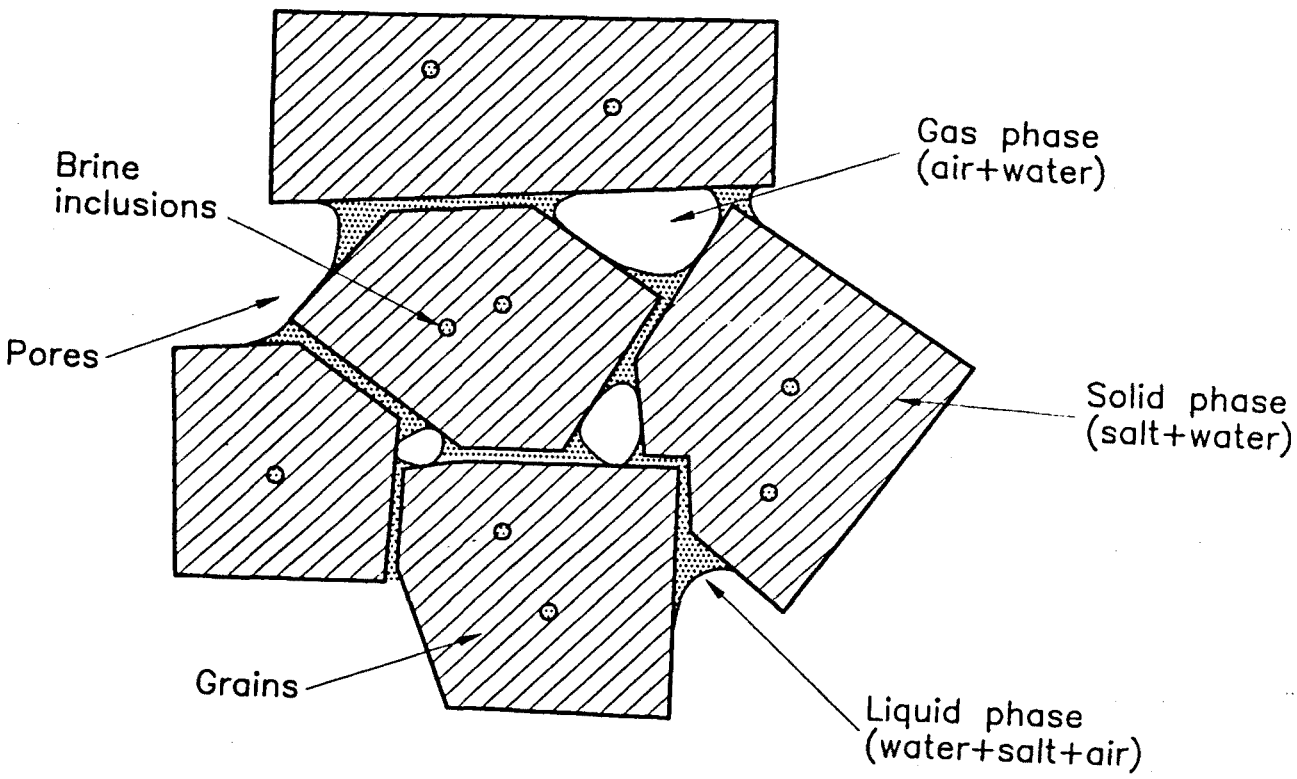

Figure 3.1: Schematic representation of the porous medium composed by salt grains, brine and gas.

liquid pressure, P_l; gas pressure, P_g; temperature, T; and mass fraction of water in the solid phase, ω_s^w. It is clear that the latter will be unimportant in most cases.

In this chapter, we derive the mass balance of different species and the total internal energy balance. Balance of momentum for the medium as a whole is reduced to the equation of stress equilibrium. Balance of momentum for dissolved species and for fluid phases are reduced to constitutive equations (Fick's and Darcy's laws).

Table 3.I: Equation and Variable Summary

EQUATION NAME	VARIABLE	EQUATION NUMBER
Balance equations		
Salt mass balance	ϕ	(3.5, A3)
Water mass balance	P_l	(3.10, A5)
Air mass balance	P_g	(3.14, A6)
Water in inclusions mass balance	ω_s^w	(3.15, A7)
Stress equilibrium	$\dot{\boldsymbol{u}}$	(3.16)
Internal Energy	T	(3.26, A8)
Constitutive equations		
Fick's law (vapour and salt)	$\boldsymbol{i}_g^w, \boldsymbol{i}_l^h$	(3.28)
Darcy's law (liquid and gas)	$\boldsymbol{q}_l, \boldsymbol{q}_g$	(3.29)
Inclusion migration law	$\boldsymbol{i}_s^w$	(3.32)
Fourier's law	$\boldsymbol{i}_c$	(*)
Retention curve	S_l	(*)
Mechanical constitutive model	σ	(*)
Phase density (brine)	ρ_l	(*)
Gases law (gas)	ρ_g	(*)
Equilibrium restrictions		
Solubility	ω_l^h	(3.34)
Henry's law	ω_l^a	(*)
Psychrometric law	ω_g^w	(3.35)
Definition constraints		
$\dot{\varepsilon} = \frac{1}{2}(\nabla\dot{\boldsymbol{u}} + \nabla\dot{\boldsymbol{u}}^t)$	$\dot{\varepsilon}$	
$\omega_s^h + \omega_s^w = 1$	ω_s^h	
$\omega_l^w + \omega_l^h + \omega_l^a = 1$	ω_l^w	
$\omega_g^w + \omega_g^a = 1$	ω_g^a	
$S_l + S_g = 1$	S_g	
$\boldsymbol{i}_s^w + \boldsymbol{i}_s^h = \boldsymbol{0}$	$\boldsymbol{i}_s^h$	
$\boldsymbol{i}_l^h + \boldsymbol{i}_l^a + \boldsymbol{i}_l^w = \boldsymbol{0}$	$\boldsymbol{i}_l^w$	
$\boldsymbol{i}_g^w + \boldsymbol{i}_g^a = \boldsymbol{0}$	$\boldsymbol{i}_g^a$	

Number of equations: 27 Number of variables: 27 (*) Not included in this chapter
(1-dimension is assumed for vectorial and tensorial quantities)

3.5 Mass balance equations

The compositional approach (Panday and Corapcioglu, 1989) is followed to establish the mass balance equations. This approach consists of balancing the species rather than the phases. If the basic equation for each species in each phase is established, either phase equation or total species equation can be obtained. Phase equations are obtained by adding the equations of balance of all species contained in each phase. Often, this is advantageous when writing the flux terms, because, from the general theory of miscible displacement (Bear, 1972), nonadvective fluxes of species inside the phase would cancel. On the other hand, total species equations are obtained by adding over all phases the equation of balance of each species. In this way, phase exchange terms cancel out, which is particularly useful when equilibrium is assumed. In either case, the required final number of equations depends on the number of unknowns and, on occasions it may be necessary to recall some of these basic equations. For example, water in the solid phase (brine inclusions) can not be considered in equilibrium with water in the connected pores, so that the mass balance equation for water in the solid phase will be required.

3.5.1 Salt mass balance equation

The salt mass balance equation can be written as a particular case of equation (1). Salt fluxes occur both in the solid and liquid phases. The former consists solely of the often negligible movement of inclusions. The latter includes the more important advective flux associated to brine flow and the nonadvective flux of solute. It should be noted that, since brine flow will be computed by means of Darcy's law (i.e. relative to the moving solid salt reference) a correction term will be required to account for the solid velocity.

The presence of brine inclusions in the solid phase has been considered by some authors (Ratigan, 1984), although it can be neglected in some problems. It has been observed that brine inclusions move (Roedder, 1984) when subject to temperature gradients (bubbles of brine migrating through the crystalline solid). Under the assumption that continuous variables can be defined to treat brine inclusions, mass fraction of water in the solid phase ω_s^w is defined as a continuous variable which represents the water content in the solid phase. On the other hand, ω_s^h is the mass fraction of salt in the solid phase and, by definition of mass fraction, $\omega_s^w + \omega_s^h = 1$ (note that solid salt and salt dissolved in inclusions are added in the same variable). If ρ_s is the solid phase density, the masses of species per unit volume of solid phase are: $\theta_s^h = \omega_s^h \rho_s$ and $\theta_s^w = \omega_s^w \rho_s$, respectively for salt and water. The content of salt dissolved in the liquid phase is $\theta_l^h = \omega_l^h \rho_l$. Thus, total

salt content per unit volume of porous medium is:

$$\theta_s^h(1-\phi) + \theta_l^h S_l \phi \tag{3.2}$$

where ϕ is porosity and S_l is the volumetric fraction of voids occupied by liquid phase (i.e., liquid saturation).

Since we are considering a nonadvective flux of water in the solid phase (i_s^w) due to inclusion displacement, a complementary nonadvective flux of salt (i_s^h) has to be considered as well (probably negligible even when the former is important). The mass flux of salt contained in the solid phase is the sum of this flux and the advective flux due to solid motion:

$$j_s^h = i_s^h + \theta_s^h(1-\phi)\dot{u} = j'^h_s + \theta_s^h(1-\phi)\dot{u} \tag{3.3}$$

where $\dot{u}$ is the velocity field of the solid phase due to the deformation of the solid skeleton and j'^h_s is the salt flux with respect to the solid phase (in this case, identical to the nonadvective flux i_s^h). On the other hand, the mass flux of salt in liquid phase is given by:

$$j_l^h = i_l^h + \theta_l^h q_l + \theta_l^h S_l \phi \dot{u} = j'^h_l + \theta_l^h S_l \phi \dot{u} \tag{3.4}$$

where i_l^h is the nonadvective mass flux of salt in the liquid phase, q_l is the advective volumetric flux of the liquid phase with respect to the solid phase and j'^h_l includes these two terms and represents the mass flux of salt in liquid phase with respect to the solid phase. The last equivalence in (3.3) and (3.4) is made in order to distinguish the relative motion of species j' (with respect to the solid phase) from the absolute motion j (with respect to a fixed reference system).

The total mass balance of salt in the porous medium is established by substituting (3.2), (3.3) and (3.4) in (3.1), which leads to:

$$\frac{\partial}{\partial t}(\theta_s^h(1-\phi) + \theta_l^h S_l \phi) + \nabla \cdot (j_s^h + j_l^h) = f^h \tag{3.5}$$

where f^h is an external supply of salt. An internal production term is unnecessary because this equation accounts for the total salt mass balance. At this point of the development, it is convenient to transform the equation using the material derivative with respect to the solid velocity field. Some additional algebra allows us to obtain a form of this equation which is more convenient for programming purposes (see Appendix).

3.5.2 Water mass balance equation

As discussed at the beginning of section 5, we prefer water mass balance equation instead of liquid balance equation, which is more common in general formulations (Hassanizadeh, 1986b), because the phase change terms do not appear explicitly.

Water is the main component in the brine, it is a minor component in the gas phase and it occurs in the solid phase in form of brine inclusions. The total mass of water per unit volume of porous medium is expressed as:

$$\theta_s^w(1-\phi) + \theta_l^w S_l \phi + \theta_g^w S_g \phi \tag{3.6}$$

where each term accounts for water in one phase, solid, liquid and gas, respectively. Note that $S_l + S_g = 1$ is a constraint which comes from the definition of fluid phase saturations.

Similarly to (3.3) and (3.4), water fluxes in each phase can be written as:

$$\boldsymbol{j}_s^w = \boldsymbol{i}_s^w + \theta_s^w(1-\phi)\dot{\boldsymbol{u}} = \boldsymbol{j}'^w_s + \theta_s^w(1-\phi)\dot{\boldsymbol{u}} \tag{3.7}$$

$$\boldsymbol{j}_l^w = \boldsymbol{i}_l^w + \theta_l^w \boldsymbol{q}_l + \theta_l^w S_l \phi \dot{\boldsymbol{u}} = \boldsymbol{j}'^w_l + \theta_l^w S_l \phi \dot{\boldsymbol{u}} \tag{3.8}$$

$$\boldsymbol{j}_g^w = \boldsymbol{i}_g^w + \theta_g^w \boldsymbol{q}_g + \theta_g^w S_g \phi \dot{\boldsymbol{u}} = \boldsymbol{j}'^w_g + \theta_g^w S_g \phi \dot{\boldsymbol{u}} \tag{3.9}$$

where $\boldsymbol{i}_l^w$ and $\boldsymbol{i}_g^w$ are the nonadvective fluxes of water, respectively, in the liquid and in the gas phases, and $\boldsymbol{i}_s^w$ is the flux of water in the solid phase due to inclusion movement. The other terms are advective and take into account the motion of phases. Again, the last equivalence is made in order to distinguish the relative motion of species $\boldsymbol{j}'$ (with respect to the solid phase) from the absolute motion $\boldsymbol{j}$ (with respect to a fixed reference system).

With these definitions, the total water mass balance is expressed as:

$$\frac{\partial}{\partial t}(\theta_s^w(1-\phi) + \theta_l^w S_l \phi + \theta_g^w S_g \phi) + \nabla \cdot (\boldsymbol{j}_s^w + \boldsymbol{j}_l^w + \boldsymbol{j}_g^w) = f^w \tag{3.10}$$

where f^w is an external supply of water. An internal production term is not included because the total mass balance inside the medium is performed. This might be our final equation for water mass balance. However, dependence of the storage term on porosity variations, which are deemed important, do not appear explicitly. For this purpose we need to recall the salt mass balance equation (3.5) or its more convenient form (A3). The algebraic development which leads to the final equation is included in an Appendix.

3.5.3 Air mass balance equation

Air (dry) is considered a single species and the gaseous phase is a mixture of air and water vapour. Air is also dissolved in the liquid phase. The total air content in the porous medium is expressed by:

$$\theta_l^a S_l \phi + \theta_g^a S_g \phi \tag{3.11}$$

where it is assumed that air cannot be present in the solid phase. Sometimes, inclusions contain gaseous bubbles (Roedder, 1984). However this is not the most frequent case. Moreover, on occasions these bubbles are not originated naturally. Furthermore, we cannot envision any problem in which air in inclusions can play an important role. In any case, it is clear that if gas inclusions are deemed important, then one should consider an additional independent variable (air content in the solid phase) and write the corresponding balance equation.

The mass fluxes of air in each fluid phase are:

$$\boldsymbol{j}_l^a = \theta_l^a \boldsymbol{q}_l + \theta_l^a S_l \phi \dot{\boldsymbol{u}} = \boldsymbol{j}'^a_l + \theta_l^a S_l \phi \dot{\boldsymbol{u}} \tag{3.12}$$

$$\boldsymbol{j}_g^a = \boldsymbol{i}_g^a + \theta_g^a \boldsymbol{q}_g + \theta_g^a S_g \phi \dot{\boldsymbol{u}} = \boldsymbol{j}'^a_g + \theta_g^a S_g \phi \dot{\boldsymbol{u}} \tag{3.13}$$

where $\boldsymbol{i}_g^a$ is the nonadvective air flux in the gas phase and nonadvective air flux in the liquid phase is neglected. The air mass balance equation is:

$$\frac{\partial}{\partial t}(\theta_l^a S_l \phi + \theta_g^a S_g \phi) + \nabla \cdot (\boldsymbol{j}_l^a + \boldsymbol{j}_g^a) = f^a \tag{3.14}$$

The algebraic transformation of this equation is included in the Appendix.

3.5.4 Mass balance equation of water in inclusions

As mentioned earlier, we consider the presence of brine inclusions in the solid phase. The water content in the solid phase (continuous variable) ω_s^w is an unknown because it cannot be expressed in terms of the other independent variables. This forces us to formulate an equation for this unknown. The equation of mass balance of water in inclusions is proposed as the equation associated to this non-dependent variable. This equation is easily obtained using the definitions already established for the total water mass balance. The first term in (3.6) and the flux defined by (3.7) are used to write:

$$\frac{\partial}{\partial t}(\theta_s^w(1-\phi)) + \nabla \cdot (\boldsymbol{j}'^w_s + \theta_s^w(1-\phi)\dot{\boldsymbol{u}}) + f_s^w = 0 \tag{3.15}$$

where f_s^w is an internal sink/source of water due to fluid inclusions reaching grain boundaries or being produced there. The equation (15) is also algebraically transformed in the Appendix.

3.6 Stress equilibrium equation

The balance of momentum for the porous medium reduces to the equilibrium equation for macroscopic total stresses if inertial terms are neglected (Bear and Bachmat, 1986):

$$\nabla \cdot \boldsymbol{\sigma} + \boldsymbol{b} = \mathbf{0} \tag{3.16}$$

where $\boldsymbol{b}$ is the vector of body forces. This assumption is usually accepted because both velocities and accelerations are small, giving terms which are negligible in comparison with the stress terms. Bear and Bachmat also show that under certain simplifications, the Terzaghi's concept of effective stress (total stress minus fluid pressure) for saturated conditions can be obtained. Providing an adequate mechanical constitutive model, the equilibrium equation is transformed into a form in terms of the solid velocities, fluid pressures and temperature. A possible decomposition of strains is:

$$\dot{\boldsymbol{\varepsilon}} = \dot{\boldsymbol{\varepsilon}}^{e} + \dot{\boldsymbol{\varepsilon}}^{vp} + \dot{\boldsymbol{\varepsilon}}^{c} + \dot{\boldsymbol{\varepsilon}}^{o} \tag{3.17}$$

where $\dot{\boldsymbol{\varepsilon}}^{e}$ is the elastic strain rate due to stress, $\dot{\boldsymbol{\varepsilon}}^{vp}$ is the viscoplastic strain rate (except creep), $\dot{\boldsymbol{\varepsilon}}^{c}$ is the creep strain rate (see section 3.8) and $\dot{\boldsymbol{\varepsilon}}^{o}$ is the deformation due to temperature or fluid pressure changes. Hence, $\dot{\boldsymbol{\varepsilon}}$ is the total strain rate which is related with solid velocities through the compatibility conditions that can be written as:

$$\dot{\boldsymbol{\varepsilon}} = \frac{1}{2}(\nabla \dot{\boldsymbol{u}} + \nabla \dot{\boldsymbol{u}}^{t}) \tag{3.18}$$

Obviously the most simple model for a porous material is the elastic one written as: $\dot{\boldsymbol{\varepsilon}} = \boldsymbol{C}^{e}\dot{\boldsymbol{\sigma}}$ where $\boldsymbol{C}^{e}$ is the elastic compliance matrix (inverse of the stiffness matrix).

3.7 Energy balance equation

Although the energy balance reduces to enthalpy balance in most cases, it is preferable to express it in terms of internal energy. The resulting formulation is general and allows including pneumatic energy if deemed relevant. If thermal equilibrium between phases is assumed, the temperature is the same in all phases and only one equation of total energy is required. Adding the internal energy of each phase, the total internal energy per unit volume of porous medium becomes:

$$E_s \rho_s (1-\phi) + E_l \rho_l S_l \phi + E_g \rho_g S_g \phi \tag{3.19}$$

where E_s, E_l and E_g are specific internal energy corresponding to each phase, that is, internal energy per unit mass of phase.

The gas phase energy is usually expressed as:

$$E_g\rho_g = (E_g^w\omega_g^w + E_g^a\omega_g^a)\rho_g = E_g^w\theta_g^w + E_g^a\theta_g^a \tag{3.20}$$

where E_g^w and E_g^a are the specific internal energies of species (respectively, water and air), that is, internal energy per unit mass of species. This decomposition is reasonable for the gaseous phase because of the assumption of mixture, which allows us to consider easily the latent heat in water vapour. It should be noted that this decomposition is only necessary because of the existence of the nonadvective mass fluxes. If only advective phase flux was taken into account, only the phase internal energy would be required.

It is not clear that a similar decomposition can be admitted for the liquid phase (saturated brine) which is a dissolution and not a mixture. A first approximation consists of adding the specific heat capacity of the solid solute to that of pure water (Horvath, 1985) weighted with mass fractions. Another point is that phase change of salt has also an associated exchange of energy, the chemical reaction enthalpy.

Assuming that the decomposition of specific heat capacities is valid:

$$E_l\rho_l = (E_l^h\omega_l^h + E_l^w\omega_l^w + E_l^a\omega_l^a)\rho_l = E_l^h\theta_l^h + E_l^w\theta_l^w + E_l^a\theta_l^a \tag{3.21}$$

$$E_s\rho_s = (E_s^h\omega_s^h + E_s^w\omega_s^w)\rho_s = E_s^h\theta_s^h + E_s^w\theta_s^w \tag{3.22}$$

This assumption is not very strong in the context of this formulation because energy flux due to salt nonadvective mass flux is not important and, this is because salt concentration gradients are small as well.

The most important processes of energy transfer in a porous medium are conduction, advection (due to mass flux) and phase change (Bear et al., 1991). Heat conduction, $\boldsymbol{i}_c$, is usually computed by means Fourier's law with an effective thermal conductivity coefficient to account for the characteristics of the medium and also including heat dispersion (Faust and Mercer, 1979).

Using the species specific internal energies and the species mass fluxes, the energy fluxes due to phases motion can be written as:

$$\boldsymbol{j}_{Es} = \boldsymbol{j}'^h_s E_s^h + \boldsymbol{j}'^w_s E_s^w + E_s\rho_s(1-\phi)\dot{\boldsymbol{u}} = \boldsymbol{j}'_{Es} + E_s\rho_s(1-\phi)\dot{\boldsymbol{u}} \tag{3.23}$$

$$\boldsymbol{j}_{El} = \boldsymbol{j}'^h_l E_l^h + \boldsymbol{j}'^w_l E_l^w + \boldsymbol{j}'^a_l E_l^a + E_l\rho_l S_l\phi\dot{\boldsymbol{u}} = \boldsymbol{j}'_{El} + E_l\rho_l S_l\phi\dot{\boldsymbol{u}} \tag{3.24}$$

$$\boldsymbol{j}_{Eg} = \boldsymbol{j}'^w_g E_g^w + \boldsymbol{j}'^a_g E_g^a + E_g\rho_g S_g\phi\dot{\boldsymbol{u}} = \boldsymbol{j}'_{Eg} + E_g\rho_g S_g\phi\dot{\boldsymbol{u}} \tag{3.25}$$

where $\boldsymbol{j}'_{Es}$, $\boldsymbol{j}'_{El}$ y $\boldsymbol{j}'_{Eg}$ are advective energy fluxes with respect to the solid phase.

With these definitions, the energy balance equation becomes:

$$\frac{\partial}{\partial t}(E_s\rho_s(1-\phi) + E_l\rho_l S_l\phi + E_g\rho_g S_g\phi)$$

$$+ \nabla\cdot(\boldsymbol{i}_c + \boldsymbol{j}_{Es} + \boldsymbol{j}_{El} + \boldsymbol{j}_{Eg}) = f^E \qquad (3.26)$$

where f^E is an internal/external energy supply. In this case the internal production accounts, for example, energy dissipation due to medium deformation which is not explicit in the equation because it is negligible in most cases. Algebraic transformation of this equation is included in the Appendix.

3.8 Constitutive theory

3.8.1 Species and phase fluxes, Fick's and Darcy's laws

The nonadvective fluxes of the different species are subject to the constraint (see also Table 3.I):

$$\sum_i \boldsymbol{i}^i_\alpha = \boldsymbol{0} \qquad \alpha = s,l,g \qquad (3.27)$$

where $i = h,w$, for $\alpha = s,l$ and $i = w,a$ for $\alpha = g$ (air diffusion within the liquid phase is neglected). This constraint is interesting because it reduces the number of parameters in binary systems.

Gas phase is considered a mixture of two species. For most problems, molecular diffusion is dominant, hence the concept of binary diffusion is usually admitted (Bear, 1972). In fact, this concept coincides with the above constraint, so that the nonadvective flux of air is simply obtained as the opposite in sign of the nonadvective flux of vapour (Bear et al., 1991).

Since air concentration in the liquid phase is very small, compared to that of water and salt, and since its nonadvective flux can be neglected under the assumption of equilibrium, the liquid phase can be considered a two components system. This leads to more simplified nonadvective fluxes. However, liquid phase is a dissolution, in contrast to the gas phase which was considered a mixture. Hassanizadeh (1986b) considers brines as a particular case and makes the assumption that no macroscopic separation of the two ions exists and that the two are always transported together.

The nonadvective fluxes of species inside the fluid phases are computed through Fick's law which expresses them in terms of gradients of mass fraction of species (Bird et al. 1960; Pollock, 1986; Pinder and Abriola, 1986; Pruess, 1987) through a hydrodynamic dispersion tensor (molecular diffusion plus mechanical dispersion):

$$\boldsymbol{i}_\alpha^i = -\boldsymbol{D}_\alpha^i \nabla \omega_\alpha^i \qquad i = h,\ w;\ \alpha = l \qquad i = w,\ a;\ \alpha = g \tag{3.28}$$

where $\boldsymbol{D}_\alpha^i$ is the dispersion tensor. This is the simplest way to express dispersive fluxes and coupled terms could be added if they were found necessary. The dispersion tensor includes non-advective flux caused by molecular diffusion and by hydromechanical dispersion. Porosity, degree of saturation and the advective phase flux are dependent variables that appear in the definition of this tensor.

The nonadvective flux of liquid water, $\boldsymbol{i}_l^w$, has been considered because of the high solubility of salt in water. In fact, liquid phase properties are strongly affected by the presence of the solute. Corapcioglu (1991) includes this nonadvective flux for water in the liquid phase (saturated conditions). Also, Pinder and Abriola (1986) consider nonadvective flux of each species (water and nonaqueus compound) inside the liquid phase in which that species is the main component. This term is not explicit if the balance of the liquid phase is used instead of the balance of water.

Advective fluxes of fluid phases will be computed using generalized Darcy's law (Bear, 1972) which is expressed as:

$$\boldsymbol{q}_\alpha = -\boldsymbol{K}_\alpha(\nabla P_\alpha - \rho_\alpha \boldsymbol{g}) \qquad \alpha = l,\ g \tag{3.29}$$

where $\boldsymbol{K}_\alpha = \boldsymbol{k}k_{r\alpha}/\mu_\alpha$ is the permeability tensor. The intrinsic permeability (tensor $\boldsymbol{k}$) depends on the pore structure of the porous medium. Since salt deforms and dissolves/ precipitates, the volume of pores and its distribution can change. Hence, intrinsic permeability is a function of deformation or, in terms of the independent variables, a function of displacements. In our case, void volume variations are important and, for this reason, intrinsic permeability may be considered a function of porosity only as a first approximation.

In the same way as for Fick's law, this form of Darcy's law is the direct dependence. Coupled processes and other coupled effects due to the interaction between phases (Bear and Bensabat, 1989) could be included if they are considered important.

In particular, for the case of brine flow through porous medium, Hassanizadeh (1986b) proposes generalized expressions for Fick's and Darcy's laws including all possible cross coupling terms, that is, pressure, density, concentration and

temperature gradients. The relative importance of these additional terms for our problem requires further research. For one thing, it should be noted that in brine flow through saline formations, salt is both solute and solid phase. In this situation, salt concentration gradients are expected to be small because they are only induced by temperature, pressure or stress gradients.

Note that if the basic equations for Fick's (3.28) and Darcy's (3.29) laws are used together with the constraint expressed by Eq. (3.27) there is not coupling between the motion of the fluid phase and the motion of its components (Hassanizadeh, 1986a). In fact, the phase mass flux with respect to the solid matrix results in: $\rho_\alpha \boldsymbol{q}_\alpha$ and pressure and gravity are the only driving forces for phase flow.

3.8.2 Mechanical constitutive model

The complex mechanical behaviour of porous salt aggregates requires the development of a mechanical constitutive model and this implies special theoretical and experimental work. An equation relating $\boldsymbol{\sigma}$, $\dot{\boldsymbol{\sigma}}$, $\dot{\boldsymbol{\varepsilon}}$, T, P_l and P_g is sought. That is, an equation that allows us to obtain stresses and stress rates in terms of independent variables, through parameters which are related to porosity (or void ratio), grain size, medium properties, etc.

Let us assume that strains can be divided into instantaneous and time dependent components. Instantaneous drained deformation of a highly permeable porous material which does not show creep includes elastic and plastic counterparts. This behaviour has been widely studied and characterized and elastoplastic constitutive models are available. However, experimental results have shown that elastoplasticity does not seem sufficient to reproduce the yielding behaviour and an elastoviscoplastic approach is more adequate. On the other hand, saline porous aggregates show creep as salt rock itself also does. However salt rock creep models can not be easily extended to porous aggregates, because it is not clear if the deformation mechanisms are identical. According to this, total strain rate was conceptually divided into different terms in Eq. (3.17).

The basis for a comprehensive mechanical constitutive model for porous salt aggregates has been developed by Olivella et al. (1992, 1993, Chapter 4). The work is based on a theoretical and experimental research performed by Spiers and co-workers (Spiers et al., 1990) on salt aggregates. The model focuses on creep deformation due to its relative importance on the mechanical behaviour of salts. A creep law has been developed using a very simple geometry for grains and pores and applying the concepts of two different mechanisms of creep deformation: fluid assisted diffusional transfer (FADT) and dislocation creep(DC). The former one

(also called pressure solution) is a mechanism which explains deformation as a grain boundary salt migration through the liquid phase. Gradients of concentration (or chemical potential) are induced by difference in the stress state that exists in the solid grains. This mechanism is only active on wet salts, and it is very evident in volumetric deformation of granular aggregates. It is not necessary to have the voids fully saturated with brine, on the contrary, small quantities of brine (meniscus between grains) are sufficient for the mechanism to act. In the second mechanism we have included various possible processes related to dislocation movement (climb and glide) through the crystalline structure. In this mechanism, the creep deformation of the porous aggregate is explained from the creep deformation of the grains themselves.

The microstructural geometry together with basic laws for the mechanisms of deformation permit to obtain a macroscopic law for creep. Hence, creep deformation is obtained as:

$$\dot{\varepsilon}^c = \dot{\varepsilon}_1^c + \dot{\varepsilon}_2^c \tag{3.30}$$

where the creep strain rate has two components because there are two deformation mechanisms. In a similar way as for fluxes, the viscous parameters of the model depend, among other variables, on porosity (in this particular case expressed in terms of void ratio). For instance, volumetric creep strain rate experiences variations of several orders of magnitude for void ratio changes that are often encountered in real situations. For space reasons, it is not possible to include the developed mechanical constitutive law in this chapter. Details of the model are given by Olivella et al. (1992, 1993, Chapter 4).

3.8.3 Phase and interphase physical properties

The properties of phases appear in the balance equations and as parameters in constitutive laws. These are density, viscosity, surface tension and enthalpy. In general, they are considered dependent on the composition of the phase and on the independent variables (temperature and pressure).

The retention curve expresses the equilibrium between suction ($P_g - P_l$) and capillary forces (surface tension) in the meniscus. It is an empirical relationship which relates the dependence of fluid saturation and suction. If the medium is not very dry and adsorption is not important, then the dependence on temperature (Milly,1982) and concentration can be expressed in terms of surface tension. Several models for retention curve are available in the literature. Among them, the van Genuchten (1980) curve can be used. It has the advantadge that an associated relative permeability relationship can be used with the same parameters.

3.8.4 Inclusion migration law

The nonadvective term in the equation of water in inclusions or in salt balance equations represents the motion of these brine inclusions inside the solid phase. The mechanism of brine inclusions migration is different from the mechanims of nonadvective motion in fluid phases. Another relationship is required. Ratigan (1984) has proposed expressions for $\mathbf{i}_s^w$ and for f_s^w in terms of the inclusion point velocity ($\boldsymbol{v}_s^w$), the water content in solid phase (θ_s^w) and the ratio between volume and surface of grains (d):

$$\mathbf{i}_s^w = \mathbf{j}_s^{lw} = \theta_s^w(1-\phi)\boldsymbol{v}_s^w \tag{3.31}$$

and,

$$\boldsymbol{v}_s^w = -D_s^w \nabla T \tag{3.32}$$

where the inclusion velocity is primarily expressed with a linear dependence on temperature gradient. Yagnik (1983) has obtained an expression for velocity of inclusions, studying the mecanisms that cause this migration. The sink/source term of brine inclusions has been also given:

$$f_s^w = (1-\phi)\frac{|\boldsymbol{v}_s^w|\theta_s^w}{d} \tag{3.33}$$

3.9 Equilibrium restrictions

It has already been mentioned that the compositional approach has the advantadge that phase change terms do not appear explicitly. In fact, the number of equations of mass balance is reduced thanks to the assumption of equilibrium. This assumption is adequate because phase change processes are fast (instantaneous) compared to the processes (flow and deformation) in which we are interested. In this way species concentration in phases are considered dependent variables. These species are salt and air in liquid phase, and water in gas phase. The laws that express this equilibrium are solubility, Henry's law and psychrometric law.

The dependence of solubility on temperature is well documented. Although there is less experimental evidence, liquid pressure also influences salt solubility. On the other hand, the study of the pressure solution mechanism (Spiers et al. 1991) has shown that the stress state of the solid in contact with a brine does influence the concentration of salt in the liquid phase. For a preliminary version of the model, a simple dependence on temperature (T, ^{o}C) will be used (Langer and Offermann, 1982):

$$\omega_l^h = c/(100+c), \quad c = \frac{35.335 - 0.22947\,T}{1 - 0.0069059\,T} \tag{3.34}$$

This equation was obtained by fitting experimental data.

Henry's law expresses a linear relationship between the concentration of air in dissolution and the partial pressure of air in the gaseous phase. Due to the expected small influence of air dissolved in the general problem, this law is kept as an approximation.

Finally, it has been already pointed out that the classical form of psychrometric law is not valid for brines. Originally this law was obtained (Edlefson and Anderson, 1943) for pure water. The law expresses the variation of vapour density (or partial vapour pressure) in the gas due to the curvature of the surface of the liquid phase and the temperature (T, °K). That is:

$$\theta_g^w = (\theta_g^w)^o \exp\left(\frac{-(P_g - P_l)\, M_w}{RT\, \rho_l}\right) \tag{3.35}$$

where $(\theta_g^w)^o$ is the vapour density in the gaseous phase in contact with planar surface (i.e. $P_g - P_l = 0$) and depends on temperature. In the presence of a solute in the liquid phase, $(\theta_g^w)^o$ depends also on concentration. However, if a physical derivation is performed (Sprackling, 1985), it can be shown that the law is still valid when this dependence is taken into account. Therefore, the ambient relative humidity (as measured with a psychrometer) is referred to vapour in contact with pure water and does not coincide with the relative humidity which could be defined with this law which would be referred to brine. The former is related to the total suction and the latter is related to the matric suction. The osmotic suction is the difference between them and it is caused by the presence of the solute. Finally, the ideal dependence of vapour density (or partial vapour pressure) on concentration is expressed for ideal dissolutions by Raoult's law. At high concentrations, when the dissolution deviates from the ideal behaviour, empirical relationships which express the real dependence on temperature and concentration have to be used.

3.10 Summary

A general formulation for non-isothermal multiphase flow of brine and gas in saline media has been established. It has been developed with the objective of building a numerical tool to handle COupled DEformation, BRIne, Gas and Heat Transport problems (CODE-BRIGHT). It is supported on a constitutive theory, in which some laws are adopted from the literature and other are specifically developed or modified.

Apart from the general aspects of multiphase systems, the formulation also incorporates aspects which are important in saline media problems. These are: salt solubility (dissolution/precipitation, deformation by pressure solution),

instantaneous and creep deformation of the solid skeleton, inclusion migration and hygroscopic effects.

We believe that this formulation provides a sound basis on which to build general computational tools for the analysis of boundary value problems involving saline media in the form of aggregates or rock.

3.11 Appendix. Algebraic transformation of balance equations

The material derivative with respect to the solid velocity field will be very useful to obtain the final expressions for balance equations and is defined as:

$$\frac{D_s(\cdot)}{Dt} = \frac{\partial(\cdot)}{\partial t} + \dot{\boldsymbol{u}} \cdot \nabla(\cdot) \qquad (A1)$$

Reorganizing the salt mass balance equation (3.5) and using (A1) leads to the following expression for porosity evolution:

$$(\theta_s^h - \theta_l^h S_l)\frac{D_s\phi}{Dt} = (1-\phi)\frac{D_s\theta_s^h}{Dt} + \phi\frac{D_s(\theta_l^h S_l)}{Dt}$$

$$+ \nabla \cdot (\boldsymbol{j}_s'^h + \boldsymbol{j}_l'^h) + (\theta_s^h(1-\phi) + \theta_l^h \phi S_l)\nabla \cdot \dot{\boldsymbol{u}} - f^h \qquad (A2)$$

This equation expresses the variation of porosity as a result of the following causes: solid density variations, liquid-solid phase exchanges and porous medium deformation. It is interesting to see that this equation reduces to the solid balance equation when solubility and brine inclusions are not permitted. Moreover if solid phase is assumed incompressible, then a simple and well known form is obtained: $D_s\phi/Dt = (1-\phi)\nabla \cdot \dot{\boldsymbol{u}}$ which expresses the variation of porosity caused only by the volumetric deformation of the solid skeleton. A more convenient form for Equation (A2) is:

$$\frac{D_s\phi}{Dt} = \frac{1}{(\theta_s^h - \theta_l^h S_l)}\Big((1-\phi)\frac{D_s\theta_s^h}{Dt} + \phi\frac{D_s(\theta_l^h S_l)}{Dt}$$

$$+ \theta_s^h \nabla \cdot \dot{\boldsymbol{u}} + \nabla \cdot (\boldsymbol{j}_s'^h + \boldsymbol{j}_l'^h) - f^h\Big) - \phi\nabla \cdot \dot{\boldsymbol{u}} \qquad (A3)$$

The volumetric strain term ($\nabla \cdot \dot{\boldsymbol{u}}$) has been separated into two terms for algebraic reasons.

The equation of water mass balance (3.10), is transformed substituting definitions (3.7) through (3.9) and using the material derivative with respect the

solid velocity field (A1):

$$\phi\frac{D_s(\theta_l^w S_l + \theta_g^w S_g)}{Dt} + (1-\phi)\frac{D_s\theta_s^w}{Dt} + (\theta_l^w S_l + \theta_g^w S_g - \theta_s^w)\frac{D_s\phi}{Dt}$$

$$+\Big((\theta_l^w S_l + \theta_g^w S_g)\phi + \theta_s^w(1-\phi)\Big)\nabla\cdot\dot{\boldsymbol{u}} + \nabla\cdot(\boldsymbol{j}'^w_s + \boldsymbol{j}'^w_l + \boldsymbol{j}'^w_g) = f^w \quad (A4)$$

If the salt mass balance (A3) is used to express the variations of porosity, the final expression is obtained as:

$$\phi\frac{D_s(\theta_l^w S_l + \theta_g^w S_g)}{Dt} + (1-\phi)\frac{D_s\theta_s^w}{Dt} + \frac{(\theta_l^w S_l + \theta_g^w S_g - \theta_s^w)}{(\theta_s^h - \theta_l^h S_l)}\Big((1-\phi)\frac{D_s\theta_s^h}{Dt}$$

$$+\phi\frac{D_s(\theta_l^h S_l)}{Dt} + \theta_s^h\nabla\cdot\dot{\boldsymbol{u}} + \nabla\cdot(\boldsymbol{j}'^h_s + \boldsymbol{j}'^h_l) - f^h\Big) + \theta_s^w\nabla\cdot\dot{\boldsymbol{u}}$$

$$+\nabla\cdot(\boldsymbol{j}'^w_s + \boldsymbol{j}'^w_l + \boldsymbol{j}'^w_g) = f^w \quad (A5)$$

For the equation of air mass balance (3.14), using (3.12) and (3.13), rearranging the resulting equation, using the material derivative (A1) and the salt mass balance equation (A3), the final expression is obtained:

$$\phi\frac{D_s(\theta_l^a S_l + \theta_g^a S_g)}{Dt} + \frac{(\theta_l^a S_l + \theta_g^a S_g)}{(\theta_s^h - \theta_l^h S_l)}\Big((1-\phi)\frac{D_s\theta_s^h}{Dt} + \phi\frac{D_s(\theta_l^h S_l)}{Dt}$$

$$+\theta_s^h\nabla\cdot\dot{\boldsymbol{u}} + \nabla\cdot(\boldsymbol{j}'^h_s + \boldsymbol{j}'^h_l) - f^h\Big)$$

$$+\nabla\cdot(\boldsymbol{j}'^a_l + \boldsymbol{j}'^a_g) = f^a \quad (A6)$$

The reader may notice that formal differences between the equations of water (A5) and air (A6) balance are minor and arise from the adopted assumptions, mainly because the species air cannot be present in the solid phase.

The same transformations made in the previous mass balance equations are carried out on the water in inclusion balance equation (3.15) leading to:

$$(1-\phi)\frac{D_s\theta_s^w}{Dt} - \frac{\theta_s^w}{(\theta_s^h - \theta_l^h S_l)}\Big((1-\phi)\frac{D_s\theta_s^h}{Dt} + \phi\frac{D_s(\theta_l^h S_l)}{Dt}$$

$$+\theta_s^h\nabla\cdot\dot{\boldsymbol{u}} + \nabla\cdot(\boldsymbol{j}'^h_s + \boldsymbol{j}'^h_l) - f^h\Big) + \theta_s^w\nabla\cdot\dot{\boldsymbol{u}}$$

$$+ \nabla \cdot (j'^{w}_{s}) + f^{ws} = 0 \qquad (A7)$$

The equation for energy balance (3.24) is formally equal to the equation of water mass balance (3.10), hence an analogous algebraic transformation leads to:

$$\phi \frac{D_s(E_l\rho_l S_l + E_g\rho_g S_g)}{Dt} + (1-\phi)\frac{D_s(E_s\rho_s)}{Dt} + \frac{(E_l\rho_l S_l + E_g\rho_g S_g - E_s\rho_s)}{(\theta^h_s - \theta^h_l S_l)}\Big((1-\phi)$$

$$\frac{D_s\theta^h_s}{Dt} + \phi\frac{D_s(\theta^h_l S_l)}{Dt} + \theta^h_s \nabla\cdot\dot{\boldsymbol{u}} + \nabla\cdot(j'^h_s + j'^h_l) - f^h\Big) + E_s\rho_s\nabla\cdot\dot{\boldsymbol{u}} +$$

$$+ \nabla\cdot(i_c + j'_{Es} + j'_{El} + j'_{Eg}) = f^E \qquad (A8)$$

3.12 References

Abriola L.M. and Pinder, G.F. (1985): A Multiphase Approach to the Modeling of Porous Media Contamination by Organic Compounds. 1. Equation Development, Water Resources Research, Vol. 21, N° 1: 11-18.

Bachmat, Y. and J. Bear, (1986): Macroscopic Modelling of Transport Phenomena in Porous Media. 1: The continuum approach, Transport is Porous Media 1, 213-240.

Bear, J. (1972): Dynamics of fluids in porous media, American Elsevier Publishing Company, inc.

Bear, J. and Y. Bachmat, (1986): Macroscopic Modelling of Transport Phenomena in Porous Media. 2: Applications to Mass, Momentum and Energy Transport, Transport in Porous Media 1, 241-269.

Bear, J. and J. Bensabat, (1989): Advective Fluxes in Multiphase Porous Media Under Nonisothermal Conditions, Transport in Porous Media 4, 423-448.

Bear, J., J. Bensabat, and A. Nir (1991): Heat anf Mass Transfer in Unsaturated Porous Media at a Hot Boundary: I. One-Dimensional Analytical Model, Transport in Porous Media 6, 281-298.

Bird, R. B., W.E. Stewart and E.N. Lightfoot (1960): Transport Phenomena, John Wiley, New York, 1960.

Corapcioglu, M.Y., (1991): Formulation of Electro-Chemico-Osmotic Processes in Soils, Transport in Porous Media 6, 435-444.

Edlefson, N.E. and A.B.C. Anderson, (1943): Thermodynamics of soil moisture. Hilgardia, 15(2): 31-298.

Engelmann, H.J., P.W. Broochs, W. Hänsel and L. Peters, (1989): Dams as Sealing Systems in Rock Salt Formations - Test Dam Construction and Determination

of Permeability, Sealing of Radioactive Waste Repositories, Proceedings of an NEA/CEC Workshop, ISBN 92-64-03290-8, 151-162.

Faust, C.R. and J.W. Mercer, (1979): Geothermal Reservoir Simulation: 1. Mathematical Models for Liquid- and Vapour- Dominated Hydrothermal Systems, Water Resources Research, vol. 15, N° 1, 23-30.

van Genuchten, R., (1980): A closed-form equation for predicting the hydraulic conductivity of unsaturated soils, Soil Sci. Soc. Am. J.: 892-898.

Hassanizadeh, S.M. and W.G. Gray (1979a): General Conservation Equations for Multiphase Systems: 1. Averaging Procedure, Adv. Water Resour. 2: 131-144.

Hassanizadeh, S.M. and W.G. Gray (1979b): General Conservation Equations for Multiphase Systems: 2. Mass, momenta, energy and entropy equations, Adv. Water Resour. 2: 191-203.

Hassanizadeh, S.M. (1986a): Derivation of basic equations of mass transport in porous media, Part 1. Macroscopic balance laws, Adv. Water Resour. 9: 196-206.

Hassanizadeh, S.M. (1986b): Derivation of basic equations of mass transport in porous media, Part 2. Generalized Darcy's and Fick's laws, Adv. Water Resour. 9 207-222.

Horvath, A. L. (1985): Aqueous Electrolyte Solutions, Physical Properties, Estimation and Correlation Methods , Ellis Horword Limited, John Wiley and Sons.

Langer, H., and H. Offermann, (1982): On the solubility of Sodium Chloride in water, Journal of Crystal Growth, 60: 389-392.

Lewis, R.W., P.J. Roberts, B.A. Schrefler, (1989): Finite Element Modelling of Two-Phase Heat and Fluid Flow in Deforming Porous Media, Transport in Porous Media 4: 319-334.

Milly, P.C.D. (1982): Moisture and Heat Transport in Hysteretic, Inhomogeneous Porous Media: A Matric Head-Based Formulation and a Numerical Model, Water Resources Research, vol. 18, N° 3: 489-498.

Olivella, S.; A. Gens, E. E. Alonso and J. Carrera (1992): Constitutive Modelling of Porous Salt Aggregates, Proceedings of the Fourth International Symposium on Numerical Models in Geomechanics - NUMOG-IV/Swansea/UK/24-27 August 1992, A. A. Balkema, ISBN 90-54-10088-5, 179-189.

Olivella, S.; A. Gens, J. Carrera, and E. E. Alonso (1993): Behaviour of Porous Salt Aggregates. Constitutive and Field Equations for a Coupled Deformation, Brine, Gas and Heat Transport Model. Proceedings of the 3rd Conference on the Mechanical Behaviour of Salt, September 14:16, 1993, Ecole Polytechnique, Palaiseau-France:255-269

Panday, S. and M.Y. Corapcioglu (1989): Reservoir Transport Equations by Compositional Approach, Transport in Porous Media 4, 369-393.

Philip, J.R. and D.A. de Vries (1957): Moisture Movement in Porous Materials under Temperature Gradients, EOS Trans. AGU, 38(2):222-232.

Pinder, G.F. and L.M. Abriola (1986): On the Simulation of Nonaqueous Phase Organic Compounds in the Subsurface, Water Resources Research, Vol. 22, N° 9: 109S-119S.

Pollock, D.W. (1986): Simulation of Fluid Flow and Energy Transport Processes Associated WIth High-Level Radioactive Waste Disposal in Unsaturated Alluvium, Water Resources Research, Vol. 22, N° 5: 765-775.

Pruess, K. (1987): TOUGH user's guide. Report LBL-20700, NUREG/CR-4640, 80 pp.

Ratigan, J.L. (1984): A Finite Element Formulation for Brine Transport in Rock Salt, Int. J. for Num. and Analit. Meth. in Geomech., Vol. 8: 225-241.

Roedder, E. (1984): The Fluids in Salt, American Mineralogist, Vol. 69: 413-439.

Spiers, C.J., Schutjens, P.M.T.M., Brzesowsky, R.H., Peach, C.J., Liezenberg, J.L. and Zwart, H.J., (1990): Experimental determination of constitutive parameters governing creep of rock salt by pressure solution, Geological Society Special Publication no. 54: Deformation Mechanisms, Rheology and Tectonics. 215:227.

Sprackling, M.T. (1985): Liquids and Solids, Student Physics Series, King's College, University of London. Eds. Routledge and Kegan Paul.

Yagnik. S.K., (1983): Interfacial stability of migrating brine inclusions in alkali halide single crystals supporting a temperature gradient, Journal of Crystal Growth, 62: 612-626.

CHAPTER 4

MECHANICAL CONSTITUTIVE MODEL FOR CREEP DEFORMATION OF POROUS SALT AGGREGATES

4.1 Introduction

The study of seals for isolating purposes in saline media leads to the necessity of developing new approaches. Processes that take place in salt are not relevant in other geological materials. As mentioned before, the level of knowledge of the mechanical behaviour of salt rock is relatively high while the behaviour of porous salt aggregates is less known.

Seals in rock salt caverns are designed to be made of porous crushed salt with different degrees of initial compaction, that is, with different initial porosities (ϕ_0). Backfilling of cavities is made with crushed salt slightly compacted ($\phi_0 \approx 0.3-0.4$) while seals (also called dams) are built with salt bricks more compacted ($\phi_0 \approx 0.1-0.2$). Temperature and brine content are crucial variables in the mechanical behaviour of these aggregates.

A saline medium is composed by three phases. Each phase containing several species. The phases are described in terms of the components as: (1) solid grains made of crystalline sodium chloride, brine inclusions are encountered in the solid matrix, (2) liquid phase as a dissolution of salt and air in water, and, (3) gas phase as a mixture of dry air and water vapour.

The behaviour of porous salt aggregates is complex because the interaction between phases involves processes not relevant in other geological media. The interaction between solid and liquid phases includes dissolution and precipitation of salt. From the mechanical point of view, saline materials show relevant creep deformation. Presence of brine in pores allows a creep deformation based on dissolution/ precipitation at the pore scale level.

Coupling mechanical and hydraulic problems is important, among other well known reasons, because salt creep is strongly dependent on the presence of brine in grain contacts and pores. In fact, one of the creeping mechanisms (will be referred later as FADT) can only be active if brine is present.

On the other hand, there are several reasons for the need of using a nonisothermal approach. Of course, the primary reason is that temperature gradients exist in the problems of waste disposal. Among the reasons related to the medium composition, it should be noticed that the following processes strongly depend on temperature: (1) creep deformation of salt rock, creep strain rates are strongly dependent on temperature, (2) solubility of salt in water, the concentration of a saturated dissolution is a function of temperature (3) water vapour concentration and motion in gas phase, (4) viscous motion of fluids.

The study of a medium which has the microstructure described here forces to a physico-mathematical approach in the field of multiphase-multicomponent flow under nonisothermal conditions and including deformation. The investigation consists of formulation of the balance equations for mass, momentum and energy; development or adaptation of constitutive laws; and numerical solution.

The formulation of the balance equations can be found in Olivella et al (1994) and in Chapter 3. Partial differential equations were established paying specific attention to the relevant processes that take place in saline media. Mass balance of water, air and salt were obtained. Since the solute is assumed in equilibrium, the equation for salt balance is not required to solving for salt concentration. Then, it is substituted in the other balance equations to account for porosity variations. Accounting for porosity changes is crucial as this variable in turn leads to changes in hydraulic, thermal and mechanical behaviour. Energy balance for the porous medium as a whole is established under the the assumption of thermal equilibrium . The equation that represents the balance of momentum for the medium is the equilibrium of stresses. This means that the variation of solid velocities is negligible. Finally, balance of momentum for species and phases is reduced to constitutive laws, i.e. Darcy's and Fick's laws.

Among the constitutive laws that are required for this formulation, the stress-strain equation is associated with the equilibrium of stresses.

4.2 Mechanical behaviour of porous salt aggregates

A mechanical constitutive model for porous salt aggregates is developed in this chapter. Two main objectives had to be achieved, good predictive capabilities for

the stress-strain processes that take place in real conditions, and implementation in a coupled numerical tool. In order to accomplish the first objective it is necessary to compare the model with test results. For the second one, the equations theoretically developed should be transformed into a viscoelastic or viscoplastic framework.

The most relevant mechanisms of deformation in saline materials are linked with creep or ductile deformation. Rock salt is crystalline and the classical example of soft rock. While rock salt shows creep deformation at room temperature, other rocks require very high temperatures and degree of confinement to behave in a similar way, otherwise they deform in a brittle way.

A stress/temperature deformation mechanism map is presented in Figure 4.1. This map shows that depending on temperature and stress level, creep deformation takes place caused by different mechanisms. Glide and climb (low and high temperature) mechanisms are related to dislocation theory, hence, they can be seen as intracrystalline mechanisms. At high temperatures (T/Tm above 0.6, where $Tm \approx 800°C$ is meelting temperature) solid diffusion mechanisms may occur. At low stresses and temperatures the important mechanism of creep deformation is based on fluid assisted diffusion. This mechanim is intercrystalline because diffusion takes place along grain boundaries. In the map, the probable conditions for stresses and temperatures in backfills and seals is represented.

Since the expected conditions in the natural environment lead to conclude that the important creep deformation mechanisms are basically of two types, the constitutive model has been based on these two main mechanisms of deformation:

- Fluid Assisted Diffusional Transfer deformation (FADT)
- Dislocation creep deformation (DC)

Fluid assisted diffusional transfer creep refers to the mechanism of deformation based on the migration of salt through the liquid phase present in pores. This migration of salt is developed from contact to contact or from contact to pore and is driven by differences in chemical potential induced by differences in contact stresses.

Dislocation creep refers to the intracrystalline mechanisms characterized by the power creep law and explained through dislocation theory. As mentioned above, solid diffusion mechanisms are only important under high temperatures and low stress states, hence these mechanisms are not relevant for our objectives.

The model is based on an idealized geometry (Figure 4.2) for the

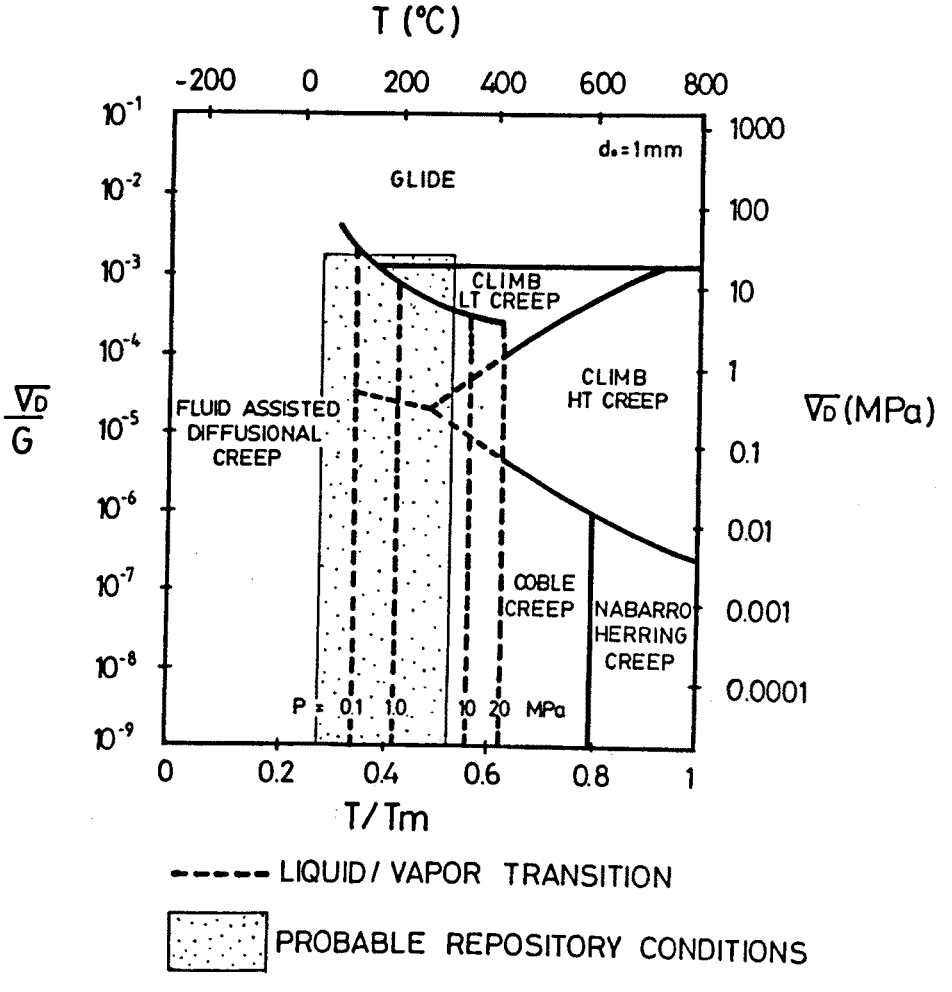

Figure 4.1: Stress/temperature deformation mechanism map for NaCl of 1 mm grain size. Adapted from Spiers (1986).

microstructure composed by a regular arrangement of polyhedrons. This idealized geometry is used as a basis for calculating strain rates and to obtain macroscopic laws. In order to provide a common framework for both mechanisms, the same idealized geometry is used. An idealized geometry for grains and pores could be based, for instance, on sperical particles. However, the microstructure of salt granular aggregates has been observed by Spiers and coworkers (1988; Schutjens, 1991), and these authors have shown micrographs where regular cubic forms can be clearly distinguished. It must be recalled that sodium cloride belongs to the crystallographic cubic system. This regular form of grains has led to idealize the geometry with polyhedral forms as simple as possible.

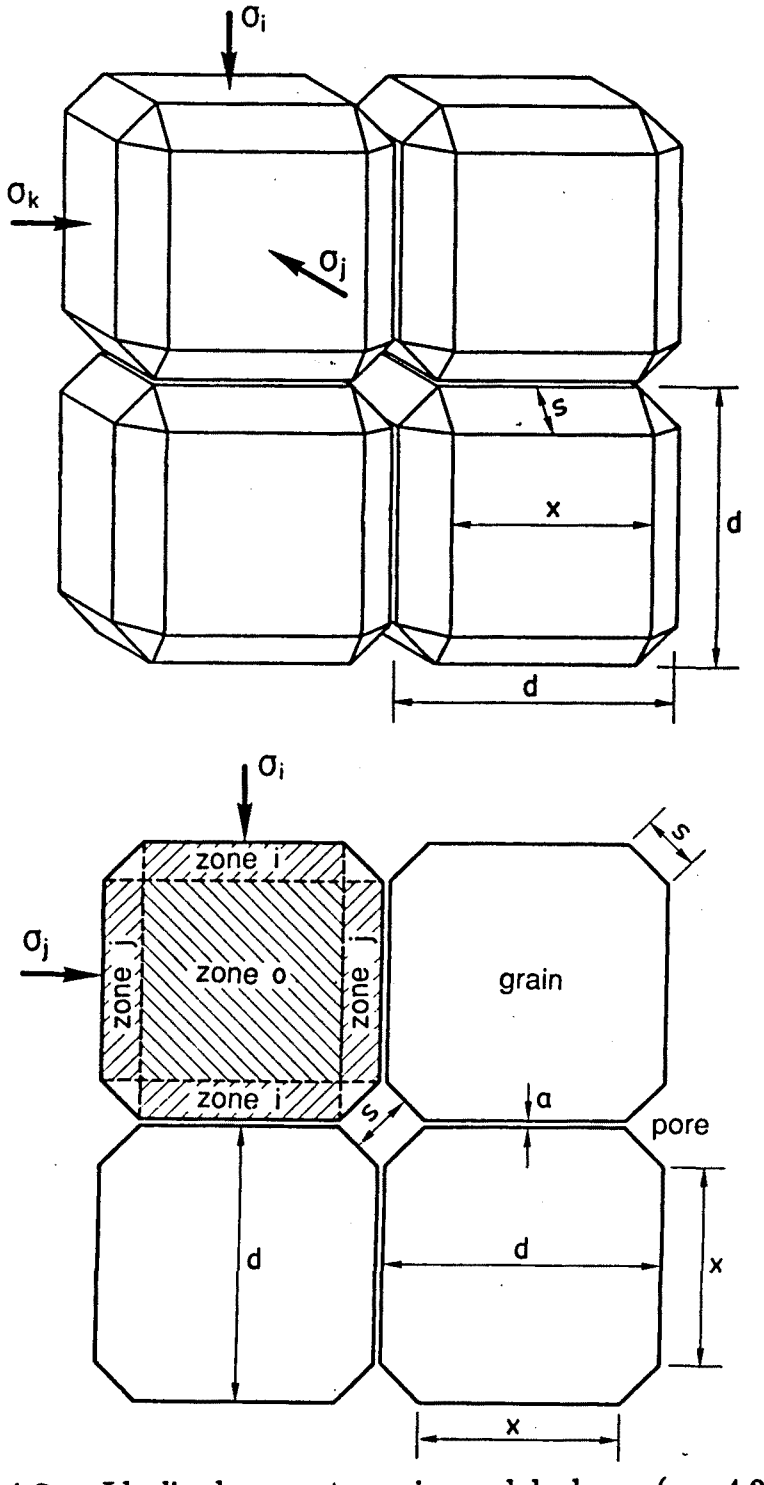

Figure 4.2a: Idealized geometry using polyhedrons (see 4.2b for variable definitions and derived expressions)

Geometrical variable	Symbol or equation	Comment
characteristic grain size	d_0	d_0^3 is the volume of the solid grain
distance between contacts	d	size of the circumscribed cube
pore size	s	
contact size	x	$x = d - \sqrt{2}s$
intercontact thickness	a	$a << s, d, d_0$
void volume	$3s^2d - \frac{4}{3}\sqrt{2}s^3 = \lambda_v s^2 d$	$\lambda_v = 3 - \frac{4}{3}\sqrt{2}\frac{s}{d}$ $\lambda_v = 3(1 - e^{3/2})$ (*)
void ratio	$e = \frac{3s^2d - \frac{4}{3}\sqrt{2}s^3}{d_0^3} = \frac{\lambda_v s^2 d}{d_0^3}$	void/solid vol.
mass conservation	$d^3 - ed_o^3 = d_o^3$	$d^3 = d_0^3(1+e)$
relative pore size	$\frac{s}{d} = \frac{\sqrt{\frac{e}{\lambda_v}}}{\sqrt{1+e}}$	only depends on e
relative contact size	$\frac{x}{d} = \frac{\sqrt{1+e} - \sqrt{\frac{2e}{\lambda_v}}}{\sqrt{1+e}}$	idem
relative stress concentration	$\frac{(\sigma_i)_c}{\sigma_i} = \frac{d^2}{x^2}$	idem

(*) modified function that improves predictions and avoids implicit expressions

Figure 4.2b: Definition of variables and derived expressions corresponding to the idealized geometry (see 4.2a). Relative pore size and contact size are variables that only depend on void ratio. They tend to zero and one, respectively, as void ratio vanishes.

In order to simplify the mathematical subsequent developments, there are two assumptions which are related with the idealized geometry. These are: the principal directions of the macroscopic stress state are normal to the faces of the idealized grain and the characteristic sizes d, s, a (see Figure 4.2) are equal in all directions.

Figure 4.2 shows the idealized geometry and several simple relationships in terms of the characteristic sizes: d grain size, s void size, and a contact thickness. For instance contact size is related with them as: $x = d - \sqrt{2}s$. Then void volume, void ratio and and ratio of stress concentration can be computed.

It is convenient to write every variable as a funtion of void ratio. In this way the introduction of these variables in physical equations, produces dependences on void ratio and not on the characteristic sizes. It should be pointed out that, unfortunately, the three-dimensional character of this geometry gives implicit expressions, hence it is not possible to put every variable in terms of void ratio. To overcome this practical dificulty the variable λ_v has been modified. The theoretical value is in Figure 4.2. In terms of the final equations of the model there is no problem of using implicit equations except that it is necessary to iterate. However, the parameter λ_v can be modified without loss of generality. The modification is also convenient because the theoretical expression predicts low stress concentrations for high void ratios. The modified λ_v has the following advantages: it is explicit, for low values of e converges to the theoretical one, and when comparing the model with experimental results for different values of e it has exhibited a better performance.

4.2.1 Fluid assisted diffusional transfer mechanism

The first mechanism that was investigated is FADT. It involves basically the deformation of grains by dissolution/ migration/ precipitation of salt from zones of stress concentration to zones of lower stress levels. Since salt migration takes place through the liquid phase, this mechanism will only operate if a brine film is present. For porous salt aggregates subject to relatively confined conditions, salt migration takes place from contacts to pores causing reduction of pore volume. This mechanism of deformation has been extensively studied by Spiers and co-workers (1986, 1988, 1990; Schutjens, 1991). Their ideas have been followed in the development of a constitutive model. Experimental data from these authors has been useful to validate the model predictions. Other results correspond to experiments carried out at our laboratory.

A solid in contact with its solution is a system where different processes take

place. Figure 4.3 shows a cross-section of the contact between two grains. It is assumed that the medium is saturated with brine at a P_l pressure and stress $\sigma_i, \sigma_j, \sigma_k$ are applyied externally in a macroscopic way.

Chemical potential (μ) is the driving force for dissolution/ transport/ precipitation of salt. For halite, and in absence of flow, the process is diffusion controlled (Schutjens, 1991). Two basic assumptions are usually accepted for developing deformation models: (1) chemical potential is the same in the solid and in the solution in contact with it, and, (2) differences in chemical potential are induced by differences in normal stress on the solid.

The diffusive mass flux of salt in solution is expressed as (Bird, 1961):

$$\mathbf{i} = -D\,\nabla\omega = -\tau\,\rho_l\,D_m\,\frac{\omega m}{RT}\nabla\mu \tag{4.1}$$

where ω is mass fraction of salt in dissolution and D is a coefficient of effective diffusion expressed as $D = \tau\rho_l D_m$, where τ a tortuosity coefficient, ρ_l liquid density and D_m molecular diffusion coefficient. The second equivalence in (4.1) has been obtained from the definition of chemical potential and the relationship between mass and mole fraction:

$$\mu = \mu_o + RT\log(\gamma\chi) \Rightarrow \frac{\nabla\chi}{\chi} = \frac{\nabla\mu}{RT}$$

$$\chi = \frac{\omega/M_h}{\omega/M_h + (1-\omega)/M_w} \Rightarrow \frac{\nabla\chi}{\chi} = \frac{\nabla\omega}{m\omega} \tag{4.2}$$

where χ is mole fraction of salt in dissolution, μ_o is a reference value for chemical potential, R is the constant of gases (8.314 J/mol/°K), T is absolute temperature, γ is activity coefficient and $m = M_w(\omega/M_h + (1-\omega)/M_w)$ is a conversion factor (M_h and M_w are molecular weights of salt and water, respectively).

The normal stress differences between contact and pores induce a mass flux of salt which reduces the grain and the pore sizes (d, s) while the mass is locally conserved. The variables used here are considered local and are used with the objective of obtaining a constitutive relationship. They should not be confused with the macroscopic ones which appear in the macroscopic balance equations.

The salt mass flux through the lateral area of the fluid film in the contact must equal the salt removed from the contact. This is expressed by:

$$4ax|\mathbf{i}| = \rho_s x^2 \dot{d} \quad \Rightarrow \quad \dot{d} = \frac{4a|\mathbf{i}|}{\rho_s x} \tag{4.3}$$

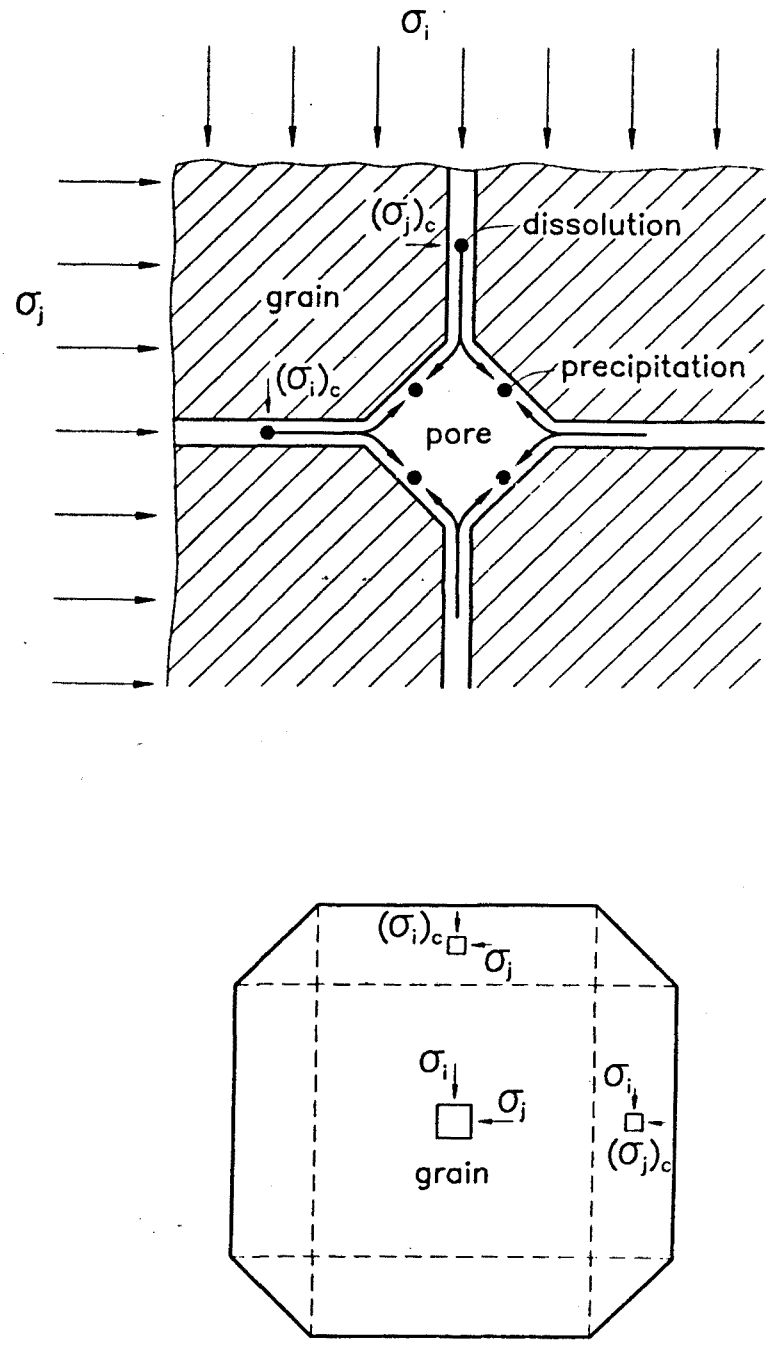

Figure 4.3: a) Fluid assisted diffusional transfer mechanism. Dissolution of salt takes place in contacts and precipitation in pores as a consequence of differences in chemical potential. b) Assumed distribution of stresses in the grain for the dislocation creep mechanism.

where | | is module, $\dot{d}$ is time variation of d, ρ_s is solid density and x is contact length. The chemical potential gradient is aproximated as:

$$\nabla\mu = \frac{\Delta\mu}{x/4} = \frac{\mu_{\text{pore}} - \mu_{\text{contact}}}{x/4} \tag{4.4}$$

assuming that the mean path of the solute in the contact is $x/4$. Considering that the medium is fully saturated with brine at pressure P_l, chemical potential in contacts and pores are approximated as:

$$\mu_{\text{contact}} = (\sigma_i')_c\, V_m + P_l\, V_m \qquad \mu_{\text{pore}} = P_l\, V_m + (p')_c\,(1-r)V_m \tag{4.5}$$

where V_m is molar volume, $\sigma_i' = \sigma_i - P_l$ is effective stress, $p' = (\sigma_1' + \sigma_2' + \sigma_3')/3$ is the mean effective stress and $()_c$ indicates contact stress (Figure 4.2). Obviously $()_c$ should be applied to the effective stress and not to the total stress.

As void ratio vanishes, chemical potential difference between contact and pore must also vanish, and consequently, the volumetric strain rate will go to zero. This is acomplished by the last term in (4.5) and $r = e^{3/2}$ has been adopted on an empirical basis. This is necessary because (4.5) does not express the change in relative areas of the contacts and pores. In other words, the surface of the grain that is exposed to the pore progressively becomes in the contact as void volume decreases.

Strain rate along principal directions (i) is obtained by combination of the above equations and the relationships derived from the geometry:

$$\dot{\varepsilon}_i = \left(\frac{\dot{d}}{d}\right)_i = 16\,\frac{\tau D_m \rho_l m\omega V_m a}{RT\rho_s}\,\frac{(\sigma_i' - p'(1-r))d^2}{dx^2x^2} =$$

$$= \frac{16\,B(T)}{d_0^3}\,\frac{(\sigma_i' - p'(1-r))(1+e)}{\left(\sqrt{1+e} - \sqrt{\frac{2e}{\lambda_v}}\right)^4} \tag{4.6}$$

where $B(T)$ includes the set of physical parameters which depend on temperature and physical properties of the mineral.

Volumetric strain rate is obtained as:

$$\dot{\varepsilon}_v = \dot{\varepsilon}_1 + \dot{\varepsilon}_2 + \dot{\varepsilon}_3 = \frac{16B(T)}{d_0^3}\,\frac{3(1+e)e^{3/2}}{\left(\sqrt[2]{1+e} - \sqrt[2]{\frac{2e}{\lambda_v}}\right)^4}\,p' \tag{4.7}$$

which correctly vanishes when void ratio tends to zero. In order to compare with experimental results, it is useful to obtain the void ratio change as: $\dot{e} = (1+e)\dot{\varepsilon}_v$.

An important result is that a linear dependence of this mechanism on stresses is found. Deviatoric strain rate is simply defined as $\dot{e}_i = \dot{\varepsilon}_i - \dot{\varepsilon}_v/3$, which leads to the corresponding expression for deviatoric deformation under deviatoric stress.

Another point that deserves further comments is the presence of brine in pores. The development presented above assumes that the medium is fully saturated with brine. However, this is not necessary for the mechanism to be active. Without loss of generality, for the unsaturated conditions effective stresses should change to net stresses in (4.5) but the term $P_l V_m$ does not change although pressure may become negative.

On the other hand, experimental results (Figure 4.4) have shown that a reduction of the strain rate takes place under unsaturated conditions, specially at low saturation levels. This can be explained by a reduction of brine film thickness (a) due to suction forces and/or an increase of tortuosity (reduction of τ). A dependence on the square root of degree of saturation (S_l) has been chosen on an empirical basis. Backfills and dams are likely to have small quantities of brine which may be sufficient for the FADT mechanism to be active. For the experimental conditions of the test in Figure 4.4 (4.2 MPa of mean stress, 22°C, $d_0 = 275$ μm) FADT seems to be the most relevant strain mechanism, at least in the range of degrees of saturation studied. If the medium becomes drier, then other strain mechanisms may become more relevant.

The final equations for FADT mechanism (here referred as mechanism I) express strain rate as a function of several variables. The linear dependence on stresses allow to use a viscoelastic approach for this mechanism:

$$\dot{\boldsymbol{\varepsilon}}_I^c = \frac{1}{2\eta_I^d}(\boldsymbol{\sigma}' - p'\boldsymbol{I}) + \frac{1}{3\eta_I^v} p'\boldsymbol{I} \tag{4.8}$$

where $\boldsymbol{\sigma}'$ is the net stress tensor (defined as $\boldsymbol{\sigma}' = \boldsymbol{\sigma} - P_f \boldsymbol{I}$, P_f is fluid pressure, gas if unsaturated and liquid if saturated), p' is the mean net stress, $\boldsymbol{I}$ is the identity tensor, and the volumetric and deviatoric (η_I^v and η_I^d) viscous functions are defined as:

$$\frac{1}{\eta_I^v} = \frac{16\, B(T)\sqrt{S_l}}{d_o^3} \frac{3\, g^2\, e^{3/2}}{(1+e)} = C(T, S_l, d_0)\, g_I^v(e) \tag{4.9}$$

$$\frac{1}{2\eta_I^d} = \frac{16\, B(T)\sqrt{S_l}}{d_o^3} \frac{g^2}{(1+e)} = C(T, S_l, d_0)\, g_I^d(e) \tag{4.10}$$

The function $C(T, S_l, d_0)$ compiles the information related essentially to grain size,

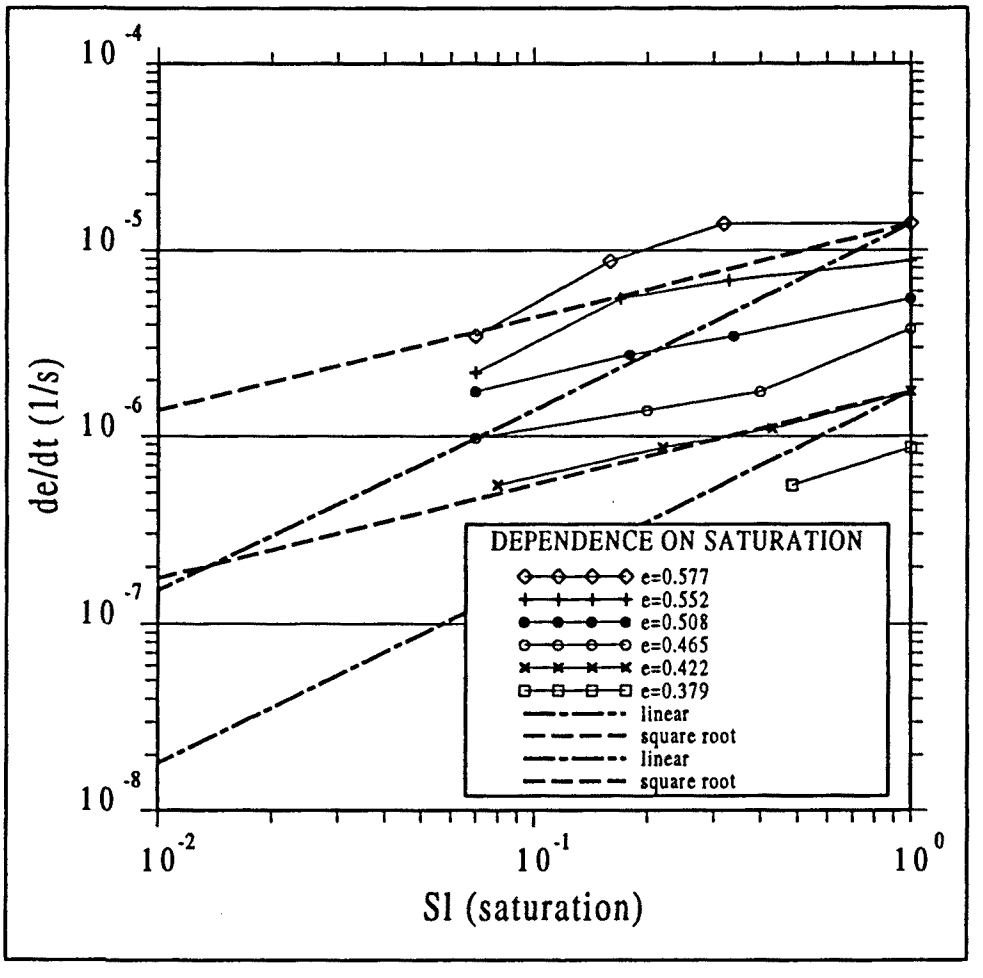

Figure 4.4: Dependence of strain rate on degreee of saturation. Strain rate as a function of brine degree of saturation (S_l). Linear and square root relationships are included. Experimental data from Spiers et al (1988).

brine content and temperature. The function g has the form:

$$g = \frac{(1+e)}{\left(\sqrt{1+e} - \sqrt{\frac{2e}{\lambda_v}}\right)^2} = \frac{1}{(1-f)^2} \qquad f = \frac{\sqrt{\frac{2e}{\lambda_v}}}{\sqrt{1+e}} \qquad \lambda_v = 3(1-e^{3/2}) \tag{4.11}$$

The function g, comes from the adopted geometry (Figure 4.2) and expresses the ratio between stress in grain contacts and external applied stress, hence g tends to one as void ratio vanishes. The function f expresses the ratio between void

size and grain size, hence f tends to zero as void ratio vanishes. Figure 4.5 shows the form of the auxiliary functions g_I^v and g_I^d that have been defined in (4.9) and (4.10). These functions contain the information that comes from the porous structure and depend on the idealized geometry used to develop the model. Hence, once the geometry is fixed, they only depend on void ratio (e). The reader may notice that, as void ratio tends to zero, the volumetric counterpart vanishes while the deviatoric counterpart goes to one. The two functions increase monotonically as void ratio increases.

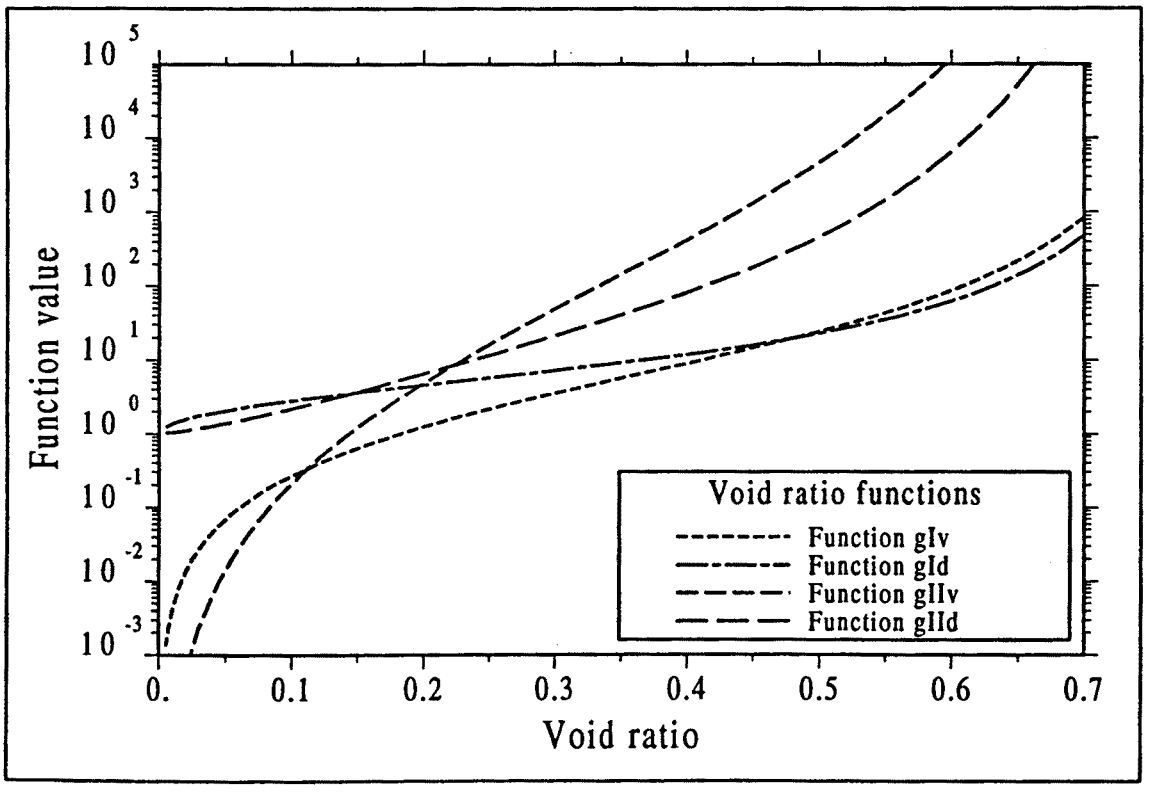

Figure 4.5: Void ratio functions. g_I^v, g_I^d, (corresponding to mechanism FADT) and g_{II}^v, g_{II}^d, (corresponding to mechanism DC).

4.2.2 Dislocation creep mechanism

The second mechanism included in the model is called DC (dislocation creep

strain). With this name several strain mechanisms related to dislocation theory are grouped. The most important one is dislocation climb, but glide of dislocations can also take place. The main reason for this grouping is that these mechanims can be represented by power law terms, i.e. the same mathematical representation corresponds to various possible strain mechanisms. A very comprehensive discussion of the relevance of the different mechanisms of crystalline deformation in salt rock can be found for instance in Munson and Dawson (1981).

For axisymmetric and generalized case, creep power law for rock salt can be respectively written as:

$$\dot{\varepsilon}_1 = A(T)(\sigma_1 - \sigma_3)^n \qquad \dot{\varepsilon} = A(T)q^n \frac{\partial q}{\partial \sigma} \tag{4.12}$$

where $A(T)$ is a temperature dependent parameter, $q = \sqrt{3J_2}$ is a deviatoric stress, J_2 is the second invariant of the deviatoric part of the stress tensor and n is the power of the law. It is important to notice that these two forms do not allow volumetric creep deformation. The power law will be combined with the geometry to obtain a law for porous aggregates.

The generalized expression can be particularized along principal directions:

$$\dot{\varepsilon}_i = A(T)q^n \frac{\partial q}{\partial J_2}\frac{\partial J_2}{\partial \sigma_i} = \frac{3}{2}Aq^{n-1}(\sigma_i - p)$$

$$J_2 = \frac{1}{6}((\sigma_1 - \sigma_2)^2 + (\sigma_2 - \sigma_3)^2 + (\sigma_3 - \sigma_1)^2) \tag{4.13}$$

where $p = (\sigma_1 + \sigma_2 + \sigma_3)/3$ is mean stress. It does not matter if net or total stress is used here because deviatoric stresses do not depend on pore pressure.

From the basic mechanism equations and the proposed geometry a macroscopic law is sought. However it is not possible to obtain analytical expressions without making further assumptions. For this reason, deformations are computed assuming a simple stress distribution inside the grain. Figure 4.2 shows the cross-section of the grain and different zones are distinguished, o, i and j (k would appear in another cross-section). It is assumed that in zone o the stress state is equal to the macroscopic one. In the i zone, the stress state shows the influence of stress concentration in contacts, and the stress state is $(\sigma_i')_c$, σ_j' and σ_k', i.e., the corresponding principal net stress is concentrated while the other remain equal to the macroscopic ones. Again concentration of stresses is made over net or effective stress. The assumption of using average stresses in the various zones considered has been demonstrated to be valid to a high degree of approximation by means of finite element computations at the grain level (Olivella et al. 1992).

With these assumptions, the following expression for strain rate along any principal direction i is obtained:

$$\dot{\varepsilon}_i = \left(\frac{\dot{d}}{d}\right)_i = \frac{3}{2}A(T)q_i^{n-1}((\sigma_i')_c - p_i')\frac{\sqrt{2}s}{d} + \frac{3}{2}A(T)q^{n-1}(\sigma_i' - p')\frac{x}{d} \qquad (4.14)$$

where p_i' and q_i are mean net stress and deviatoric stress in zone i (Figure 4.2), i.e. computed with, $(\sigma_i')_c$, σ_j' and σ_k'; and, p' and q are mean net stress and deviatoric stress in zone o, i.e. computed with σ_i', σ_j' and σ_k'. In this equation, the first term corresponds to the strain of the area near contacts and the second term corresponds to the strain in the core of the grain. As porosity tends to zero, the first term vanishes, and the original law for rock salt is obtained. In the same way as for FADT mecanism the volumetric strain law for DC can be obtained. However, a more simple expression is obtained if the stress state is considered isotropic ($\sigma_1' = \sigma_2' = \sigma_3'$):

$$\dot{\varepsilon}_v = 3A(T)((p')_c - p')^n\frac{\sqrt{2}s}{d} = 3A(T)\left(\frac{(1+e)}{\left(\sqrt{1+e} - \sqrt{\frac{2e}{\lambda_v}}\right)^2} - 1\right)^n \frac{\sqrt{\frac{2e}{\lambda_v}}}{\sqrt{1+e}}(p')^n \qquad (4.15)$$

In order to obtain a deviatoric viscous parameter in a simple way, pure shear conditions are assumed, i.e. $\sigma_3' = -\sigma_1'$ and $\sigma_2' = 0$:

$$\dot{\varepsilon}_1 = \frac{3}{2}A(T)\left(\left(\sqrt{1+g+g^2}\right)^{n-1}\left(\frac{2g+1}{3}\right)f + (\sqrt{3})^{n-1}\frac{1}{\sqrt{g}}\right)\sigma_1'^n \qquad (4.16)$$

The nonlinear dependence of strain rate on stress leads to nonlinear mathematical relationships. This implies that the extension to three dimensional stress states should be performed using a flow rule. This can be written in general as (DC mechanism is referred as II):

$$\dot{\varepsilon}_{II}^c = \frac{1}{\eta_{II}^d}\Phi(F)\frac{\partial G}{\partial \sigma'} \qquad (4.17)$$

where G is the flow rule, F is a stress function and Φ is a scalar function. G and F should be taken functions of stress invariants and of the volumetric and deviatoric viscous parameters (η_{II}^v and η_{II}^d). The following form has been adopted:

$$F = G = \left(q^2 + \left(\frac{p'}{\alpha_p}\right)^2\right)^{1/2} - 1 = 0 \qquad \Phi(F) = (F+1)^n \qquad \alpha_p = \left(\frac{\eta_{II}^v}{\eta_{II}^d}\right)^{1/(n+1)} \qquad (4.18)$$

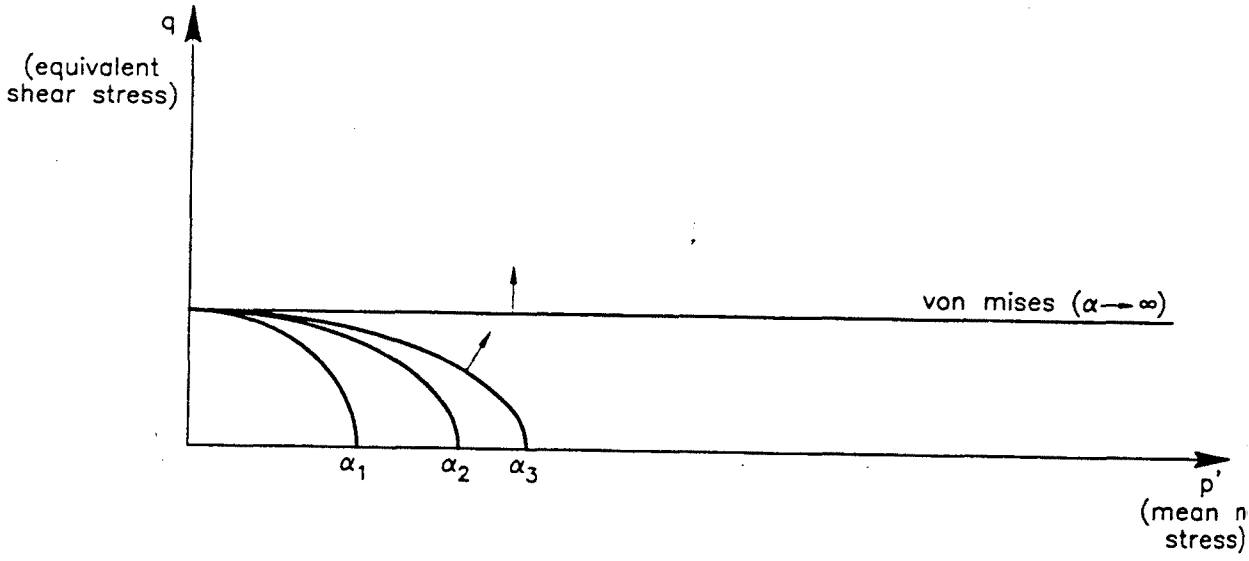

Figure 4.6: Flow rule used for the nonlinear counterpart of the model (DC mechanism).

where n is the power of the rock creep law. Figure 4.6 shows the shape of the flow rule.

Equations (4.15) and (4.16) provide volumetric and deviatoric viscous parameters, which can be written as:

$$\frac{1}{\eta_{II}^{v}} = 3A(T)(g-1)^{n} f = A(T)\, g_{II}^{v}(e) \tag{4.19}$$

$$\frac{1}{\eta_{II}^{d}} = A(T)\left[\left(\sqrt{\frac{1+g+g^2}{3}}\right)^{n-1}\left(\frac{2g+1}{3}\right) f + \frac{1}{\sqrt{g}}\right] = A(T)\, g_{II}^{d}(e) \tag{4.20}$$

where g and f have already been defined in (4.11), $A(T)$ and n come directly from the creep power law for rock salt, i.e. the nonporous material. The functions $g_{II}^{v}(e)$ and $g_{II}^{d}(e)$ depend on the idealized geometry and in turn on void ratio. However, because the originally nonlinear power law, a dependence on the power n remains in these functions. Since this parameter (n) does not change very much in saline materials, this power in the geometrical function does not represent a

practical difficulty. A value of $n = 5$ has been used to calculate these functions (Figure 4.5) which is a theoretical value for dislocation climb plus glide (Frost and Ashby, 1982). Similar comments are valid for these functions as the ones performed regarding FADT mechanism. However, for DC these functions show much higher increase as void ratio increases. This is a direct consequence of the power dependence, a smaller slope would be obtained for $n < 5$ instead of $n = 5$.

The functional-parameter α_p has been defined in such a way that the volumetric strain vanishes as void ratio tends to zero. When void ratio vanishes α_p tends to infinity and the mathematical expression of F (see Eq. 4.18) reduces to the von Mises case. In this way the creep law for rock salt is recovered (i.e. von Mises flow rule). No threshold value for creep of saline materials is usually found. Therefore it is assumed that the creep mechanisms operate under any stress level. With the flow rule adopted, the model does not allow dilatancy behaviour, and it is expected to be adequate only for high confinement situations. Another point is that the consistently derived equation (4.14) and the generalization with a flow rule practically give the same results, at least, for relatively high confinement states.

4.2.3 Final equation of the model

The physical description of the model for creep presented in this chapter indicates that two independent deformation mechanisms contribute to the total strain rate. FADT is intecrystalline while DC is intracrystalline. Hence, there is no reason that prevents to combine them in an additive way. Therefore, the creep strain rate can be written as the sum of (4.8) and (4.17), that is:

$$\dot{\boldsymbol{\varepsilon}}^c = \dot{\boldsymbol{\varepsilon}}^c_I + \dot{\boldsymbol{\varepsilon}}^c_{II} = = \frac{1}{2\eta^d_I}(\boldsymbol{\sigma}' - p'\boldsymbol{I}) + \frac{1}{3\eta^v_I}p'\boldsymbol{I} + \frac{1}{\eta^d_{II}}\Phi(F)\frac{\partial G}{\partial \boldsymbol{\sigma}'} \qquad (4.21)$$

The set of variables temperature, stress level, grain size and brine content can give a predominance of one mechanism over the other. For instance, if the medium is absolutely dry, or, it has a very large grain size, DC will predominate over FADT. On the contrary if grain size is small (say hundreds of microns) and brine is present, FADT will predominate, specially at low stresses.

Figure 4.7 shows the influence of stress level on the relative importance of mechanisms. Temperature (20 °C) and grain size (500 μm) were kept unchanged, and the medium was assumed saturated with brine. It can be observed that DC only manages to overcome FADT for high stresses (20 MPa) and high void ratios

(above 0.3) indicating that if brine is present FADT will always be predominant at this temperature and grain size. For larger grain sizes the relative importance of DC increases, in other words, not such high streses are required in order that DC overcomes FADT. On the other hand, FADT contribution decreases if the brine content goes below saturation, while DC is not affected by this variable.

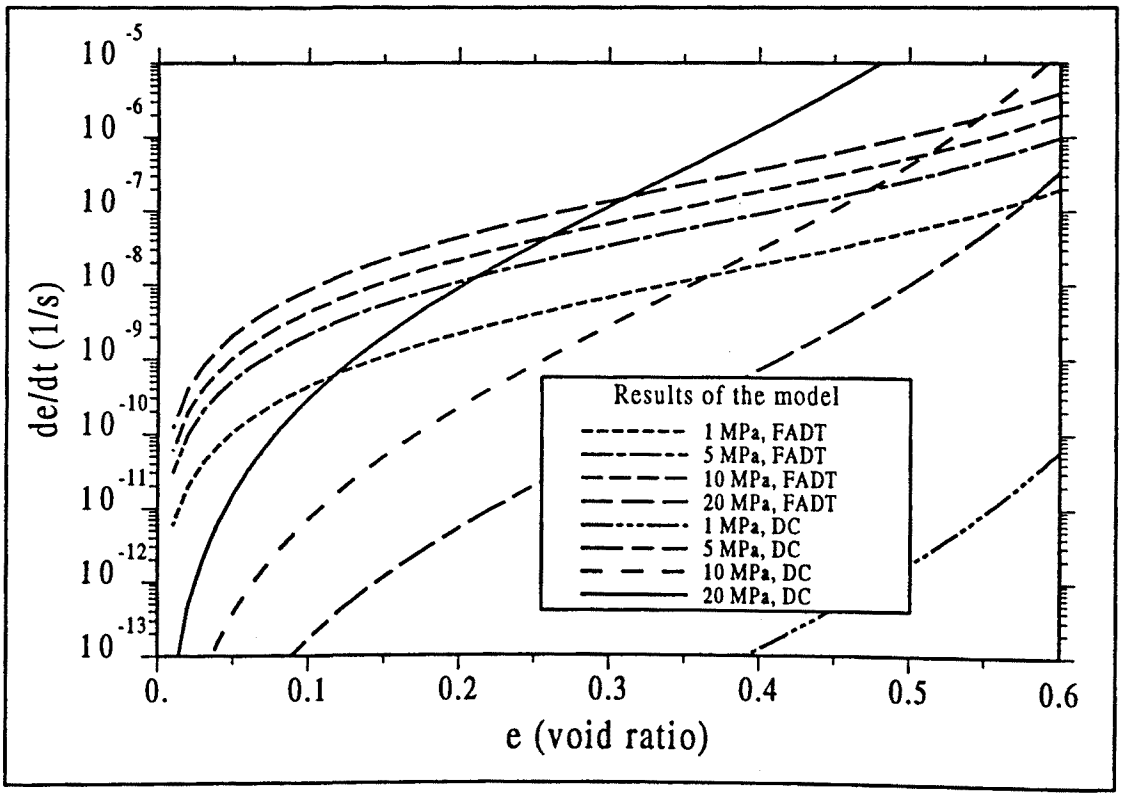

Figure 4.7: Strain rates under isotropic stress computed with the model as a function of several variables. Temperature is 20 °C and grain size is 500 μm. The contribution of DC and FADT mechanisms is shown separately in order to demonstrate that one of them may predominate over the other.

4.3 Model predictions

The model has been compared with isotropic and oedometric creep test results reported in the literature under dry and saturated conditions giving good

predictions using single values for $B(T)$ and $A(T)$ regardless of the other variables (e.g. stress, grain size). In fact $B(T)$ and $A(T)$ are for salt rock, therefore they must depend only on the nature of the medium, in this case sodium cloride. However, this is not always true and different origin of the rock may produce small variations on the coefficients.

In the model predictions included here we have used the following values: Dislocation creep (DC):

$$A(T) = 5 \times 10^{-6} \exp(\frac{-59650}{RT}) \text{s}^{-1}\ \text{MPa}^{-n} \qquad n = 5.375$$

Fluid assisted diffusional transfer creep (FADT):

$$B(T) = \frac{6 \times 10^{-13}}{RT} \exp(\frac{-24530}{RT})\ \text{s}^{-1}\text{MPa}^{-1}\text{m}^3$$

The two parameters have different units because each mechanism of deformation shows different dependences. For DC the adopted values correspond to typical values for rock salt (from Asse mine) deviatoric creep deformation. For FADT, the constant inside the exponential has been taken from Spiers et al (1990) while the pre-exponential constant has been taken suitable to reproduce the experimental test described below (Figures 4.10 and 4.11).

Figures 4.8 and 4.9 show comparisons with tests results obtained in the literature. Figure 4.8 is a clear example of deformation under the dominance of FADT mechanism because the small grain size of the material used (50-75 and 125-150 μm) and the low stress level. On the contrary, Figure 4.9 shows two tests carried out under relatively dry conditions, higher stresses and, in one of them, higher temperature. For these reasons, in this case, the predominant strain mechanism is DC. In both Figures (4.8 and 4.9), only the counterpart of the model corresponding to the predominant mechanism was represented because the remaining counterpart produces negligible contribution.

Also results of an oedometric laboratory test carried out in our Department (Chumbe, 1994) have been used to compare the predictions of the model. The test was carried out at 25 °C and under brine saturated conditions. The salt powder was obtained at the Suria mine (Spain) and the sample prepared with a controlled grain size of 0.520 mm. Four steps of stress were applied to the sample, these are: 0.6,3.7,6.0 and 30 MPa. The high load for the last stage was mainly used in order to finish the test in a shorter time. These high stresses are seldom reached in a backfilling material due to its low stiffness compared to the host rock.

Figure 4.10 creep strain rates as a function of void ratio and Figure 4.11 the time evolution of void ratio. The representation of strain rates versus void ratio

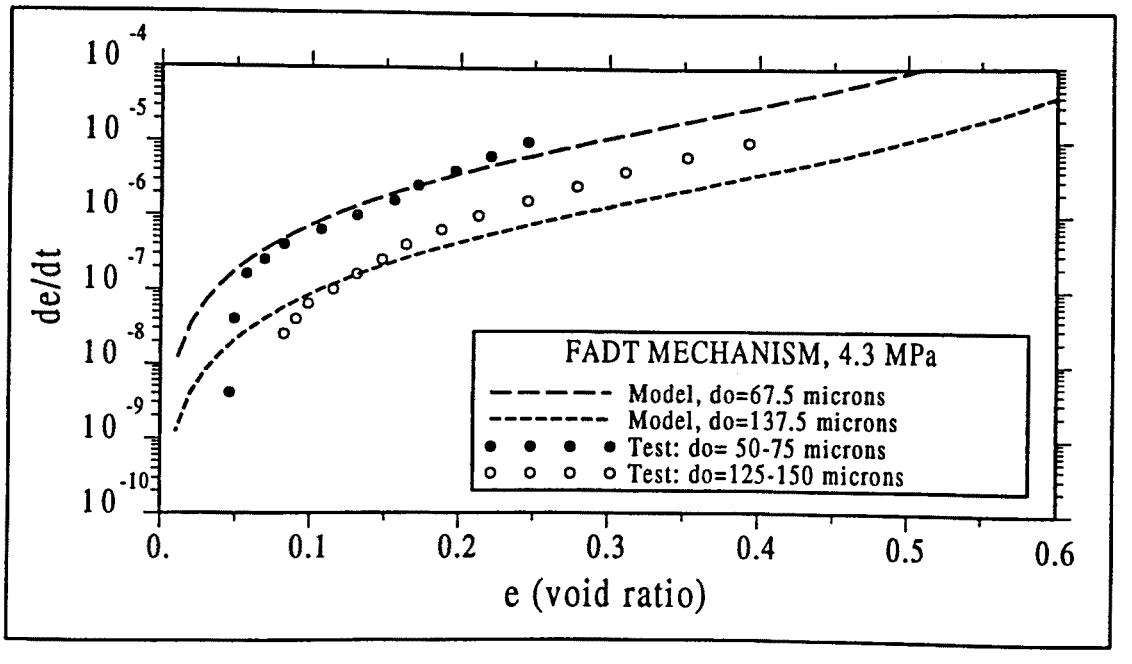

Figure 4.8: Comparison of the model (FADT mechanism) predictions with experimental results for isotropic deformation of saturated medium at 4.3 MPa, 21 °C and grain size 50-75 μm and 125-150 μm. Data adapted from Schutjens, (1991).

(for instance in Figure 4.10) is very useful because it allows the estimation of the creep parameters. In this test the contribution of both mechanisms of deformation was computed because of the high stress used during the last step (30 MPa). Which mechanism gives more contribution is deduced by comparison of the shape of the curves in Figure 4.10 with the shape of the functions g_I^v and g_{II}^v drawn in Figure 4.4. In fact, only for the higher stress value (30 MPa) DC is dominant in almost all the range of void ratios, except for $e < 0.1$ where FADT gives more contribution. For the remaining stress levels, FADT dominates in almost all the range. The exception is for void ratio $e > 0.6$ where DC is dominant for 3.7 and 6 MPa.

The creep strain rates do not predict very well the transient period immediatly after the stress increment. This behaviour was expected because instantaneous deformation is also taking place. For computing time evolution of void ratio, an instantaneous elastic behaviour is assumed which gives relatively good results. A linear model has been used with a Young modulus of 2000 MPa and a Poisson

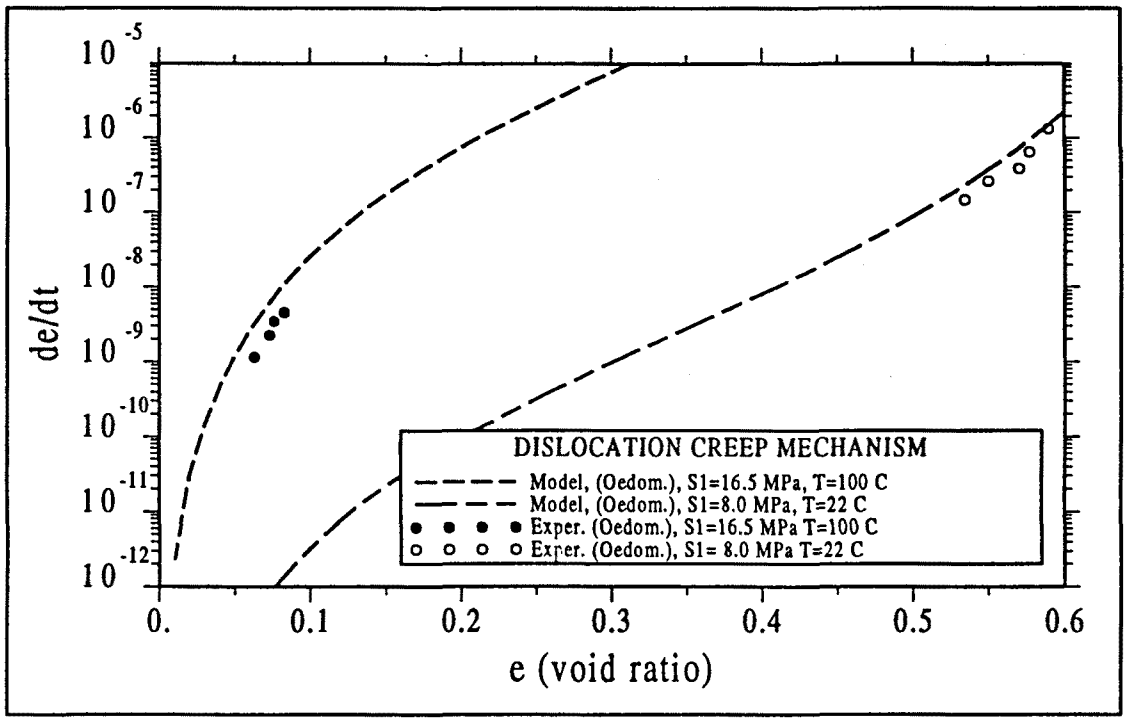

Figure 4.9: Comparison of the model (DC) predictions (for oedometric deformation) with experimental results of oedometric deformation at 16.5 MPa and 100 °C (after Stührenberg, 1990) and 8.0 MPa and 22 °C (after Spiers, 1988).

modulus of 0.30. With these values, practically no elastic contribution takes place. Also a non-linear model ($\Delta\varepsilon_v = -\lambda\Delta[\ln p']$) for the elastic counterpart has been used with $\lambda = 0.01$, and with shear modulus of 10 MPa. Elastic strain contribution is not negligible in this case, but the final void ratio is similar which is coherent because both models for instantaneous deformation are reversible.

A deviation of strain rates is obtained for low void ratios. The observed strain rates are smaller than the ones predicted. It should be pointed out that the model assumes perfect connectivity of pores until they completely close. However, as deformation progresses brine is squeezed from the sample. This is not accounted in the comparison presented here because it is required a coupled analysis. The resulting coupled strain rates are probably controlled by permeability to brine. The tests reported by Schutjens (1991) and used to compare with the model gives the same kind of behaviour (see Figure 4.8). A coupled analysis permits to model this phenomenon, brine in pores increases its pressure (effective stress decreases)

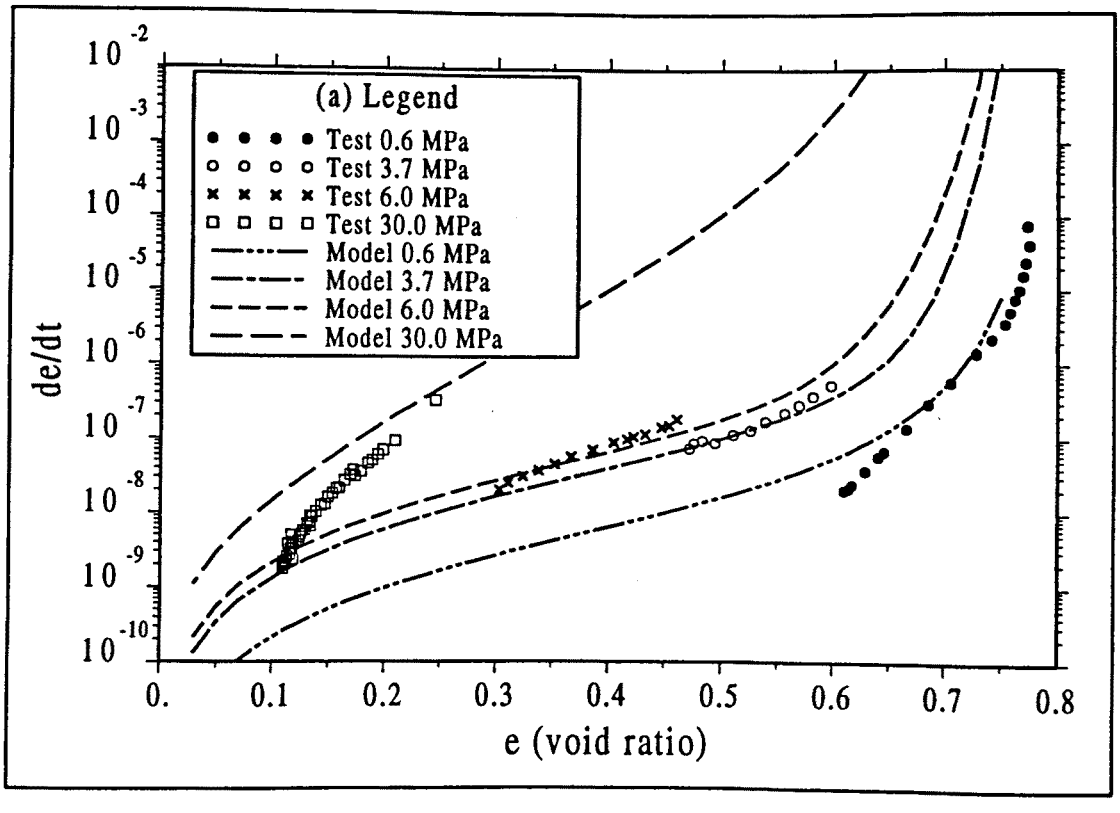

Figure 4.10: Comparison of oedometric test results with model (both mechanisms) predictions (for oedometric deformation). Creep strain rates as a function of void ratio for the different stress level periods.

and deformation takes place at a lower rate. The results of the analysis compared with the predictions of the model seem to indicate that a fraction of voids has become unconnected. Therefore brine cannot be squeezed out and strain rate reduces. However, further laboratory investigation is required. One aspect which is very important in the interpretation of laboratory tests is the measurement of porosity of the samples. At lower values of porosity the accumulated measurement error increases.

4.4 Conclusions

The mechanical constitutive model presented here is a relevant contribution in the study of the mechanical behaviour of porous salt aggregates. It has been shown how from a simple idealized geometry and theoretical considerations for two

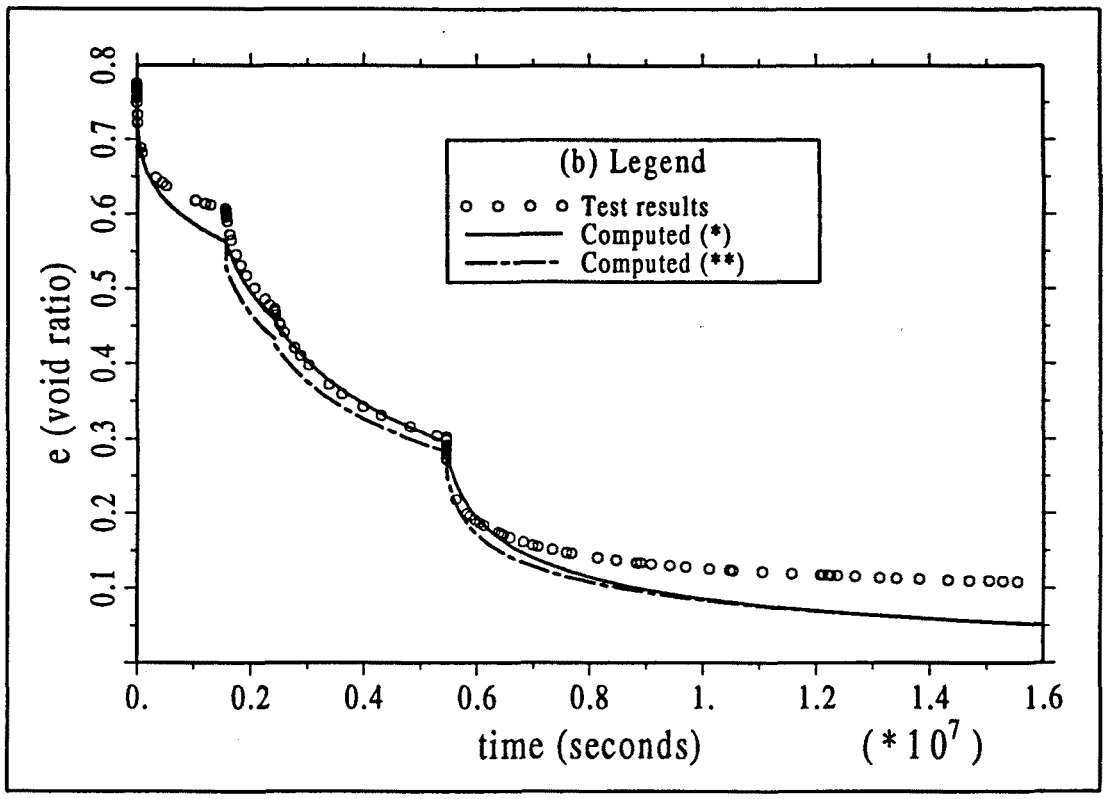

Figure 4.11: Comparison of oedometric test results with model (both mechanisms) predictions (for oedometric deformation). Time evolution of void ratio, (*) creep deformation combined with linear elasticity and (**) creep deformation combined with non-linear elasticity

mechanisms of deformation, a macrocopic stress/strain rate law can be obtained. A nonlinear viscoelastic approach is used to obtain a general form of the model.

The main variables that control creep behaviour of porous salt aggregates are: stress, void ratio, grain size, brine content and temperature. The obtained model shows the kind of dependence that is expected. Dependence on stress results linear for FADT and nonlinear (power type) for DC. Dependence on grain size is a negative cubic power for FADT while no dependence has been found for DC. The dependence on void ratio is mathematically complex because of the three dimensional geometry of the microstructure. From experimental results, the square root of brine saturation is proposed as a weighting function for the FADT mechanism counterpart, while DC is not influenced by brine content.

The strain rates predicted by the model have been compared with test results under different situations giving good agreement. The same parameters were used for the different comparisons. Finally, a simulation of void ratio evolution has been performed and compared with the experimental values. It demonstrates that creep strains predominate over elastic or plastic strains. Therefore the model can be used to study the behaviour of sealing structures made of compacted crushed salt.

4.5 References

Bird, R. B., W.E. Stewart and E.N. Lightfoot (1960):"Transport Phenomena", John Wiley, New York, 1960.

Chumbe, D., 1994, Personal communication

Frost and Ashby, 1982: Deformation-Mechanism Maps, Pergamon Press.

Munson, D.E. and P.R. Dawson, 1981: Salt Constitutive Modelling using Mechanism Maps, Proceedings of the 1st Conference on the Mechanical Behaviour of Salt, Pennsylvania State University Trans Tech Publications: 717-737

Olivella, S., A. Gens, E. E. Alonso, J. Carrera, 1992. Constitutive Modelling of Porous Salt Aggregates . Numerical Models in Geomechanics, Pande and Pietruszczak (eds) Balkema, Rotterdam, Vol 1 pp. 179:189

Olivella, S., J. Carrera, A. Gens, E. E. Alonso, 1994. Non-isothermal Multiphase Flow of Brine and Gas through Saline Media. Transport in Porous Media 15:271-293.

Schutjens, P.M.T.M. -Intergranular Pressure Solution in Halite Aggregates and Quartz Sands: an Experimental Investigation. Thesis. Geologica Ultraiectina, n° 76, Utrecht, 1991.

Spiers, C.J., Urai, J.L. ,Lister, G.S., Boland, J.N., Zwart, H.J. – The Influence of Fluid-Rock Interaction on the Rheology of Salt Rock, Nuclear Science and Technology series, EUR 10399 EN, 1986.

Spiers, C.J., Peach, C.J., Brzesowsky, R.H., Schutjens, P.M.T.M., Liezenberg, J.L. and Zwart, H.J. – Long-term Rheological and Transport Properties of Dry and Wet Salt Rocks, Nuclear Science and Technology series, EUR 11848 EN, 1988.

Spiers, C.J., Schutjens, P.M.T.M., Brzesowsky, R.H., Peach, C.J., Liezenberg, J.L. and Zwart, H.J., (1990): Experimental determination of constitutive parameters governing creep of rock salt by pressure solution, Geological Society Special Publication no. 54: Deformation Mechanisms, Rheology and Tectonics. 215:227.

Stührenberg, "Untersuchungen zum Materialverhalten von Versatz unter Berücksichtigung der Wechselwirkung Gebirge/ Versatz und anderer VarschluBkomponenten in einem Endlager im Salinar", BMFT- Forschungsvorhaben KWA 5801 9, Teilprojekt II. 1990.

CHAPTER 5

COMPUTATIONAL APPROACH FOR COUPLED THERMO-HYDRO- MECHANICAL PROBLEMS IN SALINE MEDIA

5.1 Introduction

A new theoretical approach that includes balance equations and constitutive theory has been presented in the preceding Chapters 3 and 4. The balance equations have been derived in Chapter 3 where the general aspects of the constitutive theory are also presented. The mechanical behaviour of porous salt aggregates has received specific attention in Chapter 4 where a new constitutive model has been developed. It takes into account two mechanisms of deformation and dependences on temperature and brine content are relevant. The numerical implementation of the approach is the topic of the present chapter.

Coupled thermo-hydro-mechanical problems in geomaterials is a subject of increasing interest. The possibilities of numerical analysis of coupled problems increase day by day due to the fast progress of computer sciences. In saline media, in general, uncoupled analyses do not provide sufficient information. For instance, thermo-mechanical analyses are necessary because creep strain is strongly dependent on temperature. Radioative wastes are a heat source.

This chapter concentrates first on the mechanical problem and second in the treatment of mass and energy balance equations. The partial differential equations (Appendix and Chapter 3) together with constitutive laws are strongly coupled and nonlinear. This approach is the basis for a finite element code that has been developed. CODE_BRIGHT is a simulator for COupled DEformation, BRIne, Gas and Heat Transport problems.

5.2 Numerical approach

The problem to be solved is composed by the following equations and associated unknowns (see Appendix):

- Water mass balance equation (A2) – liquid pressure (P_l)
- Air mass balance equation (A3) – gas pressure (P_g)
- Water in inclusions mass balance equation (A4) – mass fraction of water in solid (ω_s^w)
- Equilibrium of stresses (A5) – displacement field ($\boldsymbol{u}$)
- Energy balance equation (A6) – temperature (T)

The finite element method is used for the spatial discretization while finite differences are used for the time discretization. In both cases, first order integration is considered sufficient. The coupled and nonlinear nature of the problem requires special treatment of terms. This means that standard procedures of implementation may lead to large computational efforts. It is therefore necessary to optimize the algorithms in order to avoid repetitive computations. The first order approximation allows some simplifications. Sometimes excesive simplifications may cause matrix with rank defficiencies in the system of equations. For instance, reduced numerical integration may be a cause for distorted displacement fields (see for example Bićanić and Hinton, 1979) also called spurious displacements.

In the Appendix, a balance equation for salt which is the main component of solid matrix and that is also present dissolved in the water, is included. Since dissolved salt is assumed to be in equilibrium, salt concentration is not an unknown but a dependent variable. Then, salt mass balance is used to compute porosity variations once the state variables are known.

In Section 5.3 the mechanical constitutive model is discretized. This produces a vectorial (six components of the stress tensor) nonlinear function to be accomplished at every point of the medium. In Section 5.4 the model is incorporated in the equation of equilibrium of stresses. The Newton-Raphson method is used to obtain an iterative scheme to solve for the nonlinearities. Dependences on temperature, brine and gas pressure are considered.

Section 5 is devoted to the numerical implementation of the mass and energy balance equations. Details about the treatment of the different terms (accumulation, advective and nonadvective fluxes, volumetric strain) are presented. Finally the Newton-Raphson method is applyied to the residual form of these mass and energy equations. The computation of porosity variations has received also special attention because dissolution/ precipitation and volumetric strain shoud be taken into account. This is explained in Section 5.6.

5.3 Discretized form of the mechanical constitutive model

The equations presented in Chapter 4 concern the creep deformation of salt aggregates caused by stress and under varying temperature and brine content conditions. A general model to reproduce the stress-strain behaviour of a salt aggregate can be written as:

$$\dot{\varepsilon} = \dot{\varepsilon}^{evp} + \dot{\varepsilon}^{c} \tag{5.1}$$

where $\dot{\varepsilon}^{evp}$ represents any strain rate not included in the creep counterpart (elastic, elastoplastic or viscoplastic) and $\dot{\varepsilon}^{c}$ includes creep deformation (both mechanisms).

As shown in Chapter 4, creep deformation is very relevant in saline materials. On the other hand, granular aggregates are usually compacted before the sealing systems are built. On the other hand, experimental results seem to indicate that the accumulated creep deformation induces overconsolidation. For these reasons, a linear or nonlinear elastic model can be used as a first approximation to be combined with creep deformation. Elasticity plus creep is very convenient from a numerically point of view.

However, it should be pointed out that these materials are very similar to sand materials in their microstructure. Of course sand does not creep, at least at relevant rates. Therefore, a more complex approach could include a soil mechanics elastoplastic model in order to characterize the instantaneous irreversible strain and the behaviour under low confinement states.

Suction effects may be also important. It has already been shown that brine content influences creep strain rates (Chapter 4). A relationship between strain rates and suction through the degree of saturation has been found. Probably, changes in suction will also cause time independent deformation. Therefore, a term related to changes in suction can also be incorporated, both in the elastic approach or in another more complex.

Assuming an elastic nonlinear model for the instantaneous deformation, the model reads with the following dependences:

$$\dot{\varepsilon} = \dot{\varepsilon}^{e}(\dot{\sigma}', \dot{s}, \dot{T}, e) + \dot{\varepsilon}^{c}(\sigma', s, T, e) \tag{5.2}$$

where s is suction defined as $s = P_g - P_l$, i.e. the difference between gas and liquid pressures, T is temperature and e is void ratio. The elastic counterpart depends on the rate of stresses, suction and temperature, which is indicated by an overdot. Strains caused by suction variations and temperature variations have been included in the elastic counterpart indicating that they are also treated instantaneous and reversible.

If strain is written in terms of the displacement field ($\boldsymbol{u}$) and a finite difference along time is performed, Equation (5.2) can be rewritten as:

$$\boldsymbol{h}^{k+1} = -\boldsymbol{B}\,\Delta^k\boldsymbol{u} + \Delta^k\dot{\boldsymbol{\varepsilon}}^e + (\dot{\boldsymbol{\varepsilon}}^c)^{k+\epsilon}\,\Delta^k t + \boldsymbol{m}\beta\Delta^k T = \boldsymbol{0} \qquad (5.3)$$

where $\boldsymbol{B}$ is a tensor of spatial derivatives that transforms the displacement components ($\boldsymbol{u}$) into the strain components ($\boldsymbol{\varepsilon}$), Δ^k represents an increment between time t^k and t^{k+1}, $\Delta^k\dot{\boldsymbol{\varepsilon}}^e$ is an increment of elastic strain (if only stress dependence is considered and the model is linear, then $\Delta^k\dot{\boldsymbol{\varepsilon}}^e = \boldsymbol{D}^e\Delta^k\dot{\boldsymbol{\sigma}}'$), $\boldsymbol{m}$ is an auxiliary vector defined as $\boldsymbol{m}^T = (1,1,1,0,0,0)$, β is a thermal expansion coefficient (thermal expansion is assumed to be linear). The temperature term has been separated because the linear form is assumed.

The summary of this section is that $\boldsymbol{h}^{k+1}$ is a nonlinear function of stresses, fluid pressures, temperatures, void ratio and displacements. At each point of the medium, this function should vanish in order that the material behaves according to the constitutive equation. In spite of the nonlinear character of this function $\boldsymbol{h}^{k+1}$, at present, the only history variable is void ratio. Derivatives of void ratio with respect to state variables are difficult. In addition, small porosity changes will take place compared to the changes in other variables. For these reasons, void ratio is considered at time t^k. This means that for this variable, and only for this one, integration along time is explicit. The creep counterpart of deformation depends on the variables but not on their increments, then it is computed at an intermediate time $t^{k+\epsilon}$, i.e. integration is implicit along time.

5.4 Mechanical problem including creep deformation

The weighted residual method is applied to the stress equilibrium equation (A5) followed by the Green's theorem. This leads to the equation (Zienkiewicz and Taylor, 1989):

$$\boldsymbol{r}(\boldsymbol{\sigma}^{k+1}) = \int_v \boldsymbol{B}^T\boldsymbol{\sigma}^{k+1}dv - \boldsymbol{b}^{k+1} = \boldsymbol{0} \qquad (5.4)$$

where $\boldsymbol{r}(\boldsymbol{\sigma}^{k+1})$ represents the residual corresponding to the mechanical problem and $\boldsymbol{\sigma}^{k+1}$ is the stress vector at time t^{k+1}. For algebraic reasons, matrix $\boldsymbol{B}$ (composed by gradients of shape functions) is defined in such a way that stress is formally a vector and not a tensor. The body force terms and the boundary traction terms are represented together by $\boldsymbol{b}^{k+1}$. The numerical approach has been developed for the equilibrium equations and using a constitutive equation that includes creep behaviour in the form presented in Section 5.3. The approach is based on similar ones given in Zienkiewicz and Taylor (1989) for creep equations. Here the thermal and pore pressure terms have also been incorporated.

According to the notation that has been adopted, at time t^k every variable is known and its value will be computed at time t^{k+1}. In order to avoid huge notation, the superscript $()^{k+1}$ will be dropped. A new superscript will be introduced here which will refer to the iteration process. For instance, at iteration $l+1$, the unknown stress will be $\boldsymbol{\sigma}^{k+1,l+1}$ and dropping the time superscript: $\boldsymbol{\sigma}^{l+1}$.

The Newton-Raphson method will be applied here in order to find an iterative scheme. Imposing that the vector of residuals at nodal points should vanish at the next iteration $(l+1)$ and doing a Taylor expansion of the residual we obtain:

$$\boldsymbol{r}^{l+1} = \boldsymbol{r}^{l} + \int_v \boldsymbol{B}^T \delta^l \boldsymbol{\sigma} dv = \boldsymbol{0} \tag{5.5}$$

where $\delta^l \boldsymbol{\sigma} = \boldsymbol{\sigma}^{l+1} - \boldsymbol{\sigma}^l$, i.e. the difference between two iteration stress values, also referred as stress correction.

Since the constitutive equation (5.3) should also vanish (Taylor expansion of the constitutive equation) we obtain the following equation:

$$\boldsymbol{h}^{l+1} = \boldsymbol{h}^{l} + \frac{\partial \boldsymbol{h}^l}{\partial \boldsymbol{\sigma}} \delta^l \boldsymbol{\sigma} + \frac{\partial \boldsymbol{h}^l}{\partial \boldsymbol{u}} \delta^l \boldsymbol{u} + \frac{\partial \boldsymbol{h}^l}{\partial P_g} \delta^l P_g + \frac{\partial \boldsymbol{h}^l}{\partial P_l} \delta^l P_l + \frac{\partial \boldsymbol{h}^l}{\partial T} \delta^l T = \boldsymbol{0} \tag{5.6}$$

In the latter equation it is clear that the state variables that have been considered are: $\boldsymbol{u}$, P_g, P_l and T. This equation allows to obtain the stress correction at any point in the continuous as:

$$\delta^l \boldsymbol{\sigma} = -\boldsymbol{D}^{tan} \left(\boldsymbol{h}^l + \frac{\partial \boldsymbol{h}^l}{\partial \boldsymbol{u}} \delta^l \boldsymbol{u} + \frac{\partial \boldsymbol{h}^l}{\partial P_g} \delta^l P_g + \frac{\partial \boldsymbol{h}^l}{\partial P_l} \delta^l P_l + \frac{\partial \boldsymbol{h}^l}{\partial T} \delta^l T \right) \tag{5.7}$$

where the stiffness matrix $\boldsymbol{D}^{tan}$ is computed as:

$$\boldsymbol{D}^{tan} = \left(\frac{\partial \boldsymbol{h}^l}{\partial \boldsymbol{\sigma}} \right)^{-1} = \left((\boldsymbol{D}^e)^{-1} + (\boldsymbol{D}^c)^{-1} \right)^{-1} \tag{5.8}$$

where $\boldsymbol{D}^e$ and $\boldsymbol{D}^c$ are stiffness matrices for elasticity and creep respectively.

The substitution of (5.7) in (5.5) leads to the final system of equations (regarding equilibrium equations) to be solved:

$$\int_v \boldsymbol{B}^T \boldsymbol{D}^{tan} \boldsymbol{B}\, \delta^l \boldsymbol{u} dv + \int_v \boldsymbol{B}^T \boldsymbol{D}^{tan} \frac{\partial \boldsymbol{h}^l}{\partial P_g} \delta^l P_g dv + \int_v \boldsymbol{B}^T \boldsymbol{D}^{tan} \frac{\partial \boldsymbol{h}^l}{\partial P_l} \delta^l P_l dv +$$

$$+ \int_v \boldsymbol{B}^T \boldsymbol{D}^{tan} \frac{\partial \boldsymbol{h}^l}{\partial T} \delta^l T dv = -\boldsymbol{r}^l - \int_v \boldsymbol{B}^T \boldsymbol{D}^{tan} \boldsymbol{h}^l dv \tag{5.9}$$

where $\partial h^l/\partial u = B$ has been applied. It should be noticed that the residual is composed by two terms because the iterative scheme is obtained by applying the Newton-Raphson method simultaneously to the equilibrium equation together with the constitutive model. First one expresses the equilibrium of stresses and the second expresses that the constitutive equation is accomplished at every point.

The following step consists of substituting by the interpolated approach, i.e. each state variable is expressed as the weighted sum of the nodal values. The coupled terms (P_g, P_l, T) require other equations to be solved simultaneously with (5.9), these are the mass and energy balance equations.

According to the constitutive model equations (Chapter 4) as porosity vanishes, the medium recovers the properties of the salt rock and the volumetric creep counterparts vanish. This means that the medium becomes incompressible, or, at least, volumetrically very stiff. It is well known that the equations of equilibrium together with an incompressible constitutive law cause locking (not all displacemets are allowed due to element constrictions) of the elements (Zienkiewicz and Taylor, 1989). A possible technique to avoid this difficulty consists of using reduced integration, and, this is possible when the finite element interpolation is quadratic or superior order. For linear quadrilateral elements, one or two integration points could be used to integrate in a reduced way. However, reduced integration causes hourglassing effects. Bićanić and Hinton (1979) show several patterns of spurious displacement fields. In order to avoid locking and hourglassing problems the selective integration procedure has been developed and used. Hughes (1980) has extended this technique to anisotropic and nonlinear media.

The selective integration technique consists of reducing the order of integration only for the volumetric counterpart component of deformation. If volumetric and deviatoric components are not coupled, which happens in linear elasticity or viscoelasticity, the application of the method does not present difficulties. For non-linear behaviour, the generalization of this technique has received the name of B-bar method because a modified matrix $\bar{B}$ is used. If strain is written as:

$$\boldsymbol{\varepsilon} = \boldsymbol{e} + \frac{1}{3}\boldsymbol{m}^T\boldsymbol{\varepsilon}\boldsymbol{m} \tag{5.10}$$

that is, a decomposition of volumetric and deviatoric counterparts. In terms of displacements, this would read as:

$$\boldsymbol{\varepsilon} = \boldsymbol{B}\boldsymbol{u} = \boldsymbol{B}^d\boldsymbol{u} + \boldsymbol{B}^v\boldsymbol{u} \tag{5.11}$$

where the matrix $\boldsymbol{B}$ is decomposed to obtain the volumetric and deviatoric strain counterparts defined in (5.10). A numerical integration implies that $\boldsymbol{B}$ is computed at integration points. Selective integration consists of computing $\boldsymbol{B}^d$ as usual, i.e.

at integration points with the order required and $\bar{B}^v$ computed with a reduced integration rule. The modified matrix is then defined as: $\bar{B} = \bar{B}^v + B^d$. This matrix is used in every term of (5.9) as proposed by Hughes (1980). When quadrilateral elements with linear interpolation functions are used, 4 values of B^d are required (at each integration point) while only one value of $\bar{B}^v$ (centroidal point of the element).

5.5 Mass and energy balance equations

In order to explain details of the numerical treatment of mass and energy balance equations, the water mass balance equation will be used as example, and particularly, terms regarding water vapour will be written. For the other mass balance equations and for the equation of energy balance the treatment is identical. Other details and discussion can be found in Olivella et al (1994b).

The storage or accumulation terms are computed in a mass conservative approach (Milly, 1984; Allen and Murphy, 1986; Celia et al. 1990). The conservative approach dicretizes directly the accumulation terms while the capacitative approach uses the chain rule to transform time derivatives in terms of the unknowns. Milly (1984) proposes modifications of the the capacitative approach in order to conserve mass. Authors that use the mass conservative approach claim that it gives a more accurate approximation than the capacitative approach.

Mass conservation in time is achieved if the time derivatives are directly approximated by a finite difference in time. Finite element method for the space discretization conserves mass. This latter affirmation is easily proven by adding up all nodal equations. Flow terms cancel out (due to the definition of the shape functions) and the resulting equation represents mass accumulation in the entire domain. Milly (1984) concludes that if mass conservation takes place, only the distribution of moisture in the medium is affected by the discretization (spatial and temporal) and iteration. In other words, the mass balance is guaranteed independently of the discretization and iteration.

On the other hand, Celia et al. (1990) demonstrate that if the Picard iterative scheme is used the same computational effort is necessary for the conservative and the capacitative approaches. This affirmation can not be made if the Newton-Raphson method is used because in such case the conservative approach is much more economical per iteration. Celia et al. (1990) also point out that conservation of mass is insufficient to guarantee good numerical solutions and oscillations can also appear.

Galarza et al. (1992, 1994) have made a thorough comparison of several formulations for unsaturated flow. The results indicate consistently a better performance of the capacitative approach. The criteria that they use is in terms of pressures computed at nodes for a total of 7 cases. This is in agreement with the idea that although mass is conserved, the distribution of water in the medium may be not as good as with another scheme.

Despite of the latter findings, we have opted for the mass conservative approach because the capacitative method requires computing derivatives of the accumulation time derivatives with respect to unknowns. If the chain rule is used to split the accumulation time derivatives in terms of the unknowns (temperature, liquid pressure and gas pressure), the use of the Newton-Raphson method leads to second derivatives (also crossed, for example with respect to temperature and pressure) of the nonlinear terms. This results in a very uneconomical scheme.

It is assumed that the weighted residual method is applied followed by the Green's theorem. After doing so, the discrete form of equations is obtained, every equation representing the balance in cell asssociated to a node, for example, node i. Each balance equation contains several terms (for a more expanded version of the balance equations see Chapter 3), among them, four main types can be distinguished:

Type 1: Storage changes of mass or energy at constant porosity:

$$\int_{e_m} N_i \phi \frac{D_s(\theta_g^w S_g)}{Dt} dv \approx \int_{e_m} N_i \phi \frac{\partial(\theta_g^w S_g)}{\partial t} dv = \int_{e_m} N_i \phi^k \frac{\Delta^k(\theta_g^w S_g)}{\Delta^k t} dv \tag{5.12}$$

where the integral over the element e_m represents the contribution of this element to cell i (Figure 5.1). Firstly, the material derivative with respect to the solid velocities has been approximated as time derivative because the advective terms caused by solid motion are assumed to be small. Second, a mass conservative approximation has been performed simply by doing a finite diference along time of the partial derivative (Milly, 1984). The third step consists of defining porosity element-wise (constant over the elements), mass content (θ_g^w) cell-wise (constant over the cell), and degree of saturation (S_g) modified cell-wise (constant over the cell but with several values). This latter, i.e. modified cell-wise, is required for non-homogeneous medium because a cell is composed by a fraction of elements with a common node (Figure 5.1) and degree of saturation will only be a continuous variable in case of homogeneous material. Hence, modified cell-wise means that a different value of degree of saturation should be used in the cell depending on which

element is considered. The other variables such as density do not show this peculiarity because they are not material dependent. Finally, the physical quantities can go outside the integral symbol and the remaining integral is only geometrical. Therefore, it should be computed only once for a given mesh, and the values are called influence coefficients (Huyakorn et al, 1986). The treatment presented here gives rise to a concentrated matrix, i.e., storage corresponding to node i only depends on state variables (P_g, P_l, T) at this node. Another advantadge of the mass conservative approach is that when the Newton-Raphson method is applied, only first order derivatives of the nonlinear functions are required.

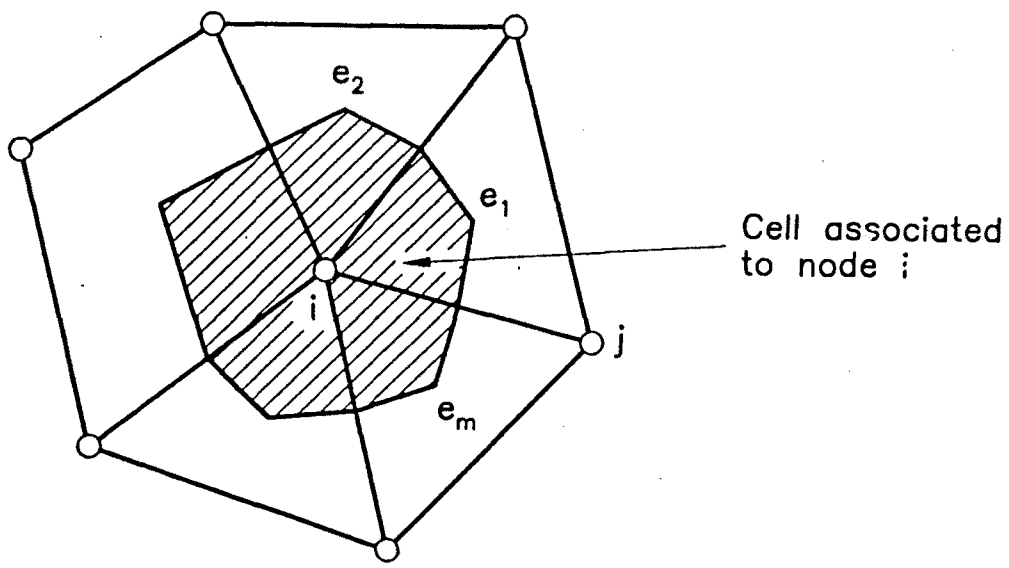

Figure 5.1: Representation of a cell in a finite element mesh.

Type 2: Advective flux due to phase motion:

$$-\int_{e_m} \nabla^T N_i \, \theta_g^w q_g dv \;=\; \Big[\int_{e_m} \nabla^T N_i \, \boldsymbol{k}^k \Big(\frac{k_{rg}}{\mu_g}\theta_g^w\Big)^{k+\varepsilon} \nabla N_j dv\Big](P_g)_j^{k+\theta} -$$

$$- \Big[\int_{e_m} \nabla^T N_i \, \boldsymbol{k}^k \Big(\frac{k_{rg}}{\mu_g} \theta_g^w \rho_g \Big)^{k+\varepsilon} \boldsymbol{g} dv \Big] \tag{5.13}$$

where j indicates a sum over element nodes and $k+\varepsilon$ and $k+\theta$ are two different itermediate time points between t^k and t^{k+1}. Generalized Darcy's law has been used and is written as (Bear, 1972):

$$\boldsymbol{q}_g = -\frac{\boldsymbol{k} k_{rg}}{\mu_g} (\nabla P_g - \rho_g \boldsymbol{g}) \tag{5.14}$$

where $\boldsymbol{k}$ is the tensor of intrinsic permeability, k_{rg} is the relative permeability of the gas phase, μ_g is the dynamic viscosity of gas and $\boldsymbol{g}$ is a vector of gravity forces. Among the coefficients that appear in Darcy's law, intrinsic permeability $\boldsymbol{k}$ contains the tensorial information regarding porous structure of the medium. In Equation (5.13), all variables that appear inside the integral are considered element-wise. With this approximation, all quantities can go outside the space integral. For the tensorial quantity (intrinsic permeability), it is necessary to split the product with the gradients of shape functions ∇N_i and then, the coefficients of the matrix $\boldsymbol{k}$ can be removed outside. The remaining integrals (also called influence coefficients) are again only geometrical and hence, computed once for a given mesh (Huyakorn et al, 1986). Finally, evaluation of density element-wise is convenient is order to correctly balance pressure gradients with gravity forces.

Type 3: Nonadvective flux due to species motion:

$$- \int_{e_m} \nabla^T N_i \boldsymbol{i}_g^w dv = \Big[\int_{e_m} \nabla^T N_i (\phi\tau)^k (\rho_g S_g D_g^w)^{k+\varepsilon} \boldsymbol{I} \, \nabla N_j dv \Big] (\omega_g^w)_j^{k+\theta} \tag{5.15}$$

where j indicates a sum over element nodes. Fick's law has been used and can be written as:

$$\boldsymbol{i}_g^w = -\phi\tau\rho_g S_g D_g^w \boldsymbol{I} \, \nabla\omega_g^w \tag{5.16}$$

where τ is a tortuosity parameter, D_g^w is the molecular diffusion coefficient which is a function of temperature and gas pressure and $\boldsymbol{I}$ is the identity matrix. Again element-wise approximation will be used for the variables inside the integral. In (5.15) it should be pointed out that the driving variable (ω_g^w, i.e. mass fraction of vapour in gas phase) has been considered node-wise, in the same way as for gas pressure in the advective term. It should be noticed that the classical approach splits the gradient of any dependent variable in terms of the corresponding unknowns (here P_g, P_l, T). The treatment proposed here is possible

because the Newton-Raphson method will be used to solve the non-linear system of equations. As for the type 1 terms, only first order derivatives of the nonlinear functions are required. Here, a diffusive term has been written, however the case of dispersion is similar except that the dispersion tensor is not isotropic. The tensor of mechanical dispersion is defined in terms of phase velocities which are considered element-wise as well and computed at the intermediate time $t^{k+\epsilon}$. Dispersivities are also considered element-wise.

Type 4: Storage changes caused by volumetric deformation of the medium:

$$\int_{e_m} N_i \, (\theta_g^w S_g \frac{\theta_s^h}{\theta_s^h - \theta_l^h S_l}) \, \nabla \cdot \dot{\boldsymbol{u}} dv \; = \; \int_{e_m} N_i \, (\theta_g^w S_g \alpha)^{k+\epsilon} \, \boldsymbol{m}^T \boldsymbol{B} \dot{\boldsymbol{u}} dv \; =$$

$$= \Big[\int_{e_m} N_i (\theta_g^w S_g \alpha)^{k+\epsilon} \boldsymbol{m}^T \boldsymbol{B}_j dv \Big] \frac{(\Delta^k \boldsymbol{u})_j}{\Delta^k t} \qquad (5.17)$$

where j indicates a sum over element nodes, α has been defined for comodity and $\boldsymbol{B}_j$ is the j-submatrix of $\boldsymbol{B}$. The same strategy as with the other terms, i.e. the physical variables inside the integral are element-wise and, hence, removed outside. The remaining integral is only geometrical. The selective integration also applies to this term and, consequently, matrix $\bar{\boldsymbol{B}}$ should be used if this technique is required.

Once all terms are transformed into their discrete form, the partial diferential equations are converted into a set of nodal balance equations. For water, air and energy, the balance can be written as:

$$\boldsymbol{r}_w^{k+1} = \boldsymbol{0} \qquad \boldsymbol{r}_a^{k+1} = \boldsymbol{0} \qquad \boldsymbol{r}_e^{k+1} = \boldsymbol{0} \qquad (5.18)$$

where the superscript $()^{k+1}$ indicates that the unknowns will be computed at time t^{k+1} while at time t^k everything is assumed known. An iterative scheme should be found simply by Taylor's expansion around a previous iteration value. The time superscript will be dropped and the new superscripts $()^l, ()^{l+1}$ indicate iteration. For any of the balance equations:

$$\boldsymbol{r}^{l+1} = \boldsymbol{r}^l + \frac{\partial \boldsymbol{r}^l}{\partial \boldsymbol{u}} \delta^l \boldsymbol{u} + \frac{\partial \boldsymbol{r}^l}{\partial P_g} \delta^l P_g + \frac{\partial \boldsymbol{r}^l}{\partial P_l} \delta^l P_l + \frac{\partial \boldsymbol{r}^l}{\partial T} \delta^l T = \boldsymbol{0} \qquad (5.19)$$

where $\delta^l() = ()^{l+1} - ()^l$, i.e. the difference between two iteration values, also referred as variable correction. In equation (5.19), derivatives with respect to the unkonws should be computed. Looking at the types of terms that appear in the equations (Eqs 5.12 to 5.17), it can be seen that the derivatives with

respect to displacements are very simple because displacements only appear in (5.17). There are two reasons for this fact. First, the derivatives of porosity have already been substituted using the salt mass balance. Second, porosity and intrinsic permeability (this latter is a function of porosity) are computed at time t^k.

Derivatives with respect to the nodal vectors of unknowns, i.e., $\boldsymbol{P}_g^{k+1}, \boldsymbol{P}_l^{k+1}, \boldsymbol{T}^{k+1}$ appear in all term types due to the nonlinear character of the problem. These derivatives should take into account if the dependent variables are cell-wise or element-wise. Cell-wise variables only depend on the unknowns at the node associated to the cell, in contrast, element-wise variables depend on the various nodes defining the element.

Finally, the Equations summarized by (5.9) and (5.19) are solved simultaneously. This means that the vector of unknowns is $\boldsymbol{X} = (\boldsymbol{x}_1, ..., \boldsymbol{x}_n)$ for n nodes, with $\boldsymbol{x}_j = (u_{xj}, u_{yj}, u_{zj}, P_{gj}, P_{lj}, T_j)$ for example for node j.

A sequential solution scheme would simplify the mathematical development and subsequent implementation because derivatives of each equation only would have to be made with respect to its associated variable. For instance, only derivatives with respect to displacements would be required in the equilibrium equations. This alternative approach is specially convenient when existing uncoupled models are combined to solve a coupled problem. The simultaneous solution is much more robust.

5.6 Porosity variations

The equation of salt balance given in the Appendix (see also Chapter 3) is used to compute porosity variations. This equation (A1) can be written as:

$$\frac{D_s\phi}{Dt} - b \approx \frac{\partial\phi}{\partial t} - b = 0 \tag{5.20}$$

where the material derivative has been approximated by a time derivative. When deformation is the only cause for porosity variation, this equation can be used to compute porosity at every point of the medium very easily because $b = (1-\phi)\nabla\cdot\dot{\boldsymbol{u}}$, i.e. porosity only depends on volumetric strain variations. For the case of dissolution/ precipitation processes, a further development is required.

Since (5.20) is a balance equation, the weighted residual method and the Green's theorem are also applied leading to:

$$\int_v N_i \frac{\partial\phi}{\partial t} dv - \int_v N_i b dv = \int_v N_i \frac{\Delta^k\phi}{\Delta^k t} - b_i^{k+1} = 0 \tag{5.21}$$

Once the problem is solved b_i^{k+1} are known in this same integrated form because they appear in the balance equations. However, this equation is nodal while porosity has been defined as an element-wise variable. Therefore, a special algorithm is used to obtain element variations of porosity. Basically, it consists of partitioning cell salt mass balance into the elements that share the given node. The distribution is made according to element area and porosity (e.g. more precipitation in a bigger and more porous element). This approximated method is only used to compute porosity variation caused by other processes than deformation, i.e. mainly dissolution/ precipitation of salt. The porosity variation caused by deformation is treated in the classical way but using only one value per element because porosity is treated element-wise. This technique is used in an application presented in Chapter 7.

5.7 Conclusions

A numerical approach for solving thermo - hydro - mechanical problems in saline media is presented. A computer code (CODE_BRIGHT) has been developed and can be used to simulate a variety of situations. Further development of the code is expected, for instance, by implementation of mechanical constitutive models also for other geological materials.

The mechanical side of the numerical approach requires to overcome the difficulties associated to incompressible behaviour which takes place in the rock because deformation is essentially deviatoric. The iterative scheme of solution has been proposed using the Newton-Raphson method. The mechanical equations are coupled with the mass and energy balance equations through different terms.

The equations of balance of species and the equation of balance of energy are complex because different types of terms appear. Each of these has received special attention and the adopted computational techniques are presented. It is shown that we may find ways of implementation that are more convenient for reducing the computational cost. We have also proposed a special method for computing porosity variations in a medium where deformation takes place together with dissolution and precipitation.

5.8 Appendix. Balance equations

Balance of mass of salt for the porous medium as a whole:

$$\frac{\partial}{\partial t}(\theta_s^h(1-\phi)+\theta_l^h S_l \phi) \; + \; \nabla \cdot (j_s^h + j_l^h) = f^h \qquad (A1)$$

The storage terms (time derivative) include salt in solid phase and salt dissolved in the liquid phase. Flux of salt in liquid (j_l^h) is the sum of a non-advective

counterpart (diffusion/dispersion) and two advective terms: one caused by liquid motion, the other by solid motion. Flux of salt in solid is a term originated by the motion of inclusions.

Balance of mass of water for the porous medium as a whole:

$$\frac{\partial}{\partial t}(\theta_s^w(1-\phi)+\theta_l^w S_l\phi+\theta_g^w S_g\phi) \; + \; \nabla\cdot(\boldsymbol{j}_s^w+\boldsymbol{j}_l^w+\boldsymbol{j}_g^w)=f^w \qquad (A2)$$

The storage term includes water in the solid (brine inclusions), water in the liquid and water in the gas phase. Motion of water takes place in the three phases. Each of these three fluxes is a sum of advective and non-advective terms.

Balance of mass of air for the porous medium as a whole:

$$\frac{\partial}{\partial t}(\theta_l^a S_l\phi+\theta_g^a S_g\phi) \; + \; \nabla\cdot(\boldsymbol{j}_l^a+\boldsymbol{j}_g^a) \; = \; f^a \qquad (A3)$$

Similar ideas as in the previous equations except that air is not considered as present in the solid phase.

Balance of mass of water in inclusions that are contained in the solid phase:

$$\frac{\partial}{\partial t}(\theta_s^w(1-\phi))+\nabla\cdot(\boldsymbol{j}_s^w)+f_s^w=0 \qquad (A4)$$

This equation is necessary to study the influence of brine inclusions because water in solid can not be considered in equilibrium with the water in pores.

Equilibrium of stresses for the porous medium as a whole:

$$\nabla\cdot\boldsymbol{\sigma} \; + \; \boldsymbol{b} \; = \; \mathbf{0} \qquad (A5)$$

This equation corresponds to the balance of momentum for the porous medium.

Balance of energy for the porous medium as a whole:

$$\frac{\partial}{\partial t}(E_s\rho_s(1-\phi) \; + \; E_l\rho_l S_l\phi \; + \; E_g\rho_g S_g\phi)$$

$$+\nabla\cdot(\boldsymbol{i}_c \; + \; \boldsymbol{j}_{Es} \; + \; \boldsymbol{j}_{El} \; + \; \boldsymbol{j}_{Eg}) \; = \; f^E \qquad (A6)$$

The internal energy for each phase appears in the storage term. Conductive flux of heat is the non-advective term which is added to advective heat fluxes.

Details regarding this formulation can be found in Olivella et al. (1994a) and in Chapter 3.

5.9 References

Allen, M.B. and Murphy C.L. (1986): A Finite-Element Collocation Method for Variably Saturated Flow in Two Space Dimensions, Water Resources Research, 22, no. 11: 1537:1542.

Bear, J. (1972): Dynamics of fluids in porous media, American Elsevier Publishing Company, inc.

Bićanić and Hinton, 1979: Spurious Modes in Two-dimensional Isoparametric Elements, International Journal for Numerical Methods in Engineering, vol 14, 1545-1557.

Celia, M.A., Boulotas, E.T. and Zarba, R. (1990): A General Mass Conservative Numerical Solution for the Unsaturated Flow Equation, Water Resources Research, 26, no. 7: 1483:1496.

Galarza, G., Carrera, J., Abriola, L., Medina, A. (1992): Comparison of Several Formulations for the Time Discretization of Non-linear Flow Equations, Proceedings of the 9th Conference on Computational Methods in Water Resources. Computational Methods in Water Resources, IX, 1: 193-202.

Galarza, G. and J. Carrera, (1994): Computational Aspects of Parameter Estimation in Unsaturated Flow Problems, Journées Numériques de Besançon Computational Methods for Transport in Porous Media, Ed. by J.M. Crolet, 229-245

van Genuchten, R., (1980): A closed-form equation for predicting the hydraulic conductivity of unsaturated soils, *Soil Sci. Soc. Am. J.*: 892-898.

Hughes, T.J.R. (1980): Generalization of Selective Integration Procedures to Anisotropic and Nonlinear Media, Int. J. Num. Meth. Eng. 15, 1413-1418.

Huyakorn, P.S., Springer, E.P., Guvanasen, V. and Wadsworth, T.D. (1986): A Three-dimensional Finite-Element Model for Simulating Water Flow in Variably Saturated Porous Media, Water Resources Research, 22, no. 13 : 1790:1808

Milly, P.C.D. (1984): A mass-conservative procedure for timestepping in models of unsaturated flow, in Proceedings Fifth International Conference on Finite Elements in Water Resources, edited by J. P. Laible et al., Springer-Verlag, New York: 103-112.

Munson, D.E. and P.R. Dawson, 1981: Salt Constitutive Modelling using Mechanism Maps, Proceedings of the 1st Conference on the Mechanical Behaviour of Salt, Pennsylvania State University Trans Tech Publications: 717-737

Olivella, S., J. Carrera, A. Gens, E. E. Alonso, 1994a. Non-isothermal Multiphase Flow of Brine and Gas through Saline Media. Transport in Porous Media 15:271-293.

Olivella, S.; J. Carrera, A. Gens, and E. E. Alonso, 1994b: Nonisothermal

Multiphase Flow of Brine and Gas Thorough Saline Media. Numerical aspects. Journées Numériques de Besançon Computational Methods for Transport in Porous Media, Ed. by J.M. Crolet, 131-150.

Voss, C.I. (1984): SUTRA Users's Guide, U.S. Geological Survey, Water Resources investigations, Report 48-4369.

Zienkiewicz O.C. and R.L. Taylor (1989): The Finite Element Method, Fourth Edition. McGraw-Hill Book Company

CHAPTER 6

VERIFICATION OF THE PROGRAM CODE_BRIGHT

This chapter contains four cases for which CODE_BRIGHT was verified. Although the examples compiled here are relatively simple the exercise is necessary. In fact the process of verification for such a complex numerical program should start from a level of simplicity and proceed towards more complicated cases. In this way the errors are detected more easily. As the problems become more complicated the basic errors can be disregarded. Complete verification is limitted by the existence of analytical solutions. On the other hand, the comparison with available analytical solutions requires double effort because the calculations with the program and with the analytical solution should be carried out. In some cases, the analytical solution is very simple or is available in a tabulated form, but in other, it is very complex because the solution is expressed in terms of functions which require numerical computations.

Another possibility is to use available verified programs. Again an extra effort is required because another program, and usually the researcher is not very familiar with it, should be run.

For these reasons, the most practical way to advance at a moderated cost in verification and validation is participating in intercomparison exercises. At present, the program CODE_BRIGHT and the DIT-UPC Department participate in the EVEGAS^{mm} (European Validation Exercise on GAS Migration Models), some aspects related to the first exercise are presented in Chapter 9.

Test-cases based on analytical solutions from the COSA (1986) and HYDROCOIN (1992) international intercomparison exercises have been very useful to obtain analytical results directly comparable to numerical result analysis. The program CODE-BRIGHT had not been written when these exercises took place, therefore the comparison has been carried out with the availability of the reports of these projects.

6.1 Heat flow, a mathematically linear problem

A heat flow problem in a homogeneous medium is one of the most simple problems that can be simulated with CODE_BRIGHT. Only temperature should be computed and the balance of energy equation is reduced to the heat flow equation:

$$\rho_s c_s \frac{\partial T}{\partial t} + \lambda_s \nabla^2 T = 0 \tag{6.1}$$

where ρ_s is solid density, c_s is solid specific heat, and λ_s is thermal conductivity. If the parameters, i.e. heat capacity and conductivity, are constant the problem is mathematically linear. If the flow is radial and a source or sink at constant heat rate Q_h is assumed at $r = 0$, then the solution of the problem is given by:

$$T - T_o = \frac{Q_h}{4\pi\lambda_s} W(u); \quad u = \frac{r^2}{4Dt}; \quad D = \frac{\lambda_s}{\rho_s c_s} \tag{6.2}$$

where $W(u) = \int_u^\infty \frac{1}{y} \exp(-y)dy$ is an integral function, u is a dimensionless variable and D is a thermal diffusivity. This solution is very popular in groundwater hydrology. For a pumping well in a homogeneous confined aquifer with constant thicknes, the mass balance of water produces the same mathematical equation and hence the same analytical solution. In this field it receives the well known name of Theis solution.

Figure 6.1 shows the simulation of the model for the radial flow for two different finite element grids and the analytical results ($r = 0.25$ m and $T_o = 40°$C). The parameters that have been used here are: $\rho_s = 2163$ kg/m^3, $c_s = 874$ J/kgK, $\lambda_s = 5.1$ W/mK and $Q_h = 930$ W/m, which roughly correspond to salt rock. It should be pointed out that an even more accurate solution would have been obtained if the well radius had been neglected. The above mentioned analytical solution stands for a an infinitesimal point source. However, the temperature computed at the borehole wall contains a very small error.

6.2 Gas flow, a nonlinear problem

The second verification exercise presented here, the gas flow in an axisymmetric medium. It is not possible to consider the gas flow problem mathematically linear because gases are highly compressible. Perfect gas law shows a linear dependence of density with pressure:

$$\rho_g = \frac{M_g P_g}{RT} \tag{6.3}$$

where M_g is the gas molecular mass, ρ_g is gas density, P_g is gas pressure, R is the gas constant and T is absolute temperature.

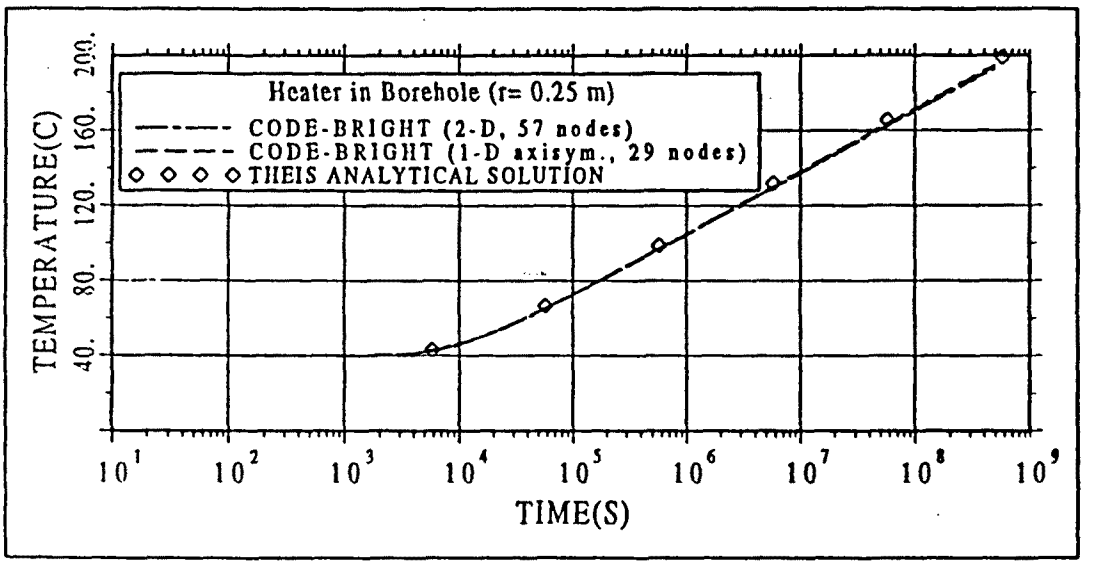

Figure 6.1: Linear radial flow, analytical and numerical predictions.

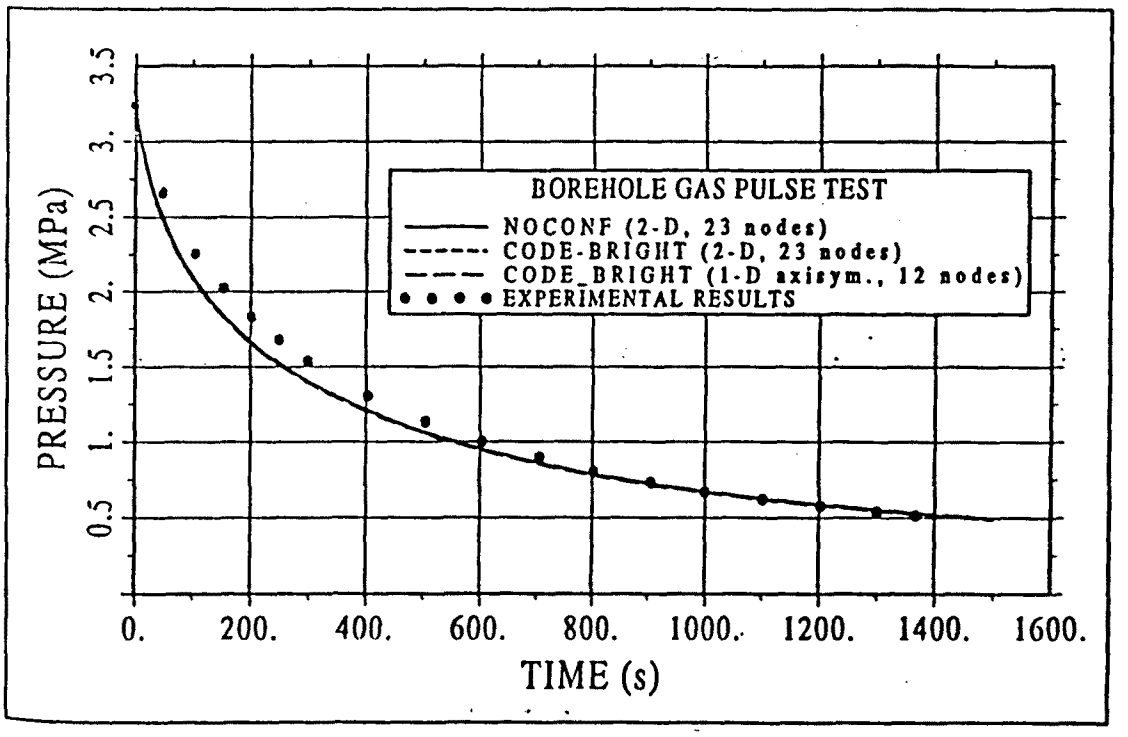

Figure 6.2: Non-linear radial flow, gas pulse test, field test results (Kloska et al. 1989) and numerical simulations with CODE-BRIGHT and NOCONF.

The general equation of air conservation is simple when only one gas is assumed present in pores and the medium is considered undeformable. In such a case, the relevant equation is the gas flow equation. If Darcy's law and perfect gas law are used, the air mass balance equation becomes (after some algebra):

$$\phi \frac{\partial P_g}{\partial t} + \nabla \cdot (\frac{k}{\mu_g} P_g \nabla P_g) = 0 \qquad (6.4)$$

where k is intrinsic permeability, ϕ is porosity and μ_g is gas viscosity (does not depend on pressure if pressure is sufficiently high). This equation is nonlinear because the unknown variable appears inside the divergence term multiplying the gradient of pressures. The storage term is linear.

This equation for gas flow is formally identical to the equation of water flow in a free surface aquifer. In therms of piezometric heads, the equation of water mass balance is expressed as:

$$S_s \frac{\partial h}{\partial t} + \nabla \cdot (K(h - h_o) \nabla h) = 0 \qquad (6.5)$$

where S_s is storage coeficient, h is piezometric head and $K = k\rho_l g/\mu_l$ is hydraulic conductivity. This equation is solved by the computer code NOCONF (1989) which has been developed for academic purposes.

A gas flow simulation has been performed to compare CODE_BRIGHT and NOCONF (1989) computations. The example that was chosen corresponds to a real gas pulse test performed in the Konrad mine and reported by Kloska et al. (1989), which allows a validation at the same time. In this kind of tests the medium goes back towards the static initial situation from an instantaneous overpressure. In this case an initial pressure value of 3.25 MPa decays to the original value of 0.10 MPa.

Figure 6.2 shows the model predictions and test measurements. The test was carried out in a $r = 0.048$m borehole. The values that were used for the simulation are: $\phi = 0.005$, $k = 1.66 \times 10^{-16}$ m ^{2}, $\mu_g = 1.9 \times 10^{-11}$ MPa s at 29 ^{o}C. The values of porosity and permeability that have been used are different from those reported by the authors ($\phi = 0.02$, $k = 7.6 \times 10^{-16}$ m ^{2}), mainly because the authors interpreted the results with an analytical model (other factors were included, such as skin effect) while a simplified numerical model has been used for the simulations. Here, the parameters have been adjusted using a "trial and error" procedure.

6.3 Rock salt creep. COSA-project benchmark

The first benchmark exercise corresponding to the European Community Project COSA (1986) has been used to verify that the constitutive model for

salt rock deformation had been correctly implemented. This exercise consists of the creep deformation of thick walled sphere subject to an internal pressure. The temperature field is constant in time but variable in space from two boundary values.

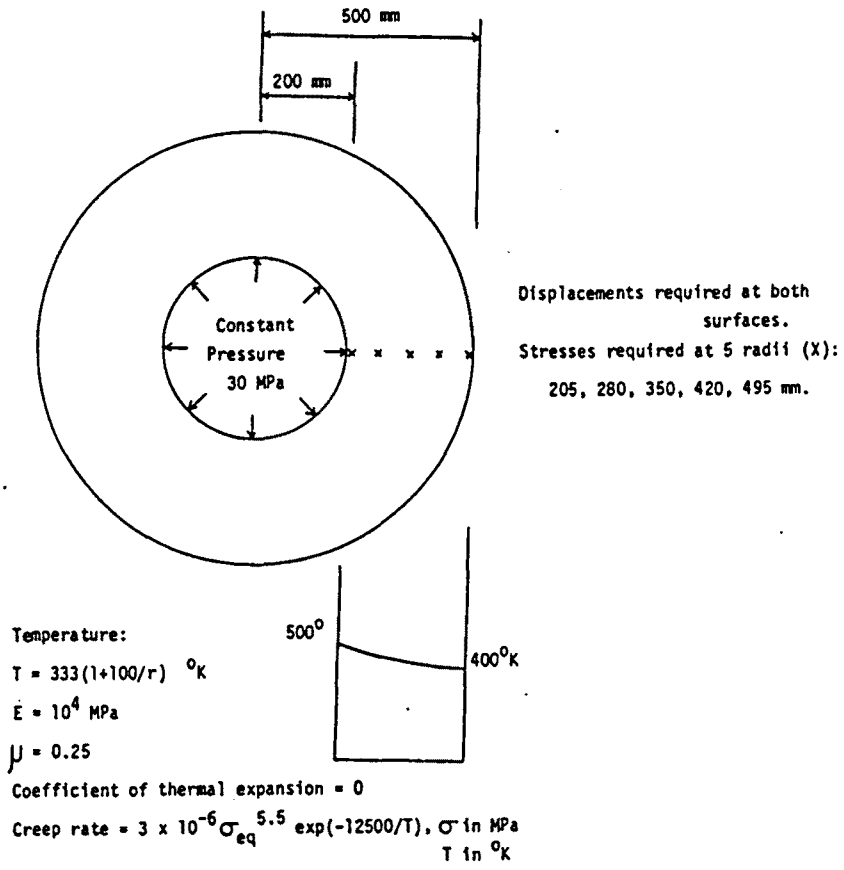

Figure 6.3: Description of the first Benchmark of the COSA intercomparison project. Thick walled sphere.

Figure 6.3 shows the description of the problem with the spherical domain and the prescribed temperature profile. Figure 6.3 also contains the values of the parameters and the required results. Analytical solutions for this particular problem or other similar can be found, for example, in Prij et al. (1987).

The results of the computations carried out with CODE_BRIGHT are summarized in Figures 6.5, 6.6 and 6.7. A two-dimensional 32 node triangle grid

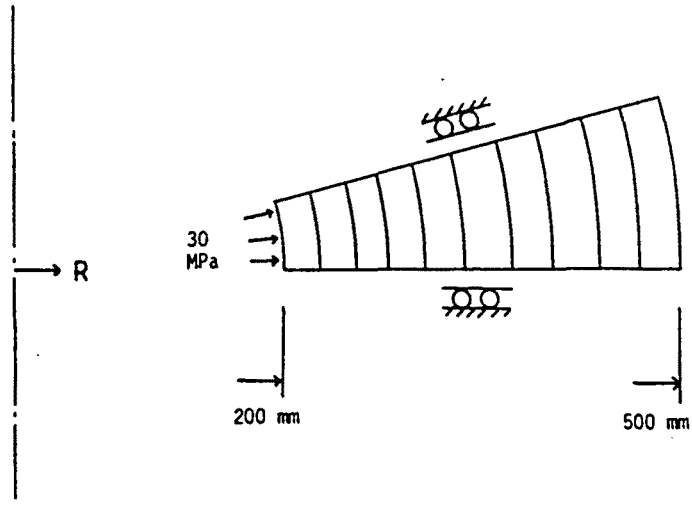

Figure 6.4: Typical finite element mesh to represent a spherical domain

was used. Axisymmetry allowed to model a spherical region. Figure 6.4 shows the form of a typical finite elemet mesh.

Although constant strain triangles are not adequate for uncompressible situations, they were used in this case because the computation was performed when no other element types were available. The results are sufficiently accuracy because only the equivalent stress is shown. The equivalent stress does not present an exagerated oscillatory behaviour as the radial or the tangential stresses would give.

The simulation was carried out using 80 time steps. The results obtained with CODE_BRIGHT completely agree with the computations performed in the COSA project and with the theoretical values. Obviously, today the computations would have been performed using quadrilateral elements and selective integration method. This methodology is explained in Chapter 5.

6.4 Thermal convection. HYDROCOIN-project benchmark

A coupled thermohydraulic analysis is presented in this section. Some computations of the Case 4, Level 1 from the International HYDROCOIN project (1992) have been performed with the program CODE_BRIGHT. The problem

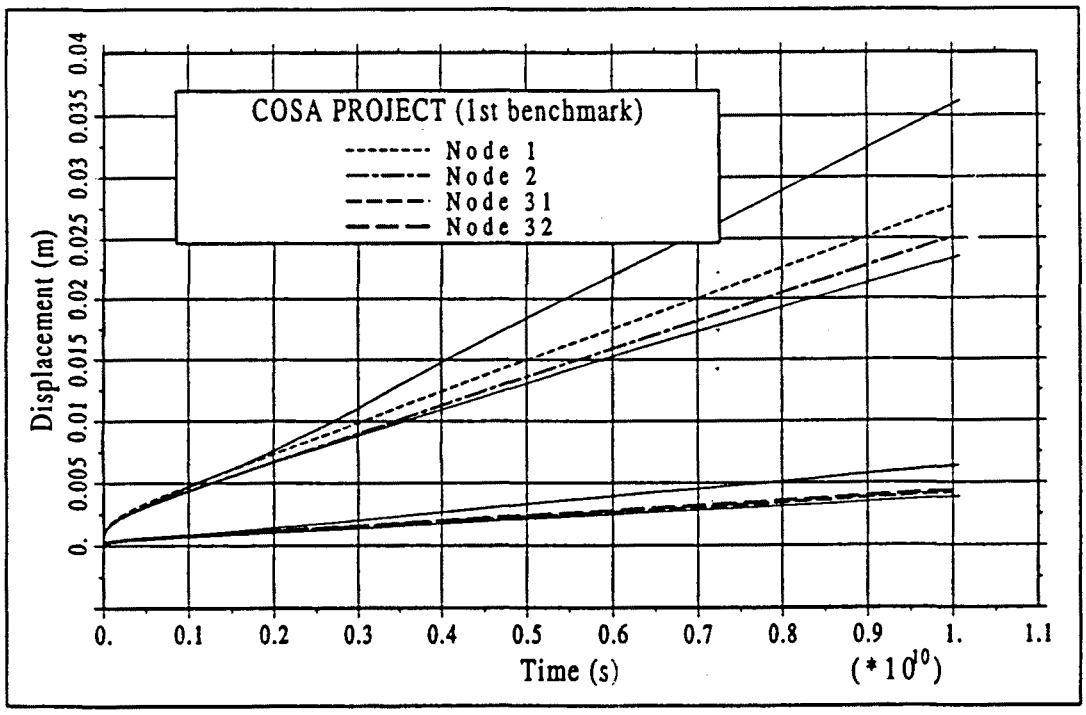

Figure 6.5: Time evolution of displacement at inner boundary (nodes 1 and 2) and at the outer boundary (nodes 31 and 32). The difference between nodes 31 and 32 is caused by the non-symmetry of the grid. Continuous lines define the max. and min. values according to the COSA project.

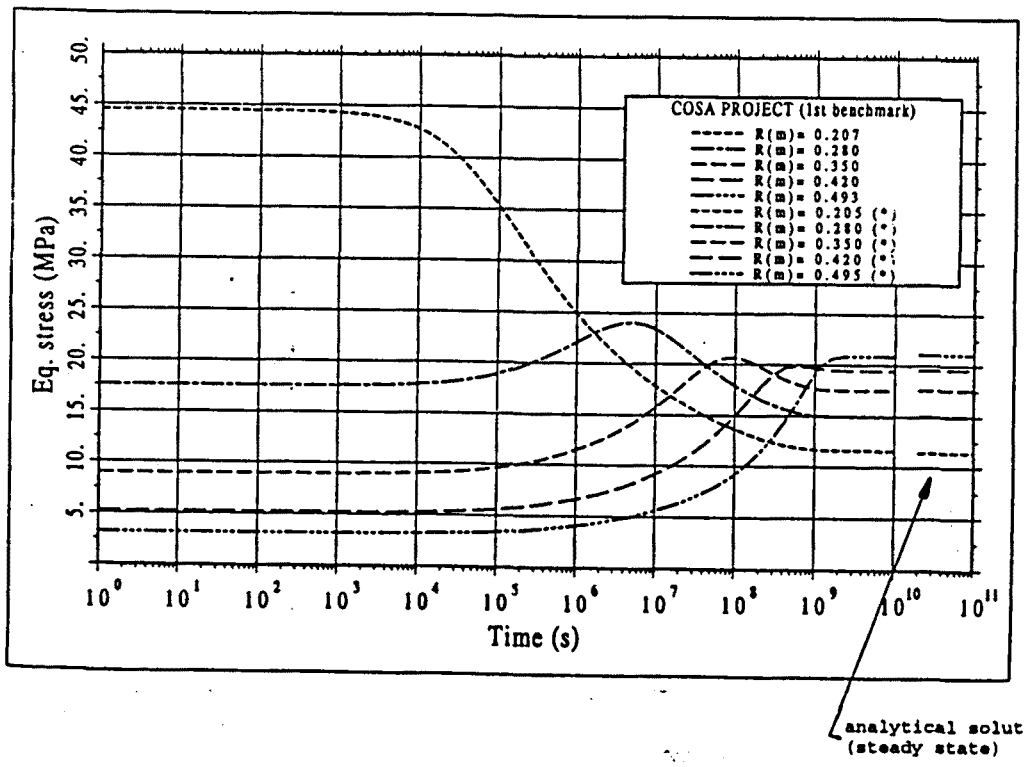

Figure 6.6: Time evolution of equivalent stress at selected points. The computed values tend to the analytical ones. Theoretical values are drawn for times greather than 10^{10} seconds.

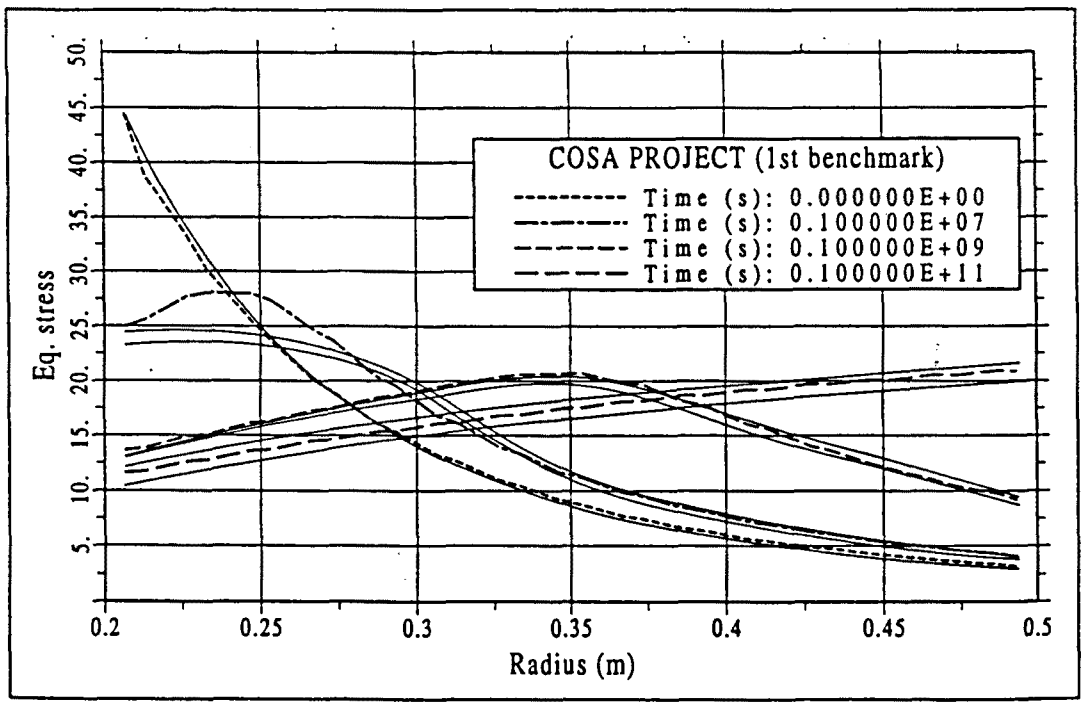

Figure 6.7: Equivalent stress variation with distance and for different times. Continuous lines define the max. and min. values according to the COSA project. (The differences for 10^6 seconds are probably caused by the kind of elements used, see text for discussion).

to be simulated is the thermal convection of a liquid through a porous saturated medium. Flow is induced by heat which is generated inside a spherical region with radius $R_o = 250$ m.

Assuming that the water flow transient terms related to compressibility effects are negligible, the equations of water mass and energy balance reduce to the form:

$$\frac{1}{r}\frac{\partial}{\partial r}(r\frac{\partial P_{ld}}{\partial r}) + \frac{\partial^2 P_{ld}}{\partial z^2} = g\beta\rho_{lo}\frac{\partial T}{\partial z} \tag{6.6}$$

$$\rho_s c_s \frac{\partial T}{\partial t} = \lambda\frac{1}{R^2}\frac{\partial}{\partial R}(R^2\frac{\partial T}{\partial R}) + f \tag{6.6}$$

where r is a cylindrical coordinate and R is a spherical one, P_{ld} is excess pressure over the initial hydrostatic state, f represents the source/ sink term which is equal to $3W_o\exp(-\lambda' t)/(4\pi R_o^3)$ inside the sphere of radius R_o and zero outside. These equations represent well this problem in very low porosity media because the accumulation terms that have been neglected are small.

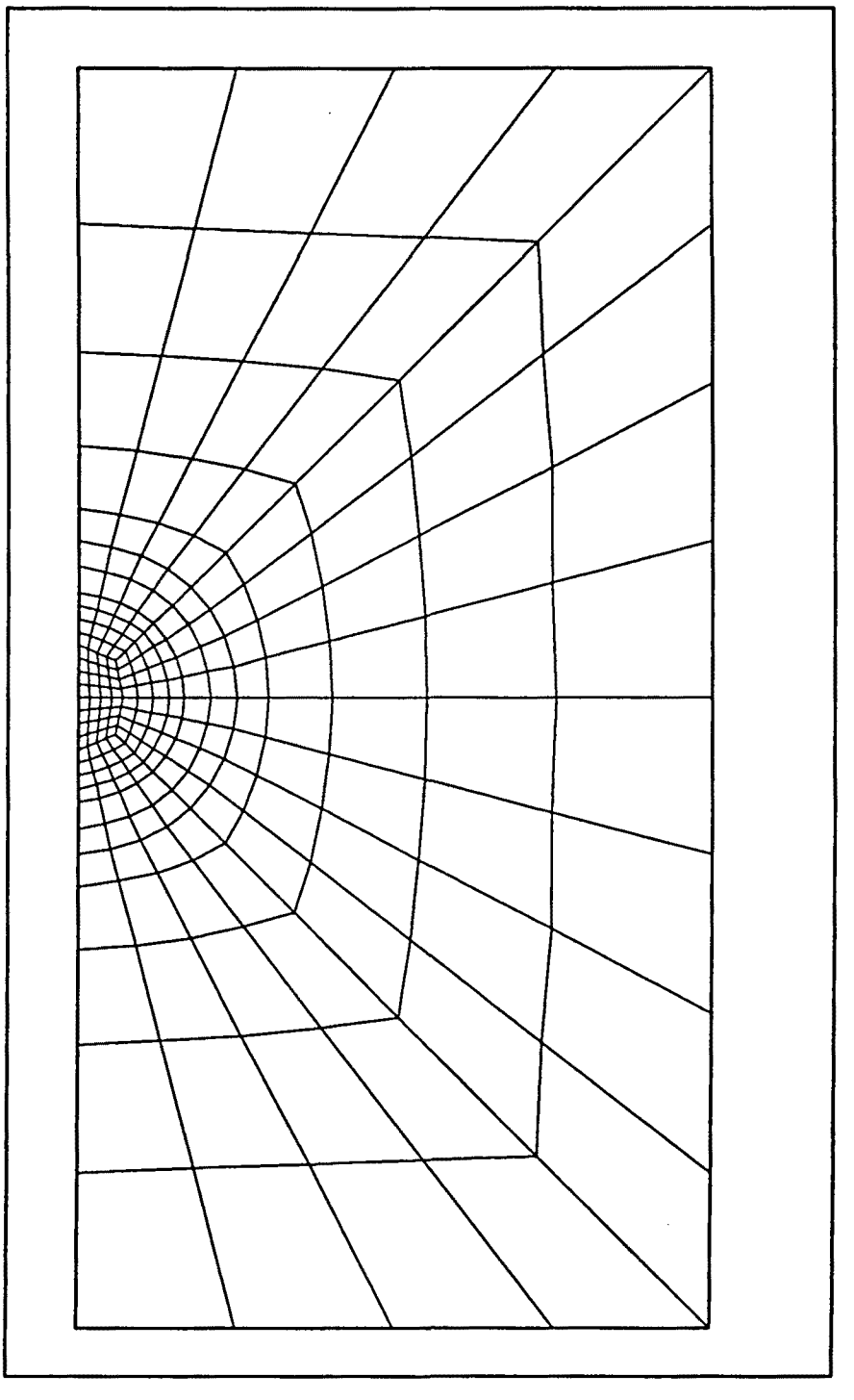

Figure 6.8: Finite element grid (249 nodes) used in the thermal convection problem. Axisymmetry is around the vertical (y) axis (left vertical boundary). The coordinate origin ($x = 0, y = 0$) is at the centre of the sphere. Sphere radius is R_o =250 m. Total simulated region is 1500-radius × 3000-height.

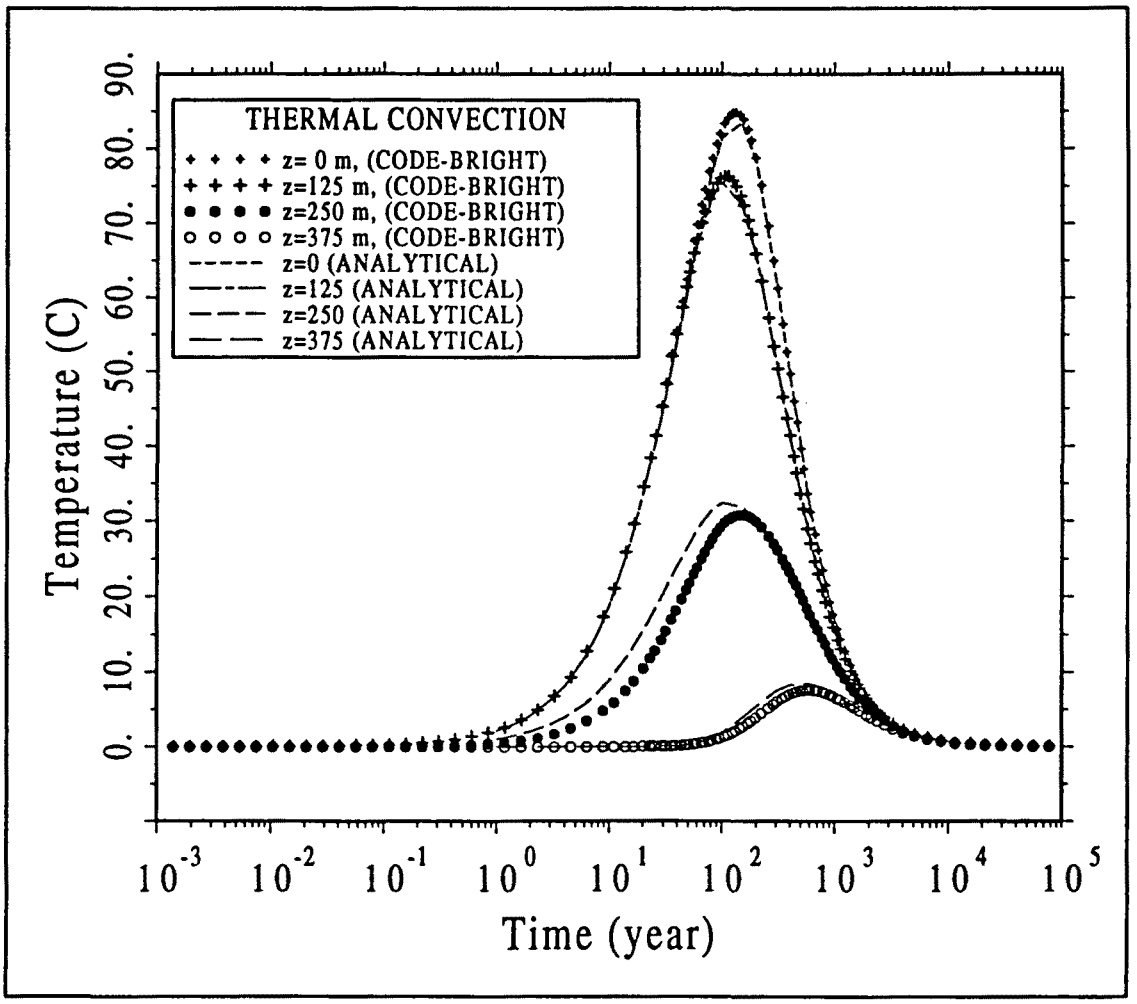

Figure 6.9: Time evolution of temperature at selected points. Computed (symbols) and analytical (dashed lines) results.

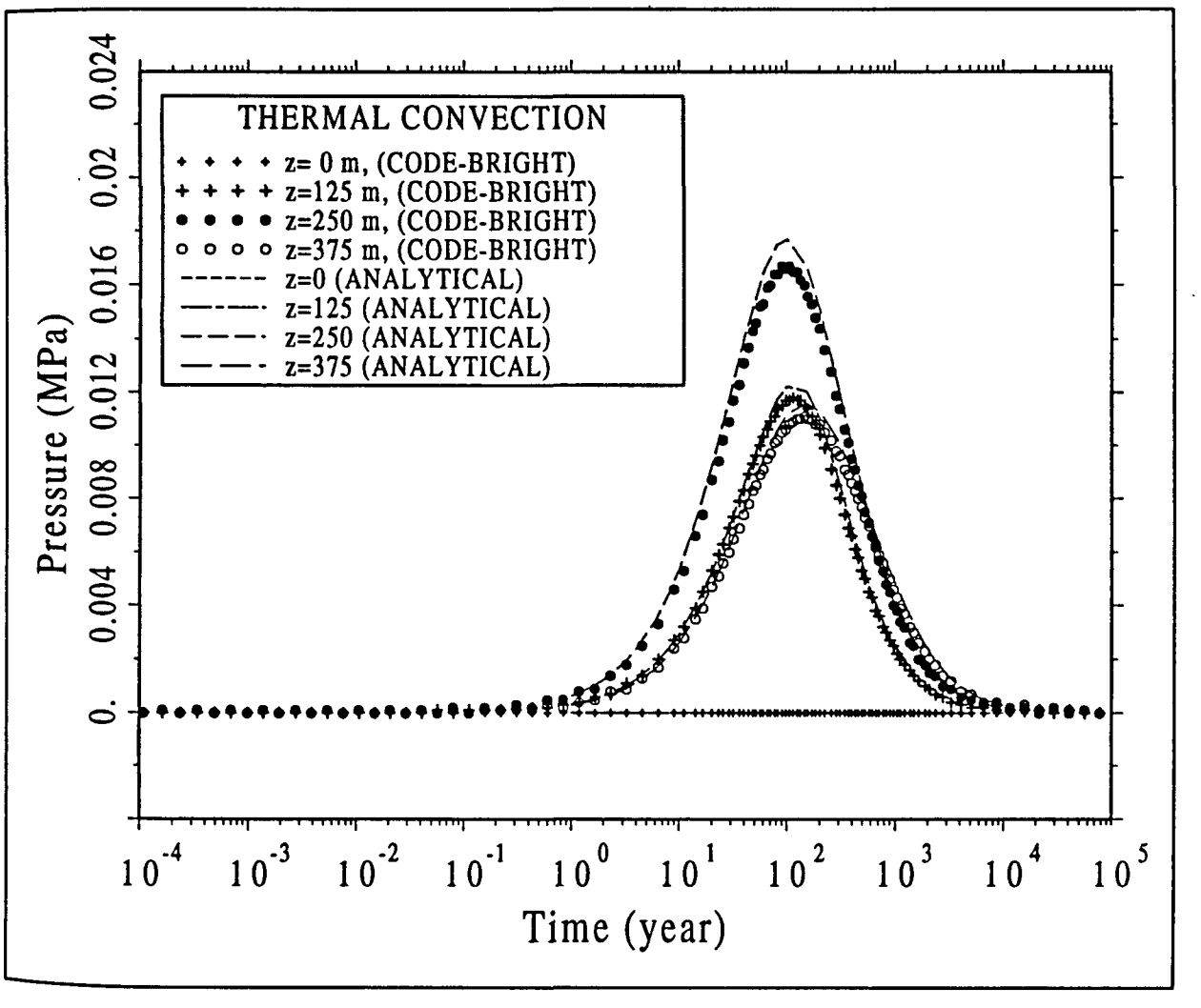

Figure 6.10: Time evolution of liquid pressure at selected points. Computed (symbols) and analytical (dashed lines) results.

The parameters that have been used in the computations are those reported in the project and summarized here:

Radius of the sphere, $R_o = 250$ m
Initial power output, $W_o = 10$ MW
Decay constant, $\lambda' = 7.3215 \times 10^{-10}$ s^{-1}
Thermal conductivity of rock, $\lambda = 2.51$ W m^{-1} K^{-1}
Density of rock, $\rho_s = 2600$ kg m^{-3}
Specific heat of rock, c_s=879 J kg^{-1} K^{-1}
Intrinsic permeability of rock, $k = 1.0 \times 10^{-16}$ m^2
Reference density of water, $\rho_{lo} = 992.2$kg m^{-3}
Expansion coefficient of water, $\beta = 3.85 \times 10^{-4}$ K^{-1}
Viscosity of water, $\mu = 6.529 \times 10^{-10}$ MPa s
Porosity(*), $\phi = 1.0 \times 10^{-10}$
Compressibility of water (**), 1×10^{-14} MPa^{-1}

(*) a low value is used in order to avoid transient terms in the flow equation. Porosity does not appear in the equations because storage terms were neglected.
(**) a low value is used in order to avoid transient terms in the flow equation.

Figure 6.8 shows the finite element grid (249 nodes) used in computations with CODE_BRIGHT. The size of the simulated region is 1500-radius × 3000-height. Axisymmetry is along the vertical axis. The boundaries are far enough to avoid their influence in the computations.

Figure 6.9 and 6.10 show temperatures and liquid pressures computed at the selected points. They are compared with the analytical solution which was tabulated in the project reports. Analytical solutions for this problem and others sinilar can be found in Hodgkinson (1979). The grid used here is relatively coarse compared to those used in the project (all grids used in the intercomparison exercise have more than 300 nodes).

6.5 Concluding remarks

The chapter contains four verification exercises with the intended objective of checking that the results obtained with CODE_BRIGHT really correspond to the solution of the equations coded. This process of verification will continue in the future together with the process of validation. As mentioned, the participation in intercomparison exercises may be very useful for this purpose.

6.6 References

Carrera, J. and J. Samper, (1989): "NOCONF" Programa de elementos finitos

para la solución de la ecuación de flujo no confinado", user's guide, ETSICCP-DIT-UPC.

COSA project, 1986, The Community Project COSA: Comparison of Geomechanical Computer Codes for Salt, EUR 10760 EN

Hodgkinson, D.P., "A mathematical model for hydrothermal convection around a radioactive waste depository (*sic*) in hard rock", Annal of Nuclear Energy, Vol 7. pp, 313:334

HYDROCOIN project, 1992, The International HYDROCOIN project, Nuclear Energy Agency, OECD-OCDE.

Kloska, M., L. Ostrowski, G. Pusch, and Yerby (1989): "Gas pulse Test- A new test method for low permeability formations", Rock at Great Depth, Maury and Fourmaintraux (eds), Balkema, pp. 219:226.

Prij, J. Beemsterboer, C.J.J., Ruiter, A, 1987, Convergentie, Eindrapportage Deelrapport 6, ECN, in English.